

Universidade de São Paulo  
Instituto de Física

# O sistema $\Lambda nn$ em Teoria de Campos Efetiva

Breno Agatão Garcia



Orientador: Prof. Dr. Renato Higa

Dissertação de mestrado apresentada ao Instituto de Física como requisito parcial para a obtenção do título de Mestre em Ciências.

Banca Examinadora:

Prof. Dr. Renato Higa - orientador (IFUSP)

Prof. Dr. Diogo Rodrigues Boito (IFSC/USP)

Prof. Dr. Tobias Frederico (ITA)

São Paulo  
2023

**FICHA CATALOGRÁFICA**  
**Preparada pelo Serviço de Biblioteca e Informação**  
**do Instituto de Física da Universidade de São Paulo**

Garcia, Breno Agatão

O sistema Lambda-n-n em Teoria de Campos Efetiva. São Paulo, 2023.

Dissertação (Mestrado) - Universidade de São Paulo. Instituto de Física. Depto. de Física Nuclear.

Orientador: Prof. Dr. Renato Higa.

Área de Concentração: Física Nuclear.

Unitermos: 1. Física nuclear; 2. Interações nucleares; 3. Teoria quântica de campo.

USP/IF/SBI-069/2023

University of São Paulo  
Physics Institute

# *Ann* system in Effective Field Theory

Breno Agatão Garcia

Supervisor: Prof. Dr. Renato Higa

Thesis submitted to the Physics Institute of the  
University of São Paulo in partial fulfillment of the  
requirements for the degree of Master of Science.

Examining Committee:

Prof. Dr. Renato Higa - Supervisor (IFUSP)

Prof. Dr. Diogo Rodrigues Boito (IFSC/USP)

Prof. Dr. Tobias Frederico (ITA)

São Paulo  
2023

# Acknowledgments

I would like to thank, at first, my parents Rogério Garcia and Fátima Agatão Garcia, who from very early ages always encouraged me to seek knowledge. They gave me the most solid base to continue pursuing my goals. I remember each day both of them, patiently, taught me the school basics. Each talk I had with my father, trying to teach him differential calculus or some complicated electromagnetism concept. I would also like to thank all my family for understanding all the times I could not attend to some family's celebration.

I would like to thank my fiancé, Claudia Maria Moraes Silva, who guided me through my darkest times and lighted up the path for me to see the life's brightness. She always encouraged and motivated me to be the best version of myself.

I would like to thank my supervisor, Prof. Dr. Renato Higa, for teaching me from the simplest mathematical trick to the most complicated physical concepts. Our discussions were of extremely importance for my scientific career. I would also like to thank my group colleagues Leandro Guedes, Matheus Cichocki, Vinícius Bet Ader and Pedro Betitto (who recently left the group) for important discussions on physics.

I would like to thank my undergraduate friends André Rodrigues, Beatriz Tucci, Francisco Maion, Gustavo Filbrich, Luigi Pierre, Marcello Cemin, Murillo de Godoy, Nathália Fukase, Pedro Fortini e Rodrigo Franco. Each one of them taught me much more than physics or mathematics. The coffee breaks, the afternoons singing and playing the acoustic guitar, the ping pong games. Every moment will be forever remembered.

I would like to thank every person I met at Xamanismo Lua Nova. I was able to strengthen myself mentally and understand so much about my own self.

Furthermore, I would specially like to thank my late grandmother, Neyde Pirozzi, who left us during the pandemics. She always took some time to genuinely show interest in things that I was studying, even knowing nothing about any scientific knowledge. Her willing to learn new things and her energy to live each day with a big smile on her face will always motivate me.

# Resumo

Apesar de recentes estudos experimentais parecerem estar cada vez mais próximos de obterem informações sobre a interação  $\Lambda n$ , até hoje, nenhum dado de espalhamento  $\Lambda n$  foi publicado. A informação disponível sobre o sistema é obtida por meio de modelos fenomenológicos, como o Nijmegen model D. Através deles, é possível obter números para os parâmetros de espalhamento de dois corpos como o comprimento de espalhamento  $a_2$  e o alcance efetivo  $r_2$ . Mais informações sobre essa interação de dois corpos é importante, tendo em vista que, nos últimos anos, estudos experimentais apontam para a existência de um estado de três corpos  $\Lambda nn$ . Estudos teóricos são categóricos em apontar que é bastante improvável a existência de um estado ligado  $\Lambda nn$ . No entanto, a existência de um estado ressonante  $\Lambda nn$  parece ser mais plausível de ser formado usando os escassos dados fenomenológicos sobre a interação  $\Lambda n$ . No presente trabalho, nós focamos em procurar ressonâncias no sistema  $\Lambda nn$ . Utilizamos a teoria de campos efetiva chamada pionless EFT ( $\not\propto$ EFT), na qual é baseada em interações de contato e assume expansões perturbativas na razão  $r_2/a_2$ , e o modelo fenomenológico baseado em potenciais separáveis, o qual não depende de que  $r_2/a_2$  seja pequeno. Utilizamos os valores do Nijmegen model D para os parâmetros de espalhamento. A fim de obter as trajetórias dos polos, nós utilizamos fatores de escalonamento que multiplicam a interação  $\Lambda n$ . Obtemos as trajetórias dos polos escalonando os comprimentos de espalhamento de dois corpos ( $a_s(\Lambda n)$  e  $a_t(\Lambda n)$ ) e a intensidade da força de três corpos ( $g(\Lambda)$ ), para a abordagem com teoria efetiva, e escalonamos a intensidade do potencial  $\Lambda n$  para o modelo de potencial separável. Com o último, achamos ressonâncias físicas apenas em um intervalo limitado, e com valores relativamente altos, do fator de escalonamento.

**Palavras-chave:** física nuclear, teoria de campos efetiva, ressonâncias, física de baixas energias.

# Abstract

Although recent experimental studies seem to be closer to constrain the  $\Lambda n$  interaction, until now, no scattering data from  $\Lambda n$  have been published. The available information for this system comes from phenomenological potential models, such as the Nijmegen  $\Lambda n$  interaction. From that, one gets numbers for scattering parameters such as the two-body scattering length  $a_2$  and effective range  $r_2$ . More information on this two-body interaction is important, specifically, given some experimental signs in recent years about the existence of a three-body  $\Lambda nn$  state. From the theoretical side, a couple of studies consistently assures that a bound  $\Lambda nn$  state is very unlikely to exist. However, a  $\Lambda nn$  resonant state could be more prone to be formed from the poorly available phenomenological information about the  $\Lambda n$  interaction. In the present work we focus on searching for resonances in the  $\Lambda nn$  system. We use pionless effective field theory ( $\not{\pi}$ EFT), which is based on contact interactions and assumes a perturbative expansion in the ratio  $r_2/a_2$ , and a phenomenological model based on rank-one separable potentials, which does not necessarily assume  $r_2/a_2$  to be small. We use the Nijmegen model D values as scattering parameters. In order to obtain the pole trajectories, we resort to scaling factors that multiplies the two-body  $\Lambda n$  interaction. We obtain pole trajectories by scaling the two-body scattering lengths ( $a_{s(\Lambda n)}$  and  $a_{t(\Lambda n)}$ ) and the three-body strength ( $g(\Lambda)$ ) in the EFT approach, and scaling the strength of the  $\Lambda n$  potential in the separable potential model. With the latter, one finds resonances only in a limited interval and with relatively large values of the scaling factor.

**Keywords:** nuclear physics, effective field theory, resonances, low-energy physics.

# Contents

<b>1</b>	<b>Introduction</b>	<b>6</b>
<b>2</b>	<b>Scattering Theory</b>	<b>10</b>
2.1	Lippmann-Schwinger Equation . . . . .	15
<b>3</b>	<b>Effective Field Theories</b>	<b>19</b>
3.1	2-body sector . . . . .	24
3.2	3-body sector . . . . .	28
3.2.1	3-boson integral equation . . . . .	31
3.2.2	Efimov Physics . . . . .	35
3.3	A more realistic case: $nd$ system . . . . .	38
3.3.1	Projectors . . . . .	39
3.3.2	Born Term . . . . .	46
3.3.3	Quartet channel . . . . .	48
3.3.4	Doublet channel . . . . .	49
<b>4</b>	<b><math>\Lambda nn</math> system</b>	<b>53</b>
4.1	Integral equation . . . . .	54
<b>5</b>	<b>Results</b>	<b>62</b>
5.1	EFT approach . . . . .	62
5.1.1	Scattering length $a_2$ as a parameter . . . . .	65
5.1.2	Strength $g(\Lambda)$ as a parameter . . . . .	65
5.2	Phenomenological approach: Separable potentials . . . . .	68
<b>6</b>	<b>Conclusions and perspectives</b>	<b>74</b>
	<b>Appendices</b>	<b>77</b>
<b>A</b>	<b>Generators of the angular momentum <math>3/2</math></b>	<b>78</b>

<b>B</b>	$G^{(i)}$ matrices and its properties	<b>82</b>
<b>C</b>	<b>Born terms</b>	<b>85</b>
	C.1 $nd$ system . . . . .	85
	C.2 $Ann$ system . . . . .	88
<b>D</b>	<b>Separable Potentials</b>	<b>91</b>
<b>E</b>	<b>Numerical Methods</b>	<b>93</b>
	E.1 Numerical Integration . . . . .	94
	E.2 Contour Rotation . . . . .	94
	E.3 Bound States . . . . .	95
	E.4 Resonances . . . . .	95
	E.5 Coupled Channel . . . . .	96
<b>F</b>	<b>Tabulated Values</b>	<b>99</b>



# Chapter 1

## Introduction

In 1954 Yang and Mills, influenced by the development and success of quantum electrodynamics (QED) [1], proposed a theory for the strong interactions with two different types of charges [2]. The corresponding  $SU(2)$  symmetry parallels the isospin symmetry of the strong interactions and the idea would be gauging the symmetry the same way as the electromagnetic interactions, inspired by Weyl's ideas [3]. The virtue of the Yang-Mills theory was to generate self-interactions of the gauge fields that could emulate the strong force. However, more ingredients were necessary to match the theory with the observed aspects of the strong interactions, in particular the asymptotic freedom at high energies. After a strong theoretical effort of the scientific community it was realized that gauge fields coupled to nearly massless fermions (partons) in the  $SU(3)$  gauge group provided not only qualitative but quantitative description of high-energy phenomena [4, 5, 6]. Meanwhile, in 1964, Gell-Mann postulated the existence of the up, down and strange quarks [7]. These, among others efforts, resulted in the birth, development, and nowadays, confirmation of quantum chromodynamics (QCD) as the theory of the strong interactions. QCD is a non-Abelian gauge theory respecting the  $SU(3)$  color symmetry. The theory is a quantum field theory of elementary spin-1/2 fermions named quarks, interacting via the elementary gauge bosons of the theory, named gluons. The coupling  $g$  that describes the interactions between a quark and a gluon, and among gluons themselves, is parametrized in terms of the so-called running (strong) coupling constant  $\alpha_s = g^2/4\pi$ . Due to the non-Abelian aspect of the theory,  $\alpha_s$  is large at relatively low energies and goes to zero as the energies involved go to infinity. The latter is known as asymptotic freedom while the former leads to the phenomenon of confinement. This behavior is shown in Figure 1.1. Since the decreasing of  $\alpha_s$  is logarithmic with increasing energy,  $\alpha_s$  cannot be small enough with available experimental energies to allow quarks and gluons to be detected as free particles. Thus, quarks and gluons remain confined within composed particles called hadrons. Hadrons are formally classified into baryons (particles containing an odd number of va-

lence quarks, at least three) and mesons (particles containing an even number of valence quarks, at least two).

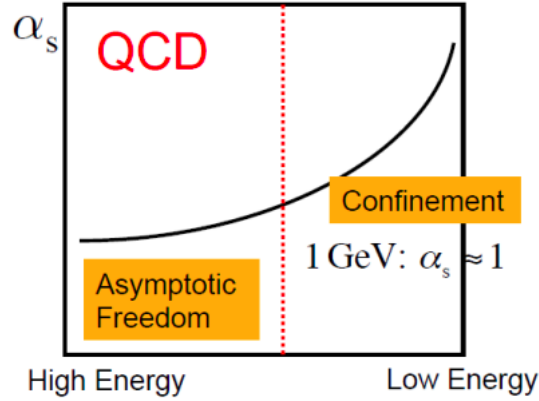


Figure 1.1: The coupling  $\alpha_s$  as a function of the energy. Taken from [8]

A central challenge for the theory of strongly interacting systems is that we cannot solve (yet) the dynamics of QCD at hadronic scales. This is mainly due to confinement— at low energies QCD is highly non-perturbative due to the increasing of  $\alpha_s$ . Some features of QCD in this regime have been lately achieved by lattice QCD, for instance, masses of baryons and mesons [9, 10, 11, 12, 13] for pion masses close to its physical value ( $m_\pi \sim 140$  MeV). However, most of these observables are static ones, and real scattering situations are still quite challenging despite some progress in this direction [14, 15, 16]. Although phenomenological models have been used to describe hadronic properties and interactions [17, 18], effective field theories (EFTs) present a controlled and model-independent description of strongly-interacting systems, based on an expansion in the ratio of short- and long-distance scales. In the last three decades, there is still an ongoing dedicated effort with the purpose of obtaining an increasingly refined interaction among hadrons from the fundamental symmetries of QCD [19, 20, 21, 22, 23, 24]. One key ingredient is the spontaneous breaking of chiral symmetry, which is well-known from several studies in the 1970s to play a major role in the description of hadron dynamics at low energies. The effective field theory that incorporates chiral symmetry (present in the QCD Lagrangian), its spontaneous and explicit breaking, and phenomenological implications, is known as Chiral Effective Field Theory ( $\chi$ EFT). The main aspect of this theory is the pion identified as the Goldstone boson of the spontaneous chiral symmetry breaking. Regarding the nuclear scenario, pionic interactions are extremely predominant at large distances, but non-perturbative aspects characteristic of nuclear bound states need to be accounted for. These non-perturbative aspects are not necessarily due to the long-range pion exchanges, but as seen in Chapter 3 due to the large two-body scattering length compared to the range of interactions. If one tries to describe such non-perturbative physics

in a limited range of energy, where pion interactions can be considered short-ranged, pion dynamics become “frozen” as heavy degrees of freedom, and their effects are condensed into simpler contact interactions of another effective theory. This theory with only contact interactions, commonly referred to as pionless EFT, has been applied with success to several nucleon-nucleon processes at momenta below  $\sim 40$  MeV, as well as to light nuclei with up to  $A \sim 6$  (for a review, see Refs. [68, 61]). Throughout this work, pionless EFT is applied, which is convenient when treating few-body systems with large scattering lengths for momenta below the energy/momentum scale set by the pion mass.

Regarding systems with strangeness, up to now, no  $\Lambda n$  scattering data exist. This is due to the difficulty in obtaining both  $\Lambda$  and/or  $n$  stable targets/beams experimentally, with good intensities and interaction cross sections (both are electrically neutral). In 2013, the HypHI Collaboration [25] had reported a  ${}^3_{\Lambda}n$  or  $\Lambda nn$  bound state. It was measured in the scattering of  ${}^6\text{Li}$  on graphite

$${}^6\text{Li} + \text{C} \rightarrow \begin{cases} \cdots + \pi^- + d \\ \cdots + \pi^- + t \end{cases} \quad (1.1)$$

which means, that a peak observed in the invariant mass of  $\pi^- + d$  and  $\pi^- + t$ . Actually, the peak in the  $\pi^- + d$  and  $\pi^- + t$  invariant mass is approximately at  $m_{\Lambda} + m_n$  and  $m_{\Lambda} + 2m_n$ , respectively. This highly suggests the existence of such bound state, also because of their comparable lifetimes. This would put strong constraints upon the  $\Lambda n$  interaction. The possible existence of a  $\Lambda nn$  bound state was investigated by different theoretical approaches. Dalitz and Downs, in the 1950s, investigated the possibility of a hypernuclear bound state using variational methods [26, 27, 28]. Garcilazo solved the Faddeev equations using both a separable model and full-fledged calculation with realistic baryon-baryon interactions [29, 30]. Hiyama studied the system by taking the  $\Lambda N - \Sigma N$  coupling explicitly into account [31], and Gal derived constraints from several hypernuclear systems with full consideration of  $\Lambda N \leftrightarrow \Sigma N$  coupling [32]. The conclusions were all consistent: no  $\Lambda nn$  bound state could be determined. To understand this, one can think of a system where  $\Lambda$  is just barely bound to a deuteron, the  ${}^3_{\Lambda}\text{H}$  or  $\Lambda np$  (hypertriton). When comparing  ${}^3_{\Lambda}\text{H}$  with  ${}^3_{\Lambda}\text{n}$ , there is a replacement of a  $np$  interaction, which supports a bound state (the deuteron) by an  $nn$  interaction, which is unbound. Although the existence of a bound state seems to be almost impossible, theoretical studies have predicted  $\Lambda nn$  resonances [34, 35] and also addressed that using a  ${}^3\text{H}(e, e'K^+)_{\Lambda}$  electro-production reaction at JLab would be an ideal experiment in order to explore such system. A recent publication from JLab facility could not see any clear peak in the missing mass distribution of the  $\Lambda nn$  [33]. In 2022, the Hall A Collaboration published a work reporting a possible

$\Lambda nn$  resonance [36]. This resonance could be used to constrain the  $\Lambda n$  interaction.

The main formalism used in this work is effective field theory, specifically the pionless EFT, which is based on contact interactions due to the low energies compared with the pion mass  $m_\pi$ , and assumes as expansion parameter the ratio between the two-body effective range and scattering length,  $r_2/a_2$ . However, based on the numbers of  $a_2 \sim 2$  fm and  $r_2 \sim 3$  fm from the phenomenological Nijmegen model D [37] for the  $\Lambda n$  interactions, it is not possible to expand the amplitudes in powers of  $r_2/a_2$  as this ratio is greater than 1. Nevertheless, we assume that we can use  $r_2/a_2 \ll 1$ , and apply the pionless EFT, regardless the phenomenological information from [37]. We solve the three-body homogeneous integral equation and look for poles for the  $S$ -matrix. In order to trace the pole trajectory, we scale our  $\Lambda n$  scattering length  $a_{2(\Lambda n)}$  in both triplet and singlet channels by a scaling factor,  $s_{EFT}$ , while the three-body force strength  $g(\Lambda) = 0$ . We also considered varying the three-body force strength  $g(\Lambda)$  maintaining the scaling factor  $s_{EFT} = 1$ .

Since there is no clear power counting in pionless EFT for the case  $r_2/a_2 > 1$ , to cover this possibility, we employ a phenomenological rank-one separable potential with Yamaguchi form factors. As in the previous case, we solve a homogeneous integral equation and search for the poles of the  $S$ -matrix, scaling the strength of the potential by a factor  $s$ .

The work is structured in the following way. Chapter 2 is a review about some of the basic concepts in scattering theory, which will be applied in the following Chapters. The pole structure (bound states, resonances and virtual states) is presented using the complex momentum- and energy-plane and the Lippmann-Schwinger equation is derived. In Chapter 3 there is a brief introduction to the idea of an effective field theory. Using pionless EFT, two- and three-body sectors at very low energies are explored. The three-boson system is detailed in order to present some key ideas of the Efimov physics.  $nd$  system is unraveled in both quartet and doublet channels, in order to define the spin-isospin projectors. In Chapter 4 we present the EFT formalism necessary to solve the three-body integral equation for the  $\Lambda nn$  system. Chapter 5 presents the results using both formalisms, EFT and Yamaguchi potentials. Also, the formalism used to solve the phenomenological model is described in this Chapter. In Chapter 6 we summarize the present work and discuss future perspectives.

# Chapter 2

## Scattering Theory

This chapter reviews some of the basic concepts of scattering theory. These concepts permeate through the structure of latter-developed theories such as the analytic  $S$ -matrix, quantum field theory, and lately, effective field theory.

Consider two non-relativistic particles with mass  $m$  interacting, for simplicity, via a short-range potential  $V(\mathbf{r})$  [38, 39]. Also, consider only elastic scattering. The process is better described at the center-of-mass reference frame, with the particles with opposite momentum  $\pm\mathbf{k}$  and kinetic energy  $E = k^2/m$  (consider from now on  $\hbar = c = 1$ ). The solution must respect the time-independent Schrödinger equation,

$$\left[ -\frac{\vec{\nabla}^2}{2m} + V(\mathbf{r}) \right] \psi(\mathbf{r}) = E\psi(\mathbf{r}). \quad (2.1)$$

The asymptotic ( $r \rightarrow \infty$ ) wave function  $\psi(\mathbf{r})$  that is a solution of the Schrödinger equation is given by

$$\begin{aligned} \psi(\mathbf{r}) &= \psi(\mathbf{r})_{\text{incident}} + \psi(\mathbf{r})_{\text{scattered}} \\ &= e^{ikz} + f(\theta, \phi) \frac{e^{ikr}}{r}, \end{aligned} \quad (2.2)$$

i.e., an incident plane wave with energy  $E$  (in our choice, traveling in the  $z$  direction) summed with an outgoing spherical wave.

The quantity  $f(\theta, \phi)$  is called *scattering amplitude* and can be understood as a three dimensional generalisation of the transmission and reflection coefficients. For our purposes, we will consider just the case where the potential is central,  $V(\mathbf{r}) = V(r)$  and then, there is no dependence on the variable  $\phi$ ,  $f = f(\theta)$ . The main goal of scattering theory is to compute the scattering amplitude.

Now one defines a quantity that is called *cross-section*. Consider the infinitesimal area  $d\sigma$ . It can be described using the impact parameter  $b$  and the angle  $\phi$

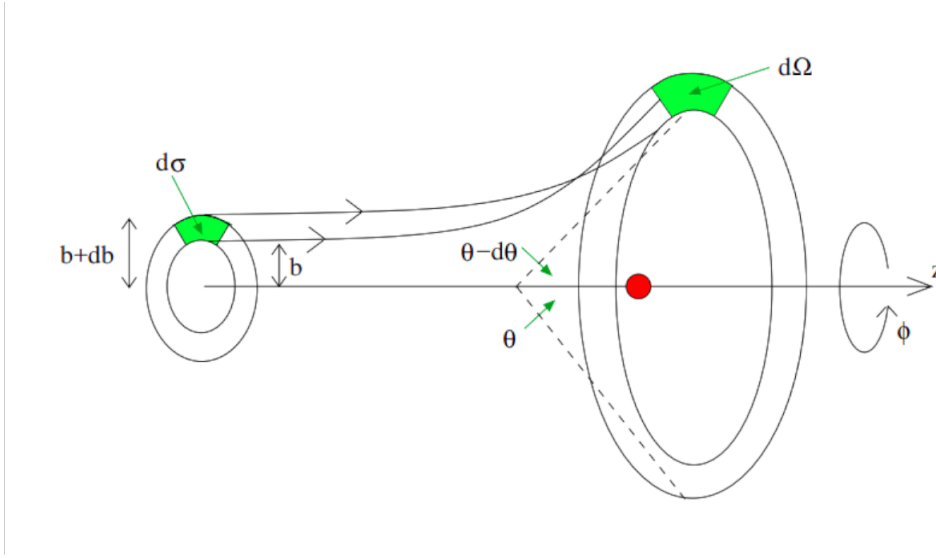


Figure 2.1: The green areas represent infinitesimal cross-sectional areas. Taken from reference [38]

$$d\sigma = b db d\phi. \quad (2.3)$$

After passing through the area  $d\sigma$  the particle flux crosses the area delimited by the cone with solid angle  $d\Omega$

$$d\Omega = \sin \theta d\theta d\phi. \quad (2.4)$$

In this sense, *the differential cross-section* is defined as

$$\frac{d\sigma}{d\Omega} = \frac{b}{\sin \theta} \frac{db}{d\theta}. \quad (2.5)$$

It is common to use the concept of flux of particles to define the differential cross-section as

$$\frac{d\sigma}{d\Omega} = \frac{\text{Scattered flux}}{\text{Incident flux}}. \quad (2.6)$$

The connection between the cross section and the scattering amplitude is established with the help of the probability current  $\mathbf{J}$

$$\mathbf{J} = -\frac{i}{2m} [\psi^* \nabla \psi - (\nabla \psi^*) \psi]. \quad (2.7)$$

The incident and scattered probability currents are

$$\mathbf{J}_{incident} = \frac{k}{m} \hat{\mathbf{z}}, \quad (2.8)$$

$$\mathbf{J}_{scattered} = \frac{k}{m} \frac{1}{r^2} |f(\theta)|^2 \hat{\mathbf{r}} + \mathcal{O}\left(\frac{1}{r^3}\right). \quad (2.9)$$

The flux of the scattered particles through an area  $dA$  implied by the solid angle  $d\Omega$  as  $r \rightarrow \infty$  becomes

$$\mathbf{J}_{scattered} \cdot \hat{\mathbf{r}} dA = \frac{k}{m} |f(\theta)|^2 d\Omega. \quad (2.10)$$

Thus the differential cross section is given by

$$\frac{d\sigma}{d\Omega} = \frac{\frac{k}{m} |f(\theta)|^2}{\frac{k}{m}} = |f(\theta)|^2, \quad (2.11)$$

and the total cross section is obtained by integrating over  $d\Omega$ ,

$$\sigma_T = \int d\Omega |f(\theta)|^2. \quad (2.12)$$

We can express the scattering amplitude  $f(\theta)$  in terms of its partial waves using

$$f(\theta) = \sum_{\ell=0}^{\infty} (2\ell + 1) f_{\ell}(\theta) P_{\ell}(\cos \theta). \quad (2.13)$$

Knowing that the probability must be conserved as the process occurs, which is known as unitarity. One can look at  $r \rightarrow \infty$  in Eq. (2.2)

$$\begin{aligned} \psi(\mathbf{r}) &= \frac{1}{(2\pi)^{3/2}} \left[ e^{ikz} + f(\theta) \frac{e^{ikr}}{r} \right] \\ &= \frac{1}{(2\pi)^{3/2}} \sum_{\ell=0}^{\infty} (2\ell + 1) P_{\ell}(\cos \theta) \left( \frac{e^{ikr} - e^{-i(kr-\ell\pi)}}{2ikr} \right) \\ &\quad + \sum_{\ell=0}^{\infty} (2\ell + 1) f_{\ell}(\theta) P_{\ell}(\cos \theta) \frac{e^{ikr}}{r}, \\ &= \frac{1}{(2\pi)^{3/2}} \sum_{\ell=0}^{\infty} (2\ell + 1) \frac{P_{\ell}(\cos \theta)}{2ik} \left\{ [1 + 2ik f_{\ell}(\theta)] \frac{e^{ikr}}{r} - \frac{e^{-i(kr-\ell\pi)}}{r} \right\}. \end{aligned} \quad (2.14)$$

The first line of Eq. (2.14) is the spherical (partial) wave expansion of the plane wave while the second line is the  $r \rightarrow \infty$  behavior of the scattering amplitude. The sum on the third line is interpreted as an incoming spherical wave with coefficient  $-1$  and an outgoing

spherical wave with coefficient  $[1 + 2ikf_\ell(\theta)]$ . This is to be compared with the pure plane wave in the first line of Eq. (2.14), with coefficients  $-1$  and  $+1$  for the incoming and outgoing spherical waves, respectively. As we are dealing with elastic scattering, conservation of the flux of particles must hold. That implies that the coefficients of each spherical wave must have the same modulus. For the outgoing spherical waves, that means  $|1 + 2ikf_\ell(\theta)| = 1$ . One can define the partial-wave  $S$ -matrix,

$$S_\ell(k) = 1 + 2ikf_\ell(\theta), \quad (2.15)$$

which satisfies the *partial wave unitarity relation*  $|S_\ell(k)| = 1$ .

That allows one to write  $S_\ell(k)$  as

$$S_\ell(k) = e^{2i\delta_\ell} \quad \Rightarrow \quad f_\ell(\theta) = \frac{1}{2i}(e^{2i\delta_\ell} - 1) = e^{i\delta_\ell} \sin \delta_\ell, \quad (2.16)$$

where the factor 2 on the definition of  $S_\ell(k)$  is a convention. The quantity  $\delta_\ell$  is called the phase-shift for the partial wave  $\ell$ . Using the *partial wave expansion* one can solve the scattering amplitude in terms of its orbital angular momentum contributions,

$$\begin{aligned} f(\theta) &= \frac{1}{k} \sum_{\ell=0}^{\infty} (2\ell + 1) \frac{e^{2i\delta_\ell} - 1}{2i} P_\ell(\cos \theta), \\ &= \frac{1}{k} \sum_{\ell=0}^{\infty} (2\ell + 1) e^{i\delta_\ell(k)} \sin \delta_\ell(k) P_\ell(\cos \theta) \\ &= \sum_{\ell=0}^{\infty} \frac{2\ell + 1}{k \cot \delta_\ell(k) - ik} P_\ell(\cos \theta). \end{aligned} \quad (2.17)$$

All the information about the scattering process is now encoded in the so-called *phase shifts*  $\delta_\ell(k)$ . At sufficiently low energies, the  $S$ -wave ( $\ell = 0$ ) phase shift can be expanded in powers of  $k^2$ , leading to the famous *effective range expansion* (ERE),

$$k \cot \delta_0(k) = -\frac{1}{a_0} + \frac{1}{2}r_0k^2 - \frac{1}{4}P_0k^4 + \dots, \quad (2.18)$$

with  $a_0$  being the  $S$ -wave scattering length,  $r_0$  the  $S$ -wave effective range and  $P_0$  the  $S$ -wave shape parameter.

It is also possible to generalize to higher partial waves and write

$$k^{2\ell+1} \cot \delta_\ell(k) = -\frac{1}{a_\ell} + \frac{1}{2}r_\ell k^2 - \frac{1}{4}P_\ell k^4 + \dots \quad (2.19)$$



The partial-wave scattering length  $a_\ell$  can be obtained through the low-energy limit

$$\lim_{k \rightarrow 0} \frac{f_\ell(\theta)}{k^{2\ell}} = -a_\ell. \quad (2.20)$$

Substituting equation (2.17) into (2.12) and using the Legendre polynomials orthogonality relation,

$$\int_{-1}^1 dx P_r(x) P_s(x) = \frac{2}{2\ell + 1} \delta_{rs}, \quad (2.21)$$

one can find an expression for the differential cross section

$$\sigma_T = \frac{4\pi}{k^2} \sum_{\ell} (2\ell + 1) \sin^2 \delta_\ell. \quad (2.22)$$

As said before,  $S_\ell(k)$  is the  $\ell$ th diagonal element of a matrix called  $S$ -matrix, sometimes referred to as the scattering matrix,

$$\mathbf{S} = \mathbf{1} + i\mathbf{T}. \quad (2.23)$$

Comparing Eqs. (2.15) and (2.23), and assuming that  $T_\ell(E)$  is the  $\ell$ th diagonal element of the  $T$ -matrix, called transition matrix,

$$T_\ell(k) = \frac{4\pi}{m} f_\ell(\theta), \quad (2.24)$$

leads to

$$S_\ell(k) = 1 + i \frac{mk}{2\pi} T_\ell(k). \quad (2.25)$$

The low-energy limit, given by Eq. (2.20), makes all but  $\ell = 0$  partial waves unimportant in this energy regime<sup>1</sup>. In such cases, the transition matrix is given by

$$T_0(k) = \frac{4\pi}{m} \frac{1}{k \cot \delta_0(k) - ik}. \quad (2.26)$$

The unitarity of the  $S$ -matrix (or, equivalently,  $S_\ell(k)$ ) holds for the physical situation when  $k$  is real. The  $S$ -matrix can, however, be analytically extended to complex  $k$ . This analytic continuation hinges on causality and its analytic properties allow one to handle resonances and non-scattering states such as bound and virtual states as poles of the  $S$ -matrix. Once the poles are located in the complex  $k$  plane, one can name them according to relevant states, i.e., bound states, resonant states or virtual states. The poles contained in the complex momentum plane are mapped into the complex energy plane, and vice-

---

<sup>1</sup>Exceptions are the presence of low-energy poles (bound/virtual states or resonances) in specific partial waves other than  $S$ -waves.

versa, through the non-relativistic dispersion relation  $E = k^2/2m$ . Given this quadratic relation with  $k$ , each half complex- $k$  plane maps to a whole distinct, complex- $E$  Riemann sheet—the upper momentum half-plane maps onto  $E_I$  (“physical” sheet) and the lower momentum half-plane maps onto  $E_{II}$  (“unphysical” sheet), both sheets are connected at the positive real axis  $E > 0$ , as Figure 2.2 shows.

The specific location of poles in the complex momentum plane (complex-energy manifold) is: for bound-states they appear as singularities in the positive imaginary  $k$ -axis  $k_0 = +i|k|$  (will be mapped onto the negative real  $E$ -axis of  $E_I$ ), for virtual-states the singularities are located at the negative imaginary  $k$ -axis  $k_1 = -i|k|$  (also mapped onto the negative real  $E$ -axis, but now onto the “unphysical” sheet  $E_{II}$ ), and for resonant states they are located at the lower half-plane, always appear in pairs  $k_2 = k_R - ik_I$  and  $k'_2 = -k_R - ik_I$  (mapped onto the lower half-plane of  $E_{II}$ ), both  $k_R$  and  $k_I$  are real positive, and  $k_I \ll k_R$  [40].

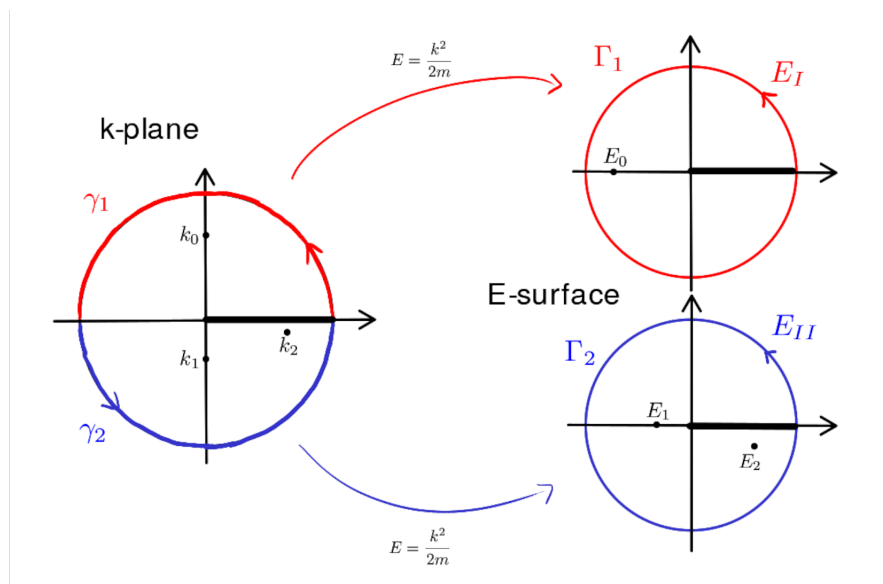


Figure 2.2: Complex momentum plane and energy manifold. Based on reference [40]

## 2.1 Lippmann-Schwinger Equation

When dealing with two-body scattering problems the Lippmann-Schwinger equation plays a central role. It consists of an integral equation for the scattering amplitude, either in momentum or position representation, with the appropriate asymptotic conditions, whose solution provides information not only for the physical scattering problem in question, but also for bound, virtual, and resonant states via analytic continuation. Sometimes one can even formally solve the scattering amplitude, as for the so-called separable potentials.

For sufficiently weak potentials unable to hold a bound state, the Lippmann-Schwinger is susceptible to approximation methods, like the Born series.

The starting point is the Schrodinger equation,

$$H |\psi\rangle = E |\psi\rangle, \quad (2.27)$$

where  $H = H_0 + V$ ,  $H_0$  stands for the free particle kinetic energy operator with eigenvalue  $\frac{\mathbf{p}^2}{2m}$ , and  $V$  is the potential operator.

The equation one needs to manipulate is

$$(H_0 + V) |\psi\rangle = E |\psi\rangle. \quad (2.28)$$

An important fact that may be considered is that, in the limit  $V \rightarrow 0$ , the equation must reduce to the well-known free particle Schrodinger equation. With that in mind, the solution must include a free Hamiltonian eigenket  $H_0 |\phi\rangle = E |\phi\rangle$ ,

$$|\psi\rangle = \frac{1}{E - H_0} V |\psi\rangle + |\phi\rangle. \quad (2.29)$$

As one may notice, the operator  $(E - H_0)^{-1}$  is singular and the energy must be slightly complex in order to avoid the singularity. With that in hand, the Lippmann Schwinger equation can be written as

$$|\psi^\pm\rangle = |\phi\rangle + \frac{1}{E - H_0 \pm i\epsilon} V |\psi^\pm\rangle. \quad (2.30)$$

The sign of the imaginary term  $i\epsilon$  in the regularized operator  $(E - H_0 \pm i\epsilon)^{-1}$  leads formally to two distinct solutions  $|\psi^\pm\rangle$ , both with different interpretations. The  $+i\epsilon$  solution corresponds to the physically meaningful solution, with a plane-wave incident plus an outgoing spherical wave, while the  $-i\epsilon$  solution contains, instead, an incoming spherical wave. Both solutions are related to each other via time-reversal [42]. Mathematically, the  $i\epsilon$  term fixes the asymptotic boundary condition of the solution in the integral equation.

So far, Eq. (2.30) is generic enough to be used in whatever basis of the Hilbert space we choose. Here we use the plane-wave momentum basis, which is more convenient for scattering processes. Multiplying Eq. (2.30) from the left by  $\langle \mathbf{p}' |$ ,

$$\langle \mathbf{p}' | \psi_p^\pm \rangle = \langle \mathbf{p}' | \phi_p \rangle + \frac{1}{E - p^2/2m \pm i\epsilon} \langle \mathbf{p}' | V | \psi_p^\pm \rangle, \quad (2.31)$$

and making use of the identity  $I = \int \frac{d^3q}{(2\pi)^3} |\mathbf{q}\rangle \langle \mathbf{q}|$ , one arrives at

$$\Psi(\mathbf{p}', \mathbf{p}) = \Phi(\mathbf{p}', \mathbf{p}) + \frac{1}{E - p^2/2m \pm i\epsilon} \int \frac{dq^3}{(2\pi)^3} V(\mathbf{p}', \mathbf{q}) \Psi(\mathbf{q}, \mathbf{p}), \quad (2.32)$$

which is the Lippmann-Schwinger equation for the scattering wave function.

In scattering theory, the transition operator  $T$  is defined as

$$T^\pm |\phi_p\rangle = V |\psi_p^\pm\rangle, \quad (2.33)$$

while the scattering amplitude is the matrix element of  $T$  between the initial and final states. Multiplying Eq. (2.30) from the left by  $\langle \mathbf{p}' | V$  leads to [41, 42]

$$\begin{aligned} \langle \mathbf{p}' | V | \psi_p^\pm \rangle &= \langle \mathbf{p}' | V | \phi_p \rangle + \int \frac{dq^3}{(2\pi)^3} \langle \mathbf{p}' | V | \mathbf{q} \rangle \frac{1}{E - q^2/2m \pm i\epsilon} \langle \mathbf{q} | V | \psi_p \rangle, \\ T(\mathbf{p}', \mathbf{p}) &= V(\mathbf{p}', \mathbf{p}) + \int \frac{dq^3}{(2\pi)^3} V(\mathbf{p}', \mathbf{q}) \frac{1}{E - q^2/2m \pm i\epsilon} T(\mathbf{q}, \mathbf{p}). \end{aligned} \quad (2.34)$$

The above Lippmann-Schwinger equation for the scattering amplitude can be schematically expanded, in the spirit of the Born series, as

$$T = V + \int VGT = V + \int VGV + \dots, \quad (2.35)$$

with  $G$  being the non-relativistic two-particle propagator, or two-particle Green's functions.

Solving Eq. (2.34) is usually technically hard as it involves a three-dimensional integral equation. There are, however, many situations, especially at low energies, where a converged partial wave expansion holds. For a generic function  $F$  of two vectors  $\mathbf{p}'$  and  $\mathbf{p}$ , the partial wave expansion [43]

$$F(\mathbf{p}', \mathbf{p}) = \sum_{\ell', m'} \sum_{\ell, m} (4\pi) Y_{\ell' m'}^*(\Omega_{p'}) Y_{\ell m}(\Omega_p) f_{\ell' m' \ell m}(p', p), \quad (2.36)$$

has the inverse relation

$$f_{\ell' m' \ell m}(p', p) = \frac{1}{4\pi} \int d\Omega_{p'} \int d\Omega_p Y_{\ell' m'}(\Omega_{p'}) Y_{\ell m}^*(\Omega_p) F(\mathbf{p}', \mathbf{p}). \quad (2.37)$$

Applying the above expansion to Eq. (2.34) yields

$$\begin{aligned}
t_{\ell' m' \ell m}(p', p) &= v_{\ell' m' \ell m}(p', p) + \frac{1}{4\pi} \int d\Omega_{p'} \int d\Omega_p Y_{\ell' m'}(\Omega_{p'}) Y_{\ell m}^*(\Omega_p) \\
&\int_0^\infty \frac{dq q^2}{(2\pi)^3} \frac{1}{E - q^2/2m + i\epsilon} \int \Omega_q \left[ \sum_{a', b'} \sum_{a, b} (4\pi) Y_{a' b'}^*(\Omega_{p'}) Y_{ab}(\Omega_q) v_{a' b' ab}(p', q) \right] \\
&\times \left[ \sum_{c', d'} \sum_{c, d} (4\pi) Y_{c' d'}^*(\Omega_q) Y_{cd}(\Omega_p) t_{c' d' cd}(q, p) \right], \quad (2.38)
\end{aligned}$$

with  $d\Omega = \sin\theta d\theta d\phi$ . The orthonormality condition,

$$\int d\Omega_p Y_{\ell' m'}^*(\Omega_p) Y_{\ell m}(\Omega_p) = \delta_{\ell' \ell} \delta_{m' m}, \quad (2.39)$$

allows one to rewrite Eq. (2.38) as

$$t_{\ell' m' \ell m}(p', p) = v_{\ell' m' \ell m}(p', p) + \sum_{c', d'} \int_0^\infty \frac{dq q^2}{2\pi^2} \frac{v_{\ell' m' c' d'}(p', q) t_{c' d' \ell m}(q, p)}{E - q^2/2m + i\epsilon}. \quad (2.40)$$

For simpler situations, for instance, central potentials or spinless particles, orbital angular momentum  $\ell$  is a good conserved quantum number, and the above equation simplifies to

$$t_\ell(p', p) = v_\ell(p', p) + \int_0^\infty \frac{dq q^2}{2\pi^2} \frac{v_\ell(p', q) t_\ell(q, p)}{E - q^2/2m + i\epsilon}, \quad (2.41)$$

which is the Lippmann-Schwinger equation for the  $\ell$ -th component of the scattering amplitude. In practical situations, one is interested in only a few specific partial waves, and for each, one needs to solve a much simpler one-dimensional integral equation.

# Chapter 3

## Effective Field Theories

Suppose a theory that could describe phenomena from all different energy scales, and name it as the most fundamental theory. This theory should be valid in any range of energy. But, in fact, one should not expect to solve the dynamics of this theory, since solving the fundamental theory in all energy scales might be impracticable, if not impossible. A situation similar to the underlying theory of the strong interactions, QCD. Instead of solving the dynamics for the most fundamental theory, one could be interested in reproducing the exact same physics as the fundamental one, but in a very specific range of validity. This defines what one calls an effective field theory (EFT). Only active and relevant degrees of freedom (effective fields) are necessary to describe this theory. The effective theory needs to include the symmetries of the underlying theory that are important in that specific range of energy. The interactions among effective fields are limited by the symmetries of a given system and in general, these interactions are organized by a set of rules called power counting, which assigns the scaling of the operators in the effective Lagrangian in terms of an expansion parameter. This expansion parameter is the ratio of the typical low-energy momentum within the validity of the EFT and the high-energy momentum that characterizes its breakdown. However, such expansion generates divergences, such ultraviolet divergences, that require special treatment.

Ultraviolet divergences is the technical expression given to certain infinities that appear in the formalism of quantum field theory (QFT). During the early days of formulation of QFT, such infinities were regarded as indication that QFT is ill-defined and incomplete. Perhaps the second point still holds, but concerning the first point, nowadays the origin of such infinities has a more robust physical interpretation. Basic quantum mechanics teaches us that quantum fluctuations, unless forbidden by certain symmetries, must be summed over all their possible states, more pragmatically, over all their energy/momentum eigenmodes. Ultraviolet divergences appear when such sum (i.e., integration) fails to converge towards the high-energy modes. From the uncertainty principle,

higher energy modes correspond to shorter distances. Thus the failure to achieve a convergent sum in the ultraviolet is, in general, due to a failure of the theory (and/or QFT itself) to provide a reliable description of arbitrarily short distance physics [44]. The predictability of QFT is rescued through the process of renormalization—unreliable short-distance physics that lead to ultraviolet divergences cannot be distinguishable from contact interactions among fields that constitute the coupling constants of the given theory, as long as one remains in its energy range of validity. Renormalization provides the mathematical prescription for assembling the ultraviolet divergences and the unknown, unreliable short-distance physics in the coupling constants in such a way that they precisely cancel each other, leaving only the physical value of these couplings.

The discussion above implies the existence of a momentum scale  $\Lambda$  that separates the physical quantum modes from the unreliable, ultraviolet divergent modes of a field theory. One of the most important, and physically robust studies of renormalization ideas is due to Kenneth Wilson [45, 46, 47]. Though his original study was addressed to critical phenomena in condensed-matter systems, the map of these ideas to QFT/particle physics can be naively established by the uncertainty principle relation between short-distances and high-energies. Translating to EFT (also to more general QFT, with appropriate adaptations), what Wilson proposed was to separate the original fields of the underlying theory based on the magnitudes of the respective momenta: high energy fields would be integrated out, leaving us with an EFT containing only the low energy fields. Wilson’s renormalization group method consists on identifying a momentum cutoff  $\Lambda$  that represents the highest energy scale of the system. For the sake of simplicity, consider a generic field  $\phi$  that can be decomposed into high- and low-momentum modes,  $\phi(k) = \phi_h(k) + \phi_l(k)$ . The definitions for the modes are

$$\phi_h(k) = \begin{cases} \phi(k) & \text{for } |k| > b\Lambda \\ 0 & \text{for } |k| \leq b\Lambda \end{cases} \quad (3.1)$$

$$\phi_l(k) = \begin{cases} 0 & \text{for } |k| > b\Lambda \\ \phi(k) & \text{for } |k| \leq b\Lambda \end{cases} \quad (3.2)$$

with  $b$  an adimensional parameter with value  $\lesssim 1$ . Renormalization group invariance imposes that observables do not depend on the value of  $b$ .

Once separated there are two different regimes involved: the soft ( $k < \Lambda$ ) and the hard physics ( $k > \Lambda$ ). The original interaction terms are Taylor-expanded in terms of the soft fields, giving rise to the so-called LECs (low-energy constants), the couplings that contain all the information one needs about the fundamental theory to calculate low-energy observables. Of course, from such expansion rises an infinite number of LECs. However,

an infinite number of couplings in a theory has no predictive power, therefore, the theory is useless unless there is a scheme to classify them according to their relative importance. Such a scheme is named “power counting” and, in practice, consists in organizing the LECs/operators according to their powers in the ratio  $Q/\Lambda$ , where  $Q$  stands for a typical low-momentum scale around which one is interested in working with the respective effective theory. In the lagrangian formalism, powers of  $Q$  are related to the number of derivative operators acting on the low-energy fields, the reason why this is also known as a derivative expansion. The power counting connects the order of the expansion and the number of terms one must keep in the effective Lagrangian. That leads to a finite number of constants up to a given order in  $Q/\Lambda$ . These constants can be determined from some experimental data or some model. Perhaps, one might be aware that there are no guarantee that for every system a proper power counting can be found [48]. As expected, increasing the power of  $Q/\Lambda$  improves the precision, but also increases the number of LECs to be determined from different physical observables.

After this brief introduction, one now focus the discussion on effective field theories applied to the strong (nuclear) force. Nowadays it is a consensus that the underlying theory of the strong interactions is quantum chromodynamics (QCD), a quantum field theory of quarks and gluons as elementary fields. Due to the aspect of confinement at low energies and asymptotic freedom at high energies, quark and gluon degrees of freedom can only be probed at the latter energy regime, but imprisoned within hadrons at the former. Therefore, for energies below the chiral scale ( $\Lambda_\chi \sim 4\pi\Lambda_{QCD} \sim 1 \text{ GeV}$ ) the only relevant degrees of freedom are the hadrons themselves (pions, nucleons, lambdas, etc.). As the EFT for the strong interactions must reproduce the QCD results in the appropriate low-energy domain, one must ensure that the effective Lagrangian incorporates all the relevant symmetries of the underlying theory. The first step, as mentioned before, is to identify the relevant degrees of freedom at the energy range of interest, namely, hadron fields generically represented by  $\psi$ . Then, construct the most general Lagrangian using the pertinent fields  $\psi$  constrained by the symmetries of QCD,

$$\mathcal{L} = \sum_i c_i(M_L, M_H, \Lambda)\mathcal{O}_i(\psi), \quad (3.3)$$

with  $M_L$  the typical EFT low-energy scale,  $M_H$  the EFT high-energy breakdown scale,  $\mathcal{O}_i(\psi)$  the effective operators involving fields at the same spacetime point, but with an arbitrary number of derivatives, and  $c_i(M_L, M_H, \Lambda)$  the LECs.

The first nuclear EFT was developed in the early 90’s and is best known as *Chiral Effective Field Theory*, or  $\chi$ EFT for short [49, 50, 51, 52], with typical momentum scale of the order of the pion mass. It was the first successful attempt to extend the ideas



of Chiral Perturbation Theory ( $\chi$ PT) [53, 54, 55] for two and more nucleon systems,  $A \geq 2$ . It is worth mentioning a fundamental difference between  $\chi$ PT and  $\chi$ EFT, namely, that in the former all interactions of the effective lagrangian are perturbative, while in the latter, due to the presence of a shallow bound state of two nucleons (the deuteron), non-perturbative physics takes place. Weinberg’s proposal [49, 50], pushed forward by van Kolck and collaborators [51, 52, 19] and other authors [20, 21, 22, 23, 24], was to apply the perturbative  $\chi$ PT rules to the effective potential, defined as all two-nucleon-irreducible Feynmann diagrams, and then iterate the potential in a dynamical equation like the Lippmann-Schwinger equation. This prescription is known in the literature as the Weinberg power counting (WPC).

However, a couple of years later, questions arouse regarding the consistency of the WPC. The main argument against WPC goes as follows: the one-pion exchange potential at leading order has an ultraviolet singularity due to its tensor force (in position space, this singularity is related to the  $-1/r^3$  behavior at the origin). Renormalization thus impose the existence of a two-nucleon contact interaction to absorb such divergences. The inconsistency appears in the scaling of these two terms of the potential—the one-pion exchange diagram scales as  $(Q/\Lambda)^0$  while the contact interaction, due to the presence of a shallow bound state, scales as  $(Q/\Lambda)^{-1}$ . From the EFT perspective, divergences at a certain order cancelled by operators from a different order do indicate an ill-defined power counting, and thus predictability of such EFT is put to question. This issue still remains controversial [58, 59, 60, 61], with intense discussions and interesting alternatives [58, 60, 62].

The first attempt to resolve the WPC inconsistencies were proposed by Kaplan, Savage, and Wise [58]. In the so-called KSW power counting, the leading order (LO) two-nucleon non-derivative contact interaction  $C_0$ <sup>1</sup> with scaling  $(Q/\Lambda)^{-1}$ , fine-tuned to reproduce the deuteron, is summed non-perturbatively to all orders, while pion exchanges and higher-derivative contact interactions are taken into account in perturbation theory. The KSW power counting restores, in principle, consistency of the nuclear EFT, at least formally. A shortcoming of KSW is that, with pions, the theory fails to converge in the energy domain where it is supposed to work,  $Q \sim m_\pi \sim 100\text{-}200$  MeV [63]. Nevertheless, the ideas seeded in the KSW work survived in a different type of EFT, named short-range EFT, EFT with contact interactions, or mostly well-known as pionless EFT ( $\not{\pi}$ EFT).

EFT with contact interactions is the more inclusive name for such type of EFT as it allows applications to a couple of distinct systems. It is named  $\not{\pi}$ EFT when applied to systems with only nucleons [64, 65, 74, 75], halo/cluster EFT for weakly-bound exotic

---

<sup>1</sup>In fact, due to the spin-isospin structure of two nucleons, there are two LO contact interactions,  $C_T$  and  $C_S$  for the tensor and spin-spin components, respectively.

nuclei [66, 67, 68],  $X$ EFT for heavy charmed exotic mesons [69, 70], and the generic EFT with contact interactions when applied to dilute ultracold atoms [39, 79, 78]. Even though with different names and, in principle, quite different quantum systems, the mentioned EFTs share the same lagrangian structure, symmetries, and at the two-body level it is equivalent to the Bethe's effective range expansion (ERE) theory [71]. These similarities among different systems constitute what is called universality of short-range interactions and lead to interesting phenomena like the Efimov effect (discussed below).

An intuitive way of understanding contact interactions can be grasped, for instance, in a top-down approach from a more microscopic  $\chi$ EFT to a lower resolution  $\not\chi$ EFT. In the path-integral formalism, operators that link two nucleons via pion exchanges are shrunk to two-nucleon contact interactions when pion fields are integrated out. This operation in practice can be seen in Fig. 3.1. Disregarding technical complications involving each nucleon operators in the lagrangian, the left-hand side of the figure is proportional to the pion propagator. However, when the energy and momentum of the exchanged pion are much smaller than its mass,  $q^2 \ll m_\pi^2$ , it is legitimate to Taylor-expand the propagator as

$$\frac{1}{q^2 - m_\pi^2} \approx -\frac{1}{m_\pi^2} \left[ 1 + \frac{q^2}{m_\pi^2} + \left( \frac{q^2}{m_\pi^2} \right)^2 + \dots \right], \quad (3.4)$$

which represents a series of two-nucleon contact interactions with zero, two, four, etc., derivatives. Such expansion is similar to the expansion of the  $W^\pm$  and  $Z^0$  gauge boson propagators in the full electroweak theory leading to the old Fermi contact effective theory for weak interactions. One can also work with expansions like these in SMEFT (Standard Model Effective Field Theory).

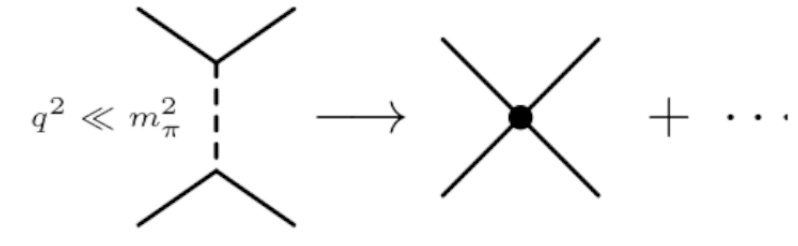


Figure 3.1: At very low-energies the interactions shrink to a point. Taken from reference [61].

The typical length scale that governs the quantum behavior is the de Broglie wavelength given by  $\lambda = 2\pi/p$ , with  $p$  being the momentum of the particle. But if the momentum  $p$  of each of the two particles is small enough, their de Broglie wavelengths are larger than the sizes of the particles themselves, which preclude them to resolve each other's internal structure.

The task at hand is to write an effective Lagrangian with contact interactions among nucleons and that respect their symmetries. These symmetries consist of, basically, invariance under small Lorentz boosts, rotations and isospin. There are also time reversal and parity, which are both discrete symmetries. It is also important to note that, as most of the nuclear EFTs, calculations are made in the non-relativistic limit, respecting Galilean invariance while relativistic corrections are accounted for at higher orders in the  $Q/m_N \sim Q/\Lambda$  expansion.

In general, the fundamental parameters of a given effective theory have a scaling driven by the high energy scale  $M_{hi}$  of the theory. In other words, the sizes of scattering parameters with length dimensions (such as the two-body scattering length  $a_2$  and the effective range  $r_2$ ) should scale with the range of the interaction  $R$ , which on the other hand scales with  $1/M_{hi}$  (from now on, the subindex 2 in  $a_2$  and  $r_2$  refers to the two-body system). In this scenario, the low-energy amplitudes reduce to a perturbative expansion in  $kR$ , with  $k$  being the low-energy momentum. In nuclear physics, the case of interest is different. The two-body scattering length  $a_2$  is much larger than the range of the two-body interaction ( $a_2 \gg R$  and  $R \sim r_2$ ). This is due to the fine-tuning of the interactions, leading to a two-body shallow bound state. It would be possible to keep a perturbative expansion of the amplitude in this case, as long as  $k \ll 1/a_2$ , but that would miss the important physics of shallow bound states. In order to keep an EFT with a perturbative expansion valid for all  $k \ll 1/R$ , it was shown [73, 58] that is enough to sum only two-body interactions that are momentum independent to all orders. Such infinite sum keeps the correct analytic dependence of the amplitude on the product  $ka_2$  while contact interactions with higher derivative operators are well accounted for in perturbation theory.

### 3.1 2-body sector

As a simpler example, let's consider a two-boson system interacting at very low energies with large scattering length. The Lagrangian for this system can be written, at leading order (LO), as [39]

$$\mathcal{L} = \psi^\dagger \left( i\partial_0 + \frac{\nabla^2}{2m} \right) \psi - \frac{g_2}{4} (\psi^\dagger \psi)^2, \quad (3.5)$$

with  $\psi$  the field representing each boson. The LEC  $g_2$  of this EFT ought to be determined by fitting to a LO low-energy observable, in this case, the scattering length  $a_2$ . To calculate the scattering amplitude  $\mathcal{A}$  in terms of the EFT parameters (in this example, only  $g_2$ ), and later be able to match with the observable  $a_2$ , one proceeds with the usual tools of QFT, namely, obtain the 4-point Green's function  $\langle 0 | T(\psi\psi\psi^\dagger\psi^\dagger) | 0 \rangle$  through Feynman diagrams. In general, the 4-point Green's function allows one to obtain the totally *off-shell*

amplitude, that is, each external leg associated with each field of the 4-point function does not necessarily obey the non-relativistic dispersion relation  $E = k^2/2m$ . In the center-of-mass (c.m.) frame, the amplitude depends on the (generally off-shell) incoming momenta  $\mathbf{k}$  and  $-\mathbf{k}$  and outgoing momenta  $\mathbf{p}$  and  $-\mathbf{p}$ , besides the total c.m. energy  $E$ . A half off-shell amplitude means that either one of the c.m. momenta  $\mathbf{k}$ ,  $\mathbf{p}$  obeys the on-shell condition. The on-shell amplitude, the only condition with physical significance, satisfies

$$T(k) = \mathcal{A}(k^2 = p^2 = 2mE). \quad (3.6)$$

This ought to be compared with Eqs. (2.20) and (2.24),

$$\begin{aligned} f_\ell(\theta) &= \frac{m}{4\pi} \mathcal{A}(E = k^2/2m), \\ a_2 &= -\frac{m}{4\pi} \mathcal{A}(0). \end{aligned} \quad (3.7)$$

(Reinforcing that the subindex 2 in  $a_2$  refers to the two-body subsystem.) The above relation allows one to relate the coupling  $g_2$  with the observable  $a_2$ . We now proceed with the calculation of the scattering amplitude  $\mathcal{A}$  using the Feynman rules for the processes depicted in Figure 3.2. In the figure, the first line is a graphical representation of the amplitude assuming a perturbative/iterative expansion from Feynman diagrams, while the second line is the same amplitude obtained via an integral equation. The latter is an alternative way of performing the infinite sum in the former.

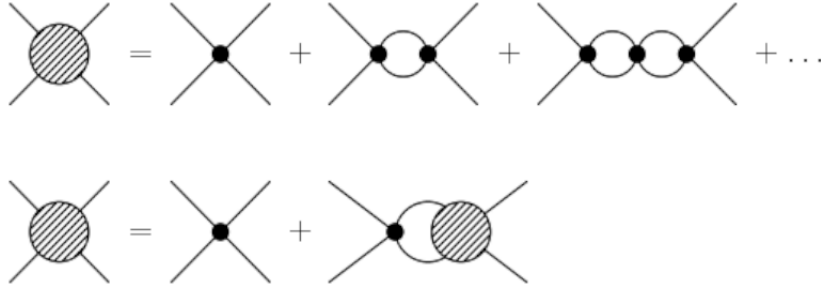


Figure 3.2: Scattering amplitude  $\mathcal{A}$  diagrammatically represented. Taken from reference [39].

Using the Feynman rules for the effective Lagrangian (3.5), one obtains the scattering

The image shows two Feynman diagrams. The top diagram is a horizontal line representing a propagator, with the equation  $= \frac{i}{E - k^2/2m + i\epsilon}$  to its right. The bottom diagram is a vertex correction, consisting of two lines crossing at a central black dot, with the equation  $= -ig_2$  to its right.

amplitude both in perturbative and integral equation forms,

$$\mathcal{A}(E) \approx -g_2 - ig_2^2 \int \frac{d^3q}{(2\pi)^3} \int \frac{dq_0}{2\pi} \frac{1}{E/2 - q_0 - q^2/2m + i\epsilon} \frac{1}{E/2 + q_0 - q^2/2m + i\epsilon} + \dots, \quad (3.8)$$

$$\mathcal{A}(E) = -g_2 - ig_2 \int \frac{d^3q}{(2\pi)^3} \int \frac{dq_0}{2\pi} \frac{1}{E/2 - q_0 - q^2/2m + i\epsilon} \frac{1}{E/2 + q_0 - q^2/2m + i\epsilon} \mathcal{A}(E). \quad (3.9)$$

Focusing on the one-loop integral in Eq. (3.8), the  $q_0$  integral can be evaluated using contour integration:

$$\begin{aligned} I_0 &= -i \int \frac{d^3q}{(2\pi)^3} \frac{(-2\pi i)}{2\pi} \frac{1}{E - q^2/m + i\epsilon}, \\ &= \int \frac{d^3q}{(2\pi)^3} \frac{m}{q^2 - mE - i\epsilon}, \\ &= \frac{1}{2\pi^2} \int_0^\infty dq q^2 \frac{m}{q^2 - mE - i\epsilon}. \end{aligned} \quad (3.10)$$

The integral  $I_0$  diverges, so it can be regularized by imposing a momentum cutoff  $\Lambda$

$$\begin{aligned} I_0 &= \frac{1}{2\pi^2} \int_0^\Lambda dq q^2 \frac{m}{q^2 - mE - i\epsilon}, \\ &= \frac{m}{2\pi^2} \left[ q - \sqrt{-mE - i\epsilon} \tan^{-1} \left( \frac{q}{\sqrt{-mE - i\epsilon}} \right) \right] \Big|_0^{\Lambda \rightarrow \infty}, \\ &\approx \frac{m}{2\pi^2} \left[ \Lambda - \sqrt{-mE - i\epsilon} \left( \frac{\pi}{2} - \frac{\sqrt{-mE - i\epsilon}}{\Lambda} \right) \right]. \end{aligned} \quad (3.11)$$

Taking the limit  $\Lambda \gg \sqrt{-mE - i\epsilon}$ , the amplitude to one loop can be expressed as

$$\mathcal{A}(E) \approx -g_2 + \frac{mg_2^2}{2\pi^2} \left( \Lambda - \frac{\pi}{2} \sqrt{-mE - i\epsilon} \right). \quad (3.12)$$

Applying the Feynman rules to the diagrams with two and more loops it is easy to notice that they can be written as multiples of the one loop integral  $I_0$ . The sum on the first line of Figure 3.2 is thus a geometric series, whose sum becomes

$$\begin{aligned}\mathcal{A}(E) &= -g_2 [1 + g_2 I_0]^{-1}, \\ &= -g_2 \left[ 1 + \frac{m g_2}{2\pi^2} \left( \Lambda - \frac{\pi}{2} \sqrt{-mE - i\epsilon} \right) \right]^{-1}.\end{aligned}\quad (3.13)$$

On the other hand, if one starts the calculation with the integral form (3.9), and the fact that under the integral the on-shell amplitude  $\mathcal{A}(E)$  does not depend on the integration variable, the remaining integral is precisely  $I_0$  already calculated. Thus,

$$\mathcal{A}(E) = -g_2 + \frac{m g_2}{2\pi^2} \left( \Lambda - \frac{\pi}{2} \sqrt{-mE - i\epsilon} \right) \mathcal{A}(E) \quad (3.14)$$

gives the same result as Eq. (3.13).

Renormalization can be implemented by eliminating the LEC  $g_2$  in favor of the scattering length  $a_2$ . We can use (3.7) to write

$$a_2 = \frac{m}{4\pi} g_2 \left( 1 + \frac{m\Lambda}{2\pi^2} g_2 \right)^{-1}. \quad (3.15)$$

Inverting the above relation to solve for  $g_2$ ,

$$\begin{aligned}g_2 &= \frac{4\pi}{m} a_2 \left( 1 - \frac{2a_2\Lambda}{\pi} \right)^{-1} \\ &= \frac{4\pi}{m} \frac{1}{1/a_2 - \frac{2\Lambda}{\pi}}.\end{aligned}\quad (3.16)$$

We write the nonperturbative on-shell amplitude eliminating  $g_2$  as

$$\mathcal{A}(E) = \frac{4\pi}{m} \frac{1}{-1/a_2 + \sqrt{-mE - i\epsilon}}. \quad (3.17)$$

The amplitude for the two-body system is independent of the momentum cutoff  $\Lambda$ , as one would, naively, expect. However, when dealing with effective field theories, observables may have a smooth dependence on the renormalization scale (in this case, the cutoff  $\Lambda$ ), which cannot happen if such dependence is logarithmic or positive powers with  $\Lambda$ . Thus, in EFT, a way to check if proper renormalization holds is to take the limit  $\Lambda \rightarrow \infty$  and to observe if the  $\Lambda$ -dependence of observables vanish as inverse powers of  $\Lambda$ .

In calculating the on-shell amplitude, one recovers the well-known expression for the scattering amplitude from quantum mechanics at LO (considering just the scattering

length  $a_2$ ) Eq (2.26)

$$f_0(\theta) = \frac{m}{4\pi} \mathcal{A}(E) = \frac{1}{-1/a_2 - ik}. \quad (3.18)$$

The on-shell amplitude  $\mathcal{A}(E)$  presents a pole at  $k = 1/a_2$  or, equivalently,  $E = -1/a_2^2$ . If  $a_2 > 0$  the pole gives rise to a bound-state, since in the complex momentum plane it is located on the positive imaginary axis. The other possibility,  $a_2 < 0$ , is located on the negative imaginary axis in the momentum plane, therefore, in the unphysical Riemann sheet. In the complex energy plane, this corresponds to a pole at  $E = e^{3\pi i}/a_2^2$ , which defines a virtual state.

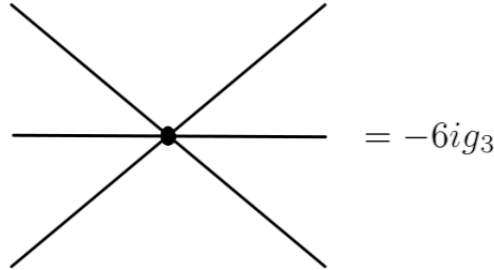
## 3.2 3-body sector

Now consider three bosons interacting at very low energies. The most general Lagrangian contains two- and three-body terms

$$\mathcal{L} = \psi^\dagger \left( i\partial_0 + \frac{\nabla^2}{2m} \right) \psi - \frac{g_2}{2} (\psi^\dagger \psi)^2 - \frac{g_3}{6} (\psi^\dagger \psi)^3, \quad (3.19)$$

with  $\psi$  the field representing each boson and  $g_2$  and  $g_3$  the two- and three-body LO low-energy constants.

The Feynman rule for the three-particle vertex reads



$$= -6ig_3$$

where the number 6 comes from the symmetry factor. The perturbative expansion in powers of  $g_2$  and  $g_3$  leads to a  $T$ -matrix that can be expanded in powers of the three-particle scattering energy  $E$ . There are several Feynman diagrams that contribute perturbatively to the three-body scattering, a few of them are illustrated in Figure 3.3. The three-body information about observables is encoded in the 6-point Green's function  $\langle 0 | T(\psi\psi\psi\psi^\dagger\psi^\dagger\psi^\dagger) | 0 \rangle$ .

### Dimer field

A convenient way of performing the three-body calculations is to introduce an auxiliary field with the appropriate quantum numbers of two particles, namely, a dimer field  $d$  [72].

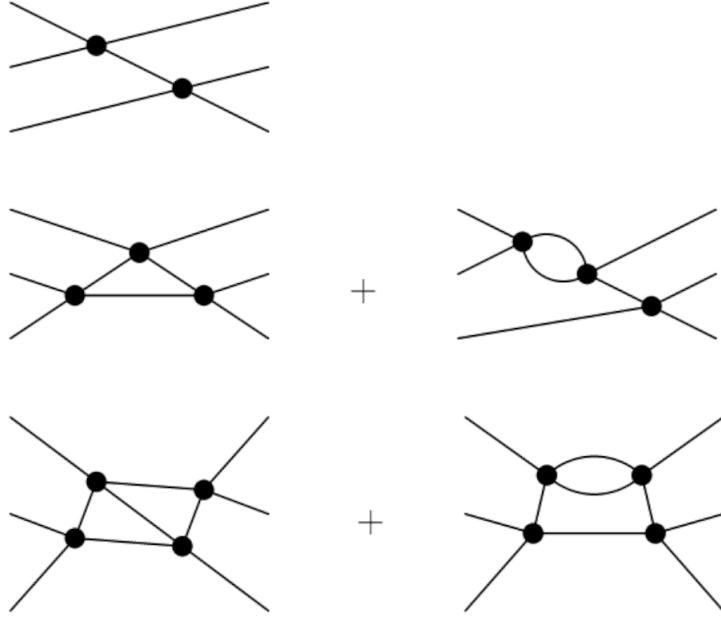


Figure 3.3: Diagrams that contributes to terms  $E^{-1}$ ,  $E^{-1/2}$  and  $\ln(E)$ . Taken from reference [39].

The mass of such field is  $2m + \Delta$ , where  $\Delta$  accounts for the two-particle binding energy. Essentially, the dimer replaces the two-body contact interaction by the  $s$ -channel ( $\ell = 0$ ) propagation of the bare dimer field. The two-body amplitude is completely determined by the full dimer propagator, which accounts for the propagation of the bare dimer dressed by two-particle loops. In the dimer formalism, the three-body interactions are replaced by dimer-particle interactions. Note that solving the 4-point (dimer-particle) Green's function  $\langle 0 | T(d\psi d^\dagger \psi^\dagger) | 0 \rangle$  is equivalent to solving the 6-point function  $\langle 0 | T(\psi\psi\psi\psi^\dagger\psi^\dagger\psi^\dagger) | 0 \rangle$ . The Lagrangian with the dimer field equivalent to (3.19) is given by

$$\mathcal{L} = \psi^\dagger \left( i\partial_0 + \frac{\nabla^2}{2m} \right) \psi + d^\dagger \left( i\partial_0 + \frac{\nabla^2}{4m} - \Delta \right) d - \frac{y}{\sqrt{2}} (d^\dagger \psi^2 + \psi^{\dagger 2} d) + h(d^\dagger d \psi^\dagger \psi). \quad (3.20)$$

The residual mass  $\Delta$ , with dimensions of mass, would naively scale as  $\Lambda$ , leading to a “natural” scattering length of size  $a_2 \sim 1/\Lambda$ . However, the case of unnaturally large scattering length  $a_2 \sim 1/Q$  enforces a fine tuning of this coupling to  $\Delta \sim Q$ , a suppression of order  $Q/\Lambda$ . One notices that, even with such suppression, the kinetic term of the dimer field,  $d^\dagger \left( i\partial_0 + \frac{\nabla^2}{4m} \right) d \sim \frac{Q^2}{\Lambda}$ , is of higher order compared to  $\Delta$ , and therefore, the bare dimer propagator is given by  $i\mathcal{D}_0 = -i/\Delta$ .

One can check the equivalence of the dimer field formalism and the original one with



only boson fields at the lagrangian level. If one solves the equation of motion for the  $d^\dagger$  field

$$d = \frac{y}{\Delta + h\psi^\dagger\psi}\psi^2, \quad (3.21)$$

and by substituting the field  $d$  on the Lagrangian, we write

$$\mathcal{L} = \psi^\dagger \left( i\partial_0 + \frac{\nabla^2}{2m} \right) \psi + \frac{y^2}{\Delta + h\psi^\dagger\psi} (\psi^\dagger\psi)^2. \quad (3.22)$$

Taylor-expanding the interaction term in powers of  $\psi^\dagger\psi$  we arrive at LO at the same Lagrangian as (3.19). We match the respective LECs as  $g_2 = y^2/\Delta$  and  $g_3 = -3y^2h/\Delta^2$ .

The Feynman rule for the bare dimer propagator is depicted in Figure 3.4.



Figure 3.4: The dimer bare propagator.

In order to obtain the full propagation, we need to dress the dimer propagator. We need to sum the bubble contribution as shown in Figure 3.5.

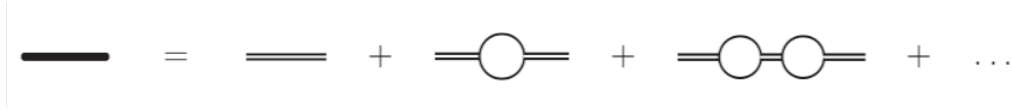


Figure 3.5: The dressed dimer propagator which is represented as an infinite sum of bubble diagrams. Taken from [39].

Using the usual Feynman rules, the expression for the dressed propagator, which forms a geometric series, is

$$\begin{aligned} \mathcal{D}(p_0; \mathbf{p}) &= \mathcal{D}_0 + \mathcal{D}_0 I_0 \mathcal{D}_0 + \mathcal{D}_0 I_0 \mathcal{D}_0 I_0 \mathcal{D}_0 + \dots, \\ &= \frac{\mathcal{D}_0}{1 - \mathcal{D}_0 I_0}, \\ &= \frac{1}{\mathcal{D}_0^{-1} - I_0}, \\ &= \frac{1}{-\Delta - I_0}. \end{aligned} \quad (3.23)$$

The integral  $I_0$  is the same as discussed in the previous section. We can absorb the divergent piece  $\Lambda$  into  $y^2/\Delta$  [74] and we can write the renormalized ratio  $y_{ren}^2/\Delta_{ren} = 4\pi a_2/m$ . The total energy is  $E = p_0 - p^2/4m$ . Thus, the expression for the full dimer

propagator is

$$i\mathcal{D}(p_0; \mathbf{p}) = \frac{i}{-\Delta + \frac{my^2}{4\pi} \sqrt{-mp_0 + p^2/4 - i\epsilon - i\epsilon}}. \quad (3.24)$$

The final expression for the renormalized dressed dimer propagator is

$$i\mathcal{D}(p_0; \mathbf{p}) = \frac{4\pi}{y^2 m} \frac{i}{-1/a_2 + \sqrt{\frac{p^2}{4} - mp_0 - i\epsilon - i\epsilon}}. \quad (3.25)$$

This dimer propagator has a pole at  $p_0 = -1/ma_2^2 + p^2/4m$ , which corresponds to a two-boson with binding energy  $E_d = 1/ma_2^2$ .

### 3.2.1 3-boson integral equation

Here we solve the three-boson spinless system in detail. The Feynman rules derived from Eq. (3.20) are illustrated in Figure 3.6. The integral equation can be diagrammatically represented by

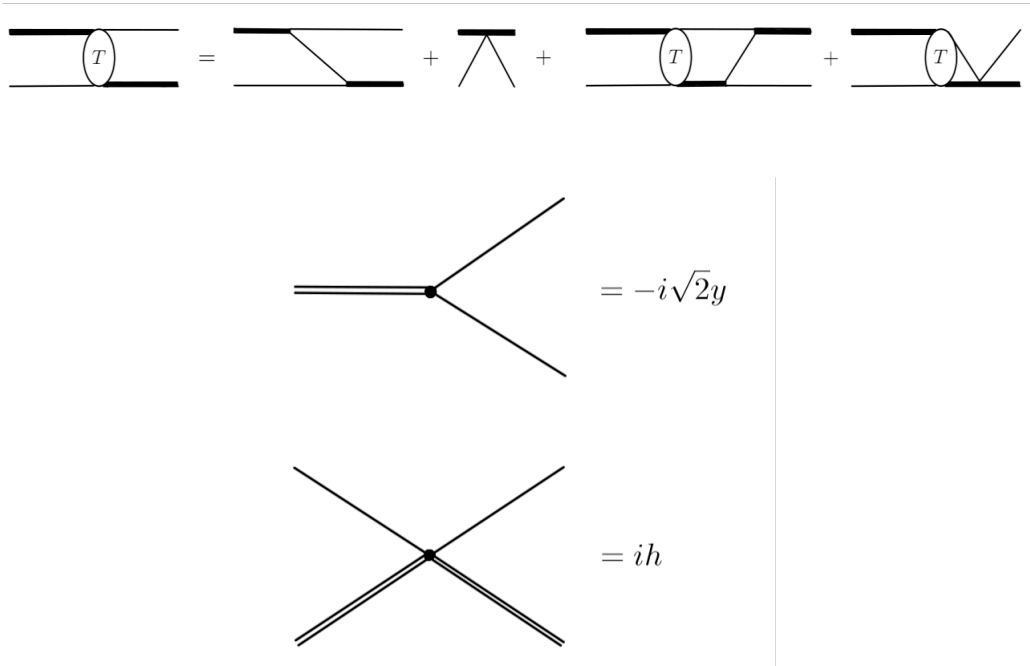


Figure 3.6: Feynman rules for the Lagrangian 3.20.

We set the kinematics as incoming 4-momenta on the energy shell  $(k^2/2m, -\mathbf{k})$  for the particle and  $(k^2/4m - B_d, \mathbf{k})$  for the dimer, and outgoing 4-momenta off-shell  $(k^2/2m - \varepsilon, -\mathbf{p})$  for the particle and  $(k^2/4m - B_d + \varepsilon, \mathbf{p})$  for the dimer. The on-shell point has  $\varepsilon = k^2/2m - p^2/2m$  and  $p = k$ . The total energy for the system is  $E = 3k^2/4m - B_d$

[74]. The integral equation from Figure 3.2.1 gives

$$\begin{aligned}
iT(\mathbf{p}, \mathbf{k}; \varepsilon) &= (-i\sqrt{2}y)^2 iS(-k^2/4m - B_d + \varepsilon; \mathbf{k} + \mathbf{p}) + ih \\
&+ \int \frac{d^4q}{(2\pi)^4} iS(k^2/2m - \varepsilon - q_0; \mathbf{q}) \left[ (-i\sqrt{2}y)^2 iS(-k^2/4m - B_d + 2\varepsilon + q_0; \mathbf{p} + \mathbf{q}) + ih \right] \\
&\quad \times i\mathcal{D}(k^2/4m - B_d + \varepsilon + q_0; \mathbf{q}) iT(\mathbf{q}, \mathbf{k}; \varepsilon + q_0), \tag{3.26}
\end{aligned}$$

resulting in

$$\begin{aligned}
T(\mathbf{p}, \mathbf{k}; \varepsilon) &= \frac{-2y^2}{-k^2/4m - B_d + \varepsilon - (\mathbf{k} + \mathbf{p})/2m + i\epsilon} + h \\
&\quad - i \int \frac{d^4q}{(2\pi)^4} \frac{1}{k^2/2m - \varepsilon - q_0 - q^2/2m + i\epsilon} \\
&\quad \times \left[ \frac{-2y^2}{-k^2/4m - B_d + 2\varepsilon + q_0 - (\mathbf{p} + \mathbf{q})/2m + i\epsilon} + h \right] \\
&\quad \times \frac{1}{-1/a_2 + \sqrt{q^2/4 - k^2/4 + mB_d - m\varepsilon - mq_0 - i\epsilon - i\epsilon}} T(\mathbf{q}, \mathbf{k}). \tag{3.27}
\end{aligned}$$

One solves the  $q_0$  integral by residues. One has  $q_0 = k^2/2m - \varepsilon - q^2/2m$  and, with the on-shell condition  $\varepsilon = k^2/2m - p^2/2m$ , the  $q_0$  integration gives (from now on, we assume  $T(\mathbf{p}, \mathbf{k}, k^2/2m - p^2/2m) = T(\mathbf{p}, \mathbf{k})$ )

$$\begin{aligned}
T(\mathbf{p}, \mathbf{k}) &= \frac{-2my^2}{-k^2/4 - mB_d - p^2 - \mathbf{k} \cdot \mathbf{p}} + h \\
&\quad - \int \frac{d^3q}{(2\pi)^3} \frac{1}{-1/a_2 + \sqrt{q^2/4 - mE}} \left[ \frac{-2my^2}{mE - q^2 - p^2 - \mathbf{p} \cdot \mathbf{q}} + h \right] T(\mathbf{q}, \mathbf{k}), \tag{3.28}
\end{aligned}$$

where omit the  $i\epsilon$  prescription to simplify the notation. Replacing  $y^2 = \frac{4\pi}{m}$  leads to

$$\begin{aligned}
T(\mathbf{p}, \mathbf{k}) &= \frac{2my^2}{k^2 + p^2 - mE + \mathbf{k} \cdot \mathbf{p}} + h \\
&+ 8\pi \int \frac{d^3q}{(2\pi)^3} \frac{1}{-1/a_2 + \sqrt{q^2/4 - mE}} \left[ \frac{1}{q^2 + p^2 - mE + \mathbf{p} \cdot \mathbf{q}} + \frac{h}{2my^2} \right] T(\mathbf{q}, \mathbf{k}) \\
&= 2my^2 B(\mathbf{p}, \mathbf{k}) + h + 8\pi \int \frac{d^3q}{(2\pi)^3} \left[ B(\mathbf{p}, \mathbf{q}) + \frac{h}{2my^2} \right] \mathcal{D}(E; \mathbf{q}) T(\mathbf{q}, \mathbf{k}). \tag{3.29}
\end{aligned}$$

We are interested in the three-body state with total angular momentum zero. One expands the above equation in partial waves and select  $\ell = 0$ . Note that the angular dependence is on the scalar product  $\mathbf{k} \cdot \mathbf{p} = |k||p| \cos \theta_{kp}$ . First we multiply both sides by

$\frac{1}{2} \int_{-1}^1 d(\cos \theta_{pk}) P_\ell(\cos \theta_{pk})$ , use the angular addition theorem

$$P_\ell(\cos \theta_{pk}) = \frac{4\pi}{2\ell + 1} \sum_{m=-\ell}^{\ell} Y_{\ell m}^*(\Omega_{pq}) Y_{\ell m}(\Omega_{qk}), \quad (3.30)$$

and also

$$P_\ell(\cos \theta) = \sqrt{\frac{4\pi}{2\ell + 1}} Y_{\ell 0}(\Omega). \quad (3.31)$$

From the partial wave expansion,

$$\begin{aligned} A(\mathbf{p}, \mathbf{k}) &= \sum_{\ell=0}^{\infty} (2\ell + 1) P_\ell(x) a_\ell(p, k) \\ \Rightarrow a_\ell(p, k) &= \frac{1}{2} \int_{-1}^1 dx P_\ell(x) A(\mathbf{p}, \mathbf{k}). \end{aligned} \quad (3.32)$$

Defining  $B(\mathbf{p}, \mathbf{k}) = (p^2 + k^2 - mE + pkx)^{-1}$  one arrives at [82]

$$\begin{aligned} b_\ell(p, k) &= \frac{1}{2} \int_{-1}^1 dx P_\ell(x) \frac{1}{p^2 + k^2 - mE + kpx}, \\ &= \frac{(-1)^\ell}{pk} Q_\ell \left( \frac{p^2 + k^2 - mE}{pk} \right). \end{aligned} \quad (3.33)$$

We choose the the  $z$ -axis along  $\mathbf{p}$ , thus only the  $m = 0$  projection contributes,

$$\begin{aligned} t_\ell(p, k) &= 2my^2 b_\ell(p, k) + h + \frac{1}{\pi^2} \frac{1}{2} \int_{-1}^1 d(\cos \theta_{pk}) P_\ell(\cos \theta_{pk}) \int_0^\infty dq q^2 \\ &\quad \times \int d\Omega_{pq} \sum_{\ell'=0}^{\infty} (2\ell' + 1) P_{\ell'}(\cos \theta_{pq}) \left[ b_{\ell'}(p, q) + \frac{h}{2my^2} \right] \mathcal{D}(E; q) \\ &\quad \times \sum_{\ell''=0}^{\infty} (2\ell'' + 1) P_{\ell''}(\cos \theta_{qk}) t_{\ell''}(q, k), \\ &= 2my^2 b_\ell(p, k) + h + \frac{1}{\pi^2} \frac{1}{2} \int_{-1}^1 d(\cos \theta_{pk}) P_\ell(\cos \theta_{pk}) \int_0^\infty dq q^2 \\ &\quad \times \int d\Omega_{pq} \sum_{\ell', \ell''=0}^{\infty} \sqrt{4\pi(2\ell' + 1)} Y_{\ell' 0}(\Omega_{pq}) \left[ b_{\ell'}(p, q) + \frac{h}{2my^2} \right] \mathcal{D}(E; q) \\ &\quad \times 4\pi \sum_{m=-\ell''}^{\ell''} Y_{\ell'' m}^*(\Omega_{pq}) Y_{\ell'' m}(\Omega_{pk}) t_{\ell''}(q, k). \end{aligned} \quad (3.34)$$

Since

$$\int d\Omega_{pq} Y_{\ell'0}(\Omega_{pq}) Y_{\ell'm}^*(\Omega_{pq}) = \delta_{\ell'\ell} \delta_{m0}, \quad (3.35)$$

we have

$$\begin{aligned} t_\ell(p, k) = & 2my^2 b_\ell(p, k) + h + \frac{1}{\pi^2} \int_{-1}^1 \overbrace{d(\cos \theta_{pk}) 2\pi P_\ell(\cos \theta_{pk})}^{=d\Omega_{pk}} \int_0^\infty dq q^2 \\ & \times \sum_{\ell'=0}^\infty \sqrt{4\pi(2\ell'+1)} \left[ b_{\ell'}(p, q) + \frac{h}{2my^2} \right] \mathcal{D}(E; q) Y_{\ell'0}(\Omega_{pk}) t_{\ell'}(q, k). \end{aligned} \quad (3.36)$$

When there is no dependence on the azimuthal angle  $\varphi \rightarrow m = 0$  and  $Y_{\ell 0}^* = Y_{\ell 0}$ . Using Eq. (3.31),

$$\int d\Omega_{pk} Y_{\ell 0}^*(\Omega_{pk}) Y_{\ell'0}(\Omega_{pk}) = \delta_{\ell\ell'}, \quad (3.37)$$

$$\begin{aligned} t_\ell(p, k) = & 2my^2 b_\ell(p, k) + h + \frac{1}{\pi^2} \int_0^\infty dq q^2 \sqrt{4\pi \frac{4\pi(2\ell'+1)}{2\ell+1}} \\ & \times \left[ b_{\ell'}(p, q) + \frac{h}{2my^2} \right] \mathcal{D}(E; q) \delta_{\ell\ell'} t_{\ell'}(q, k). \end{aligned} \quad (3.38)$$

Finally,

$$t_\ell(p, k) = 2my^2 b_\ell(p, k) + h + \frac{4}{\pi} \int_0^\Lambda dq q^2 \left[ b_\ell(p, q) + \frac{h}{2my^2} \right] \mathcal{D}(E; q) t_\ell(q, k). \quad (3.39)$$

we set the integration limited to a sharp cutoff  $\Lambda$  in order to regularize the integral. We are interested only in S-waves, then, we set  $\ell = 0$ , leading to [43]

$$Q_0(x) = \begin{cases} \frac{1}{2} \ln \frac{1+x}{1-x}, & -1 < x < 1, \\ \frac{1}{2} \ln \frac{x+1}{x-1}, & \text{outside this range.} \end{cases} \quad (3.40)$$

The Born term is written as

$$b_0(p, k) = \frac{1}{2pk} \ln \left( \frac{p^2 + k^2 - mE + pk}{p^2 + k^2 - mE - pk} \right). \quad (3.41)$$

The final expression for the three spinless bosons integral equation is given by

$$t_0(p, k) = \frac{my^2}{pk} \ln \left( \frac{p^2 + k^2 - mE + pk}{p^2 + k^2 - mE - pk} \right) + h + \frac{2}{\pi} \int_0^\Lambda dq q^2 \frac{1}{-1/a_2 + \sqrt{q^2/4 - mE}} \left[ \frac{1}{pq} \ln \left( \frac{p^2 + k^2 - mE + pk}{p^2 + k^2 - mE - pk} \right) + \frac{h}{my^2} \right] t_0(q, k). \quad (3.42)$$

This integral equation can be solved numerically by different methods. Methods used in this work are described in details in Appendix E.

### 3.2.2 Efimov Physics

A peculiar phenomenon arises when studying three-particle systems with large scattering length. This is called the Efimov effect and was first theoretically predicted by Vitaly Efimov in 1970 [76, 77]. Efimov studied three particles interacting via a short-range attractive potential that can almost or barely support a two-body bound state. A short-range interaction is characterised by decaying faster than  $1/r^3$ ,  $r$  being the interparticle distance [78]. Systems that present at least two of the three pairs with  $s$ -wave scattering length much larger than the range of the interaction ( $r_2$ ) show this effect [39, 79].

It was shown by Efimov that an effective long-range three-body attraction appears and it supports infinitely many three-body bound states, which are called Efimov states. Actually, these states are roughly geometrically spaced by a multiplicative factor  $e^{\pi/|s_0|}$ , where  $s_0$  depends on the statistics and the mass ratios of the particles. For the case of the 3-boson,  $s_0 = 1.00624$  and  $e^{\pi/|s_0|} \approx 22.7$ .

The formal explanation for the  $s_0$  value comes from solving the time independent three-body wave equation. We are not going to properly solve with all details, but using the hyper-spherical coordinates it is possible to write an equation for the hyper-radial functions  $F_n(R)$  (with  $R$  being the hyper-radius)

$$\left( -\frac{\partial^2}{\partial R^2} - \frac{1}{R} \frac{\partial}{\partial R} + \frac{s_n^2}{R^2} - k^2 \right) F_n(R) = 0, \quad (3.43)$$

with total energy  $E = k^2/m$ , leading to a one-dimensional Schrödinger equation for the hyper-radial potential  $V_n(R) = \frac{s_n^2 - 1/4}{R^2}$ ,

$$\left( -\frac{\partial^2}{\partial R^2} + V_n(R) - k^2 \right) \sqrt{R} F_n(R) = 0. \quad (3.44)$$

There is only one solution for  $s_n$  in equation (3.44) that is not real, that is, for  $n = 0$ . It

is purely imaginary and assumes the value  $s_0 \approx \pm 1.00624i$ . The corresponding potential is attractive. Any other value of  $n$  leads to a repulsive potential. This non-intuitive result for the  $s$ -channel ( $n = 0$ ) is called *Efimov attraction*.

The multiplicative factor  $\lambda_0 = e^{\pi/|s_0|} \approx 22.7$  is the one that makes the solution of (3.43) invariant,  $R \rightarrow \lambda_0^n R$ . This is called the *discrete scale invariance*. Then, if there is a solution for  $E < 0$ , there is also  $n$ -solutions for  $E/\lambda_0^{2n} < 0$  and the scaling factor is  $\lambda_0^2 \approx 515$ . This discrete scale invariance is shown on Figure 3.7, the so-called "Efimov plot".

The three-body bound states actually present some universal features that were also studied by Vitaly Efimov [80]. These universal properties are insensitive to the details of the two-body interaction that occurs in short distances. One of the universal properties is that the ratio between successive bound states are fixed

$$B_3^{(n+1)} / B_3^{(n)} \longrightarrow e^{-2\pi/|s_0|} \quad \text{as } n \rightarrow \infty \quad \text{for } a_2 = \pm\infty. \quad (3.45)$$

For instance, for three bosons this universal number is approximately 1/515.

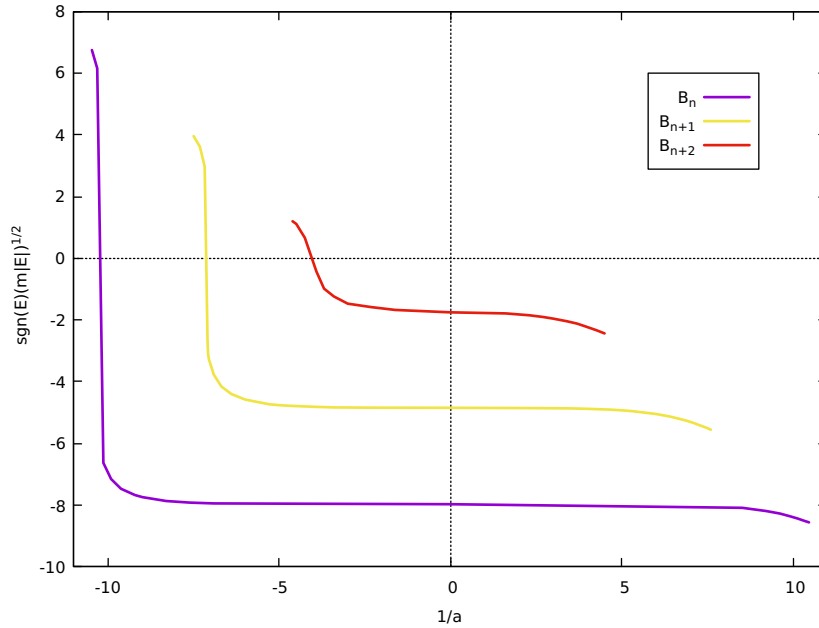


Figure 3.7: The Efimov plot showing the discrete scale invariance for the three-boson system.

In Figure 3.7 we show the spectrum of the Efimov states. The  $x$ -axis shows the inverse of the two-body scattering length  $a_2$  and the  $y$ -axis is the  $\text{sgn}(E)\sqrt{m|E|}$ . All three-body bound states show the same trajectory up to a universal scaling factor,  $\lambda \approx 22.7$ . The limit where  $1/a_2 \rightarrow 0$  (or  $a_2 \rightarrow \pm\infty$ ) is called the unitary limit or unitarity and is related to the unitarity of the  $S$ -matrix as described in Chapter 2. Near the unitary limit, the scattering

length  $a_2$  is the only parameter that governs the two-body physics. Although the Efimov states are defined only at the unitarity, where the discrete symmetry scale is exact, one can notice that the plot has an approximate symmetry for  $1/a_2 > 0$  and  $1/a_2 < 0$ . The whole spectrum shows the so-called Efimov physics. One can parcel out the spectrum into regions that have some important physical meaning. In the lower right region of the plot, going to the right (increasing  $1/a_2$ ) one notices that each curve ends at points forming a straight line with inclination of  $45^\circ$ . Physically that means that the three-body energy reaches its continuum threshold and turns into a two-body bound state and a boson. In other words, when  $1/a_2 > 0$  there is a true two-boson bound state plus a bound third boson, forming a three-body bound state—this state is sometimes called an all-bound three-body state. And as long as the curve reaches the threshold, the two-body (dimer) system remains bounded but the third boson unbinds, going to the continuum (boson-dimer scattering states). Regarding the left region of the figure, when  $1/a_2 < 0$ , there is not a true two-body bound state, but a virtual two-body state which binds to the third boson. This state is called a borromean state. As one moves towards the left (increases  $1/|a_2|$ ) the curves cross the  $y = 0$  axis and go to the continuum states, *i.e.*, states with energy  $\text{Re}[E] > 0$ . These states correspond to resonances and we can capture the physics of the resonances for the three-boson system in the Efimov plot by adapting our bound state codes. For bound states, we numerically solve a homogeneous version of Eq. (3.42), written as

$$t_0(p, k) = \frac{2}{\pi} \int_0^\Lambda dq q^2 \frac{1}{-1/a + \sqrt{q^2/4 - mE}} \times \left[ \frac{1}{pq} \ln \left( \frac{p^2 + k^2 - mE + pk}{p^2 + k^2 - mE - pk} \right) + \frac{h}{my^2} \right] t_0(q, k). \quad (3.46)$$

The true three-body bound state solutions, with  $E < b_2$  (with  $b_2$  the two-body bound state energy), result in a kernel that is purely real. The homogeneous equation can be expressed as a simple equation of the form  $(\mathbb{I} - \mathbb{K})t_0 = 0$  and search for the zeroes of the determinant of  $(\mathbb{I} - \mathbb{K})$ , where  $\mathbb{I}$  is the identity matrix. When searching for resonances, we also need to solve Eq. (3.46), however the code needs to be adapted as the kernel of the integral equation assumes complex values. Differently from the bound state code, where the search is on the real axis, resonances require a two-dimensional search, as we need to determine both real and imaginary parts. The details of the search algorithm can be seen in Appendix (E). It is also important to stress that it is not our intention to reproduce any particular physical system when describing the three-boson system. All values are fictitious, our aim is just to illustrate the Efimov physics.



### 3.3 A more realistic case: $nd$ system

The reason for studying the  $nd$  system is guided by the fact that working with fermions demand the introduction of the formalism of spin and isospin. This leads to the study of the projectors, which will be used when describing the  $\Lambda nn$  system. It was also important to check our codes for coupled integral equations and the  $nd$  system has vast results in the literature [56, 81]. The neutron-deuteron system consists of a neutron interacting with a neutron-proton pair, this pair forms a bound-state called deuteron. There are two possible S-wave channels for the  $nd$  system. Namely, the quartet channel  ${}^3S_1$  (in the spectroscopic notation  ${}^{2S+1}L_J$ ) ( $S = 3/2$ ), in which the spins of the three nucleons are aligned, and the doublet channel  ${}^1S_0$  ( $S = 1/2$ ), that is more complicated because the interaction might occur in either  ${}^3S_1$  and  ${}^1S_0$  waves, leading to a bound-state, the triton. As the latter channel is a coupled-channel, we need to solve a coupled integral equation [81]. The Lagrangian that describes the system is

$$\mathcal{L} = \mathcal{L}_0 + \mathcal{L}_I + \mathcal{L}_{3B}. \quad (3.47)$$

The first piece is the kinematic term, we need to add another dimer field describing both spin-singlet (dineutron) and -triplet (deuteron) channels. Note that, we use the convention greek letters stand for spin indices and roman letters for isospin. Then,

$$\mathcal{L}_0 = N^\dagger \left( i\partial_0 + \frac{\nabla^2}{2m_N} \right) N + s_j^\dagger \left( i\partial_0 + \frac{\nabla^2}{4m_N} - \Delta_s \right) s_j + t_\alpha^\dagger \left( i\partial_0 + \frac{\nabla^2}{4m_N} - \Delta_t \right) t_\alpha. \quad (3.48)$$

The second piece is the interaction term, that gives rise for the vertices. Here appears a object called projector  $\mathcal{P}$ , that will be derived in the next subsection. It is given by

$$\mathcal{L}_I = -g_s \left[ s_j^\dagger (N^T \mathcal{P}_s^j N) + \text{H.c.} \right] - g_t \left[ t_\alpha^\dagger (N^T \mathcal{P}_t^\alpha N) + \text{H.c.} \right]. \quad (3.49)$$

The third piece is about the three-body force term

$$\mathcal{L}_{3B} = \phi^\dagger \left[ \Omega - \sum_{\ell=1}^{\infty} h_{2\ell} \left( i\partial_0 + \frac{\nabla^2}{6m_N} + \frac{\gamma_t^2}{m_N} \right)^\ell \right] \phi - \frac{g_3}{\sqrt{3}} \{ \phi^\dagger [ (\sigma^\alpha N) t_\alpha - (\tau^j N) s_j ] + \text{H.c.} \}. \quad (3.50)$$

with  $\phi$  representing a trimer field. The trimer is similar to the dimer, but instead of being a mathematical trick representing two fields, it represents three fields, in this case, it has the quantum numbers of the triton. The trimer propagator is proportional to  $1/\Omega$ . One can write the Lagrangian using only dimers by a Gaussian integration. The reason we chose to write in this manner is to simplify the contractions.

### 3.3.1 Projectors

Since we are dealing with nucleons, spin (and also isospin) plays an important role. The way we account the spin contribution is adding a projector, that relates a channel with spin A into a channel with spin B. Of course, we will also need to add the spin of the two-particle system with the another particle spin, which will be given in the next section.

Nucleons can be understood as a doublet of isospin. The proton represents the "up" projection of the third component of the isospin  $I_3 = +1/2$  and the neutron represents the "down" projections,  $I_3 = -1/2$ . Both proton and neutron have spin-1/2. We can represent the nucleon as a vector

$$N = \begin{pmatrix} p \\ n \end{pmatrix}. \quad (3.51)$$

In the isospin space, we write

$$\text{proton} = \begin{pmatrix} 1 \\ 0 \end{pmatrix}, \quad \text{neutron} = \begin{pmatrix} 0 \\ 1 \end{pmatrix}. \quad (3.52)$$

In the same way, in the spin space, we represent

$$|\uparrow\rangle = \begin{pmatrix} 1 \\ 0 \end{pmatrix}, \quad |\downarrow\rangle = \begin{pmatrix} 0 \\ 1 \end{pmatrix}. \quad (3.53)$$

### Two-nucleon

Although we will start by deriving the expressions for the projectors using the spin space, there is no differences when working in the isospin space. The addition of two nucleons is the addition of two particles with spin-1/2. This results in a triplet and a singlet. Using  $|\uparrow\rangle$  as the positive projection of the third component of the spin  $m = +1/2$  and  $|\downarrow\rangle$  as the negative projection,  $m = -1/2$ , we write all possible spin combinations as  $|\uparrow\uparrow\rangle, |\uparrow\downarrow\rangle, |\downarrow\uparrow\rangle, |\downarrow\downarrow\rangle$ .

They sum up to spin-1 in three different combinations (normalized)

$$\text{Triplet} \quad \begin{cases} |\uparrow\uparrow\rangle, \\ \frac{1}{\sqrt{2}} [|\uparrow\downarrow\rangle + |\downarrow\uparrow\rangle], \\ |\downarrow\downarrow\rangle. \end{cases} \quad (3.54)$$

And only one combination gives spin-0

$$\text{Singlet} \quad \left\{ \frac{1}{\sqrt{2}} [|\uparrow\downarrow\rangle - |\downarrow\uparrow\rangle] \right\}. \quad (3.55)$$

Let us introduce the same states written in matrix form

$$|\uparrow\uparrow\rangle = (\uparrow, \downarrow) \begin{pmatrix} 1 & 0 \\ 0 & 0 \end{pmatrix} \begin{pmatrix} \uparrow \\ \downarrow \end{pmatrix}, \quad (3.56)$$

$$\frac{1}{\sqrt{2}} [|\uparrow\downarrow\rangle + |\downarrow\uparrow\rangle] = \frac{1}{\sqrt{2}} (\uparrow, \downarrow) \begin{pmatrix} 0 & 1 \\ 1 & 0 \end{pmatrix} \begin{pmatrix} \uparrow \\ \downarrow \end{pmatrix},$$

$$\frac{1}{\sqrt{2}} [|\uparrow\downarrow\rangle - |\downarrow\uparrow\rangle] = \frac{1}{\sqrt{2}} (\uparrow, \downarrow) \begin{pmatrix} 0 & 1 \\ -1 & 0 \end{pmatrix} \begin{pmatrix} \uparrow \\ \downarrow \end{pmatrix},$$

$$|\downarrow\downarrow\rangle = (\uparrow, \downarrow) \begin{pmatrix} 0 & 0 \\ 0 & 1 \end{pmatrix} \begin{pmatrix} \uparrow \\ \downarrow \end{pmatrix}. \quad (3.57)$$

Writing in matrix form explicit the intrinsic nature of a projector. These four matrices are projectors  $\mathcal{P}$  that project two-nucleon states ( $N^T \mathcal{P} N$ ) into spin-triplet and spin-singlet channels. Now, if we use the Pauli matrices

$$\sigma_1 = \begin{pmatrix} 0 & 1 \\ 1 & 0 \end{pmatrix}, \quad \sigma_2 = \begin{pmatrix} 0 & -i \\ i & 0 \end{pmatrix}, \quad \sigma_3 = \begin{pmatrix} 1 & 0 \\ 0 & -1 \end{pmatrix}, \quad \sigma_0 = \begin{pmatrix} 1 & 0 \\ 0 & 1 \end{pmatrix}, \quad (3.58)$$

to write the projectors and call them by  $T^{(m)}$  for triplet and  $S^{(0)}$  for singlet

$$T^{(+1)} = \begin{pmatrix} 1 & 0 \\ 0 & 0 \end{pmatrix} = \frac{1}{2}(\sigma_0 + \sigma_3), \quad T^{(-1)} = \begin{pmatrix} 0 & 0 \\ 0 & 1 \end{pmatrix} = \frac{1}{2}(\sigma_0 - \sigma_3), \quad (3.59)$$

$$T^{(0)} = \frac{1}{\sqrt{2}} \begin{pmatrix} 0 & 1 \\ 1 & 0 \end{pmatrix} = \frac{1}{\sqrt{2}}\sigma_1, \quad S^{(0)} = \frac{1}{\sqrt{2}} \begin{pmatrix} 0 & 1 \\ -1 & 0 \end{pmatrix} = \frac{i}{\sqrt{2}}\sigma_2. \quad (3.60)$$

Then, we can identify  $T^{(0)}$  as the third spin-component  $T^{(3)}$  in the Cartesian representation. Naturally, the third spin-component is proportional to  $\sigma_3$ , then using  $\sigma_i \sigma_j = \delta_{ij} \sigma_0 + i \varepsilon_{ijk} \sigma_k$

$$T^{(0)} = T^{(3)} = -\frac{i}{\sqrt{2}} \sigma_2 \sigma_3. \quad (3.61)$$

With the same prefactor the other components become

$$T^{(+1)} = -\frac{i}{\sqrt{2}}\sigma_2\frac{1}{\sqrt{2}}(i\sigma_2 - \sigma_1), \quad T^{(-1)} = -\frac{i}{\sqrt{2}}\sigma_2\frac{1}{\sqrt{2}}(i\sigma_2 + \sigma_1). \quad (3.62)$$

Defining the Cartesian components as

$$T^{(j)} = -\frac{i}{\sqrt{2}}\sigma_2\sigma_j. \quad (3.63)$$

In terms of them, we write

$$T^{(+1)} = \frac{1}{\sqrt{2}}(iT^{(2)} - T^{(1)}), \quad T^{(0)} = T^{(3)}, \quad T^{(-1)} = \frac{1}{\sqrt{2}}(iT^{(2)} + T^{(1)}). \quad (3.64)$$

The generalisation is straightforward to derive in the isospin space. Analysing the neutron-deuteron system, a spin-triplet ( $S = 1$ ) must be a isospin-singlet ( $I = 0$ ), while a spin-singlet ( $S = 0$ ) must be a isospin-triplet ( $I = 1$ ). The projectors are the direct products  $|S = 1\rangle \otimes |I = 0\rangle$  and  $|S = 0\rangle \otimes |I = 1\rangle$ . These information lead to the final expression for the projectors, denoting by  $\tau$  the same Pauli matrices but in the isospin space

$$\mathcal{P}_t^\alpha = \frac{1}{2}\tau_2\sigma_2\sigma^\alpha, \quad \mathcal{P}_s^i = \frac{1}{2}\sigma_2\tau_2\tau^i. \quad (3.65)$$

with  $\mathcal{P}_t^\alpha$  projecting into a spin-triplet (isospin-singlet) channel and  $\mathcal{P}_s^i$  into spin-singlet (isospin-triplet) channel. In the literature, one can find a  $1/\sqrt{8}$  factor in the definition of the the projector instead of the  $1/2$ . This comes from absorbing the  $1/\sqrt{2}$  from the coupling from the Lagrangian density, as in Eq. (3.49).

## Three-nucleon

Our task is to include another nucleon, in order to properly account the third particle in the system. First, we might note that there are three possible spin-states emerging from the three-nucleon system: (i) two nucleons in the singlet channel ( $j_1 = 0$ ) combining with another one ( $j_2 = 1/2$ ) to form a spin-doublet channel ( $J = 1/2$ ); (ii) two nucleons in the triplet channel ( $j_1 = 1$ ) combined with another nucleon ( $j_2 = 1/2$ ) forming a spin-doublet ( $J = 1/2$ ) and the last one (iii) two nucleons on the triplet channel combining with another one forming a spin-quartet ( $J = 3/2$ ).

For the addition of two particles, we write

$$|JM\rangle = |j_1m_1, j_2m_2\rangle. \quad (3.66)$$

Then, our previous notation now reads

$$|11\rangle = |\uparrow\uparrow\rangle = \left| \frac{11}{22}, \frac{11}{22} \right\rangle, \quad (3.67)$$

$$|10\rangle = \frac{1}{\sqrt{2}} [|\uparrow\downarrow\rangle + |\downarrow\uparrow\rangle] = \frac{1}{\sqrt{2}} \left[ \left| \frac{11}{22}, \frac{1}{2} \left( -\frac{1}{2} \right) \right\rangle + \left| \frac{1}{2} \left( -\frac{1}{2} \right), \frac{11}{22} \right\rangle \right],$$

$$|1(-1)\rangle = |\downarrow\downarrow\rangle = \left| \frac{1}{2} \left( -\frac{1}{2} \right), \frac{1}{2} \left( -\frac{1}{2} \right) \right\rangle,$$

$$|00\rangle = \frac{1}{\sqrt{2}} [|\uparrow\downarrow\rangle - |\downarrow\uparrow\rangle] = \frac{1}{\sqrt{2}} \left[ \left| \frac{11}{22}, \frac{1}{2} \left( -\frac{1}{2} \right) \right\rangle - \left| \frac{1}{2} \left( -\frac{1}{2} \right), \frac{11}{22} \right\rangle \right].$$

Adding the third particle according to the notation

$$|j_1, j_2; JM\rangle = C_{j_1 m_1, j_2 m_2}^{JM} |j_1 m_1, j_2 m_2\rangle. \quad (3.68)$$

with  $C_{j_1 m_1, j_2 m_2}^{JM}$  the Clebsch-Gordan coefficients.

The possible three-particle states are, then, given by

$$\begin{aligned} \text{Quartet} \quad & \left\{ \begin{aligned} \left| 1\frac{1}{2}; \frac{3}{2}, \frac{3}{2} \right\rangle &= \left| 11, \frac{11}{22} \right\rangle, \\ \left| 1\frac{1}{2}; \frac{3}{2}, \frac{1}{2} \right\rangle &= \sqrt{\frac{2}{3}} \left| 10, \frac{11}{22} \right\rangle + \sqrt{\frac{1}{3}} \left| 11, \frac{1}{2} \left( -\frac{1}{2} \right) \right\rangle, \\ \left| 1\frac{1}{2}; \frac{3}{2}, \left( -\frac{1}{2} \right) \right\rangle &= \sqrt{\frac{1}{3}} \left| 1(-1), \frac{11}{22} \right\rangle + \sqrt{\frac{2}{3}} \left| 10, \frac{1}{2} \left( -\frac{1}{2} \right) \right\rangle, \\ \left| 1\frac{1}{2}; \frac{3}{2}, \left( -\frac{3}{2} \right) \right\rangle &= \left| 1(-1), \frac{1}{2} \left( -\frac{1}{2} \right) \right\rangle. \end{aligned} \right. \end{aligned} \quad (3.69)$$

$$\begin{aligned} \text{Doublet} \quad & \left\{ \begin{aligned} \left| 1\frac{1}{2}; \frac{1}{2}, \frac{1}{2} \right\rangle &= \sqrt{\frac{1}{3}} \left| 10, \frac{11}{22} \right\rangle - \sqrt{\frac{2}{3}} \left| 11, \frac{1}{2} \left( -\frac{1}{2} \right) \right\rangle, \\ \left| 1\frac{1}{2}; \frac{1}{2}, \left( -\frac{1}{2} \right) \right\rangle &= \sqrt{\frac{2}{3}} \left| 1(-1), \frac{11}{22} \right\rangle - \sqrt{\frac{1}{3}} \left| 10, \frac{1}{2} \left( -\frac{1}{2} \right) \right\rangle. \end{aligned} \right. \end{aligned} \quad (3.70)$$

$$\text{Doublet} \quad \begin{cases} \left| 0\frac{1}{2}, \frac{11}{22} \right\rangle = \left| 00, \frac{11}{22} \right\rangle, \\ \left| 0\frac{1}{2}, \frac{1}{2} \left( -\frac{1}{2} \right) \right\rangle = \left| 00, \frac{1}{2} \left( -\frac{1}{2} \right) \right\rangle. \end{cases} \quad (3.71)$$

To write the expressions for the projectors for the doublet and quartet channels one needs to know what matrices relates a two-nucleon state and a nucleon to a three-nucleon state. For the doublets, we write

$$\begin{pmatrix} d_+ \\ d_- \end{pmatrix} = \sum_j [N^T \mathcal{P}^j N] F^{(j)} \begin{pmatrix} n_+ \\ n_- \end{pmatrix} = \sum_j [N^T \mathcal{P}^j N] \begin{pmatrix} f_{11}^{(j)} & f_{12}^{(j)} \\ f_{21}^{(j)} & f_{22}^{(j)} \end{pmatrix} \begin{pmatrix} n_+ \\ n_- \end{pmatrix}. \quad (3.72)$$

For the quartet

$$\begin{pmatrix} q_{++} \\ q_+ \\ q_- \\ q_{--} \end{pmatrix} = \sum_j [N^T \mathcal{P}^j N] G^{(j)} \begin{pmatrix} n_+ \\ n_- \end{pmatrix} = \sum_j [N^T \mathcal{P}^j N] \begin{pmatrix} g_{11}^{(j)} & g_{12}^{(j)} \\ g_{21}^{(j)} & g_{22}^{(j)} \\ g_{31}^{(j)} & g_{32}^{(j)} \\ g_{41}^{(j)} & g_{42}^{(j)} \end{pmatrix} \begin{pmatrix} n_+ \\ n_- \end{pmatrix}. \quad (3.73)$$

Here  $F^{(j)}$  and  $G^{(j)}$  are transition matrices that relates a two-nucleon state with Cartesian component  $j$  and a third nucleon with spin components  $n_+$ (up) and  $n_-$  (down). The components of both matrices can be determined by the Clebsch-Gordan coefficients [83]. In order to follow Griebhammer's notation [82], we use the same sign convention. Using the three-particle states as written above, we start by considering: (i) two nucleons in the singlet channel combined with another nucleon to form a spin-doublet channel ( $J = 1/2$ ).

The projector for this channel is simply  $\mathcal{P}^j = S^{(0)}$ , then

$$\begin{aligned} d_+ &= \left| 00, \frac{11}{22} \right\rangle n_+, \\ d_- &= \left| 00, \frac{1}{2} \left( -\frac{1}{2} \right) \right\rangle n_-. \end{aligned} \quad (3.74)$$

$$\begin{aligned} d_+ &= N^T S^{(0)} N n_+, \\ d_- &= N^T S^{(0)} N n_-. \end{aligned} \quad (3.75)$$

Leading to

$$F^{(0)} = \begin{pmatrix} 1 & 0 \\ 0 & 1 \end{pmatrix}. \quad (3.76)$$

The next case is: (ii) two nucleons in the triplet channel combined with another nu-

cleon forming a spin-doublet

$$\begin{aligned}
d_+ &= \sqrt{\frac{1}{3}} \left| 10, \frac{1}{2} \frac{1}{2} \right\rangle n_+ - \sqrt{\frac{2}{3}} \left| 11, \frac{1}{2} \left( -\frac{1}{2} \right) \right\rangle n_-, \\
d_- &= \sqrt{\frac{2}{3}} \left| 1(-1), \frac{1}{2} \frac{1}{2} \right\rangle n_+ - \sqrt{\frac{1}{3}} \left| 10, \frac{1}{2} \left( -\frac{1}{2} \right) \right\rangle n_-.
\end{aligned} \tag{3.77}$$

By knowing the spin projection, we can match with the two-nucleon projectors that have been derived above and write

$$\begin{aligned}
d_+ &= \sqrt{\frac{1}{3}} (N^T T^{(0)} N) n_+ - \sqrt{\frac{2}{3}} (N^T T^{(+1)} N) n_-, \\
d_- &= \sqrt{\frac{2}{3}} (N^T T^{(-1)} N) n_+ - \sqrt{\frac{1}{3}} (N^T T^{(0)} N) n_-.
\end{aligned} \tag{3.78}$$

As the  $F^{(j)}$  matrices relates the Cartesian component  $j$ , we need to use Eq. (3.64) to write

$$\begin{aligned}
d_+ &= \sqrt{\frac{1}{3}} (N^T T^{(3)} N) n_+ - \sqrt{\frac{1}{3}} [N^T (iT^{(2)} - T^{(1)}) N] n_-, \\
d_- &= \sqrt{\frac{1}{3}} [N^T (iT^{(2)} + T^{(1)}) N] n_+ - \sqrt{\frac{1}{3}} (N^T T^{(3)} N) n_-.
\end{aligned} \tag{3.79}$$

Leading to

$$F^{(1)} = \frac{1}{\sqrt{3}} \begin{pmatrix} 0 & 1 \\ 1 & 0 \end{pmatrix} = \frac{\sigma_1}{\sqrt{3}}, \quad F^{(2)} = \frac{1}{\sqrt{3}} \begin{pmatrix} 0 & -i \\ i & 0 \end{pmatrix} = \frac{\sigma_2}{\sqrt{3}}, \tag{3.80}$$

$$F^{(3)} = \frac{1}{\sqrt{3}} \begin{pmatrix} 1 & 0 \\ 0 & -1 \end{pmatrix} = \frac{\sigma_3}{\sqrt{3}}.$$

In a more compact way, one can write the expression for the projector as

$$\mathcal{P}_d^j = \frac{1}{\sqrt{3}} \sigma^j. \tag{3.81}$$

Note that, as we extend for the isospin space in the 2-nucleon projector, we can do so here and write the projector as

$$\mathcal{P}_d^{ij} = \frac{1}{\sqrt{3}} \begin{pmatrix} \sigma^i & 0 \\ 0 & \tau^j \end{pmatrix}. \tag{3.82}$$

Now, for the quartet channel

$$\begin{aligned}
q_{++} &= \left| 11, \frac{11}{22} \right\rangle n_+, \\
q_+ &= \sqrt{\frac{2}{3}} \left| 10, \frac{11}{22} \right\rangle n_+ + \sqrt{\frac{1}{3}} \left| 11, \frac{1}{2} \left( -\frac{1}{2} \right) \right\rangle n_-, \\
q_- &= \sqrt{\frac{1}{3}} \left| 1(-1), \frac{11}{22} \right\rangle n_+ + \sqrt{\frac{2}{3}} \left| 10, \frac{1}{2} \left( -\frac{1}{2} \right) \right\rangle n_-, \\
q_{--} &= \left| 1(-1), \frac{1}{2} \left( -\frac{1}{2} \right) \right\rangle n_-.
\end{aligned} \tag{3.83}$$

In terms of the two-nucleon projectors

$$\begin{aligned}
q_{++} &= \frac{1}{\sqrt{2}} [N^T (iT^{(2)} - T^{(1)}) N] n_+, \\
q_+ &= \sqrt{\frac{2}{3}} (N^T T^{(3)} N) n_+ + \frac{1}{\sqrt{6}} [N^T (iT^{(2)} - T^{(1)}) N] n_-, \\
q_- &= \frac{1}{\sqrt{6}} [N^T (iT^{(2)} + T^{(1)}) N] n_+ + \sqrt{\frac{2}{3}} (N^T T^{(3)} N) n_-, \\
q_{--} &= \frac{1}{\sqrt{2}} [N^T (iT^{(2)} + T^{(1)}) N] n_-.
\end{aligned} \tag{3.84}$$

Then, the  $G^{(j)}$  matrices are

$$\begin{aligned}
G^{(1)} &= \frac{1}{\sqrt{6}} \begin{pmatrix} -\sqrt{3} & 0 \\ 0 & -1 \\ 1 & 0 \\ 0 & \sqrt{3} \end{pmatrix}, & G^{(2)} &= \frac{i}{\sqrt{6}} \begin{pmatrix} \sqrt{3} & 0 \\ 0 & 1 \\ 1 & 0 \\ 0 & \sqrt{3} \end{pmatrix}, \\
G^{(3)} &= \frac{2}{\sqrt{6}} \begin{pmatrix} 0 & 0 \\ 1 & 0 \\ 0 & 1 \\ 0 & 0 \end{pmatrix}.
\end{aligned} \tag{3.85}$$

These matrices obey some relations

$$G^{(i)\dagger} G^{(j)} = \frac{2}{3} \delta_{ij} - \frac{i}{3} \varepsilon_{ijk} \sigma_k, \tag{3.86}$$

$$G^{(i)} G^{(j)\dagger} = \frac{3}{4} \delta_{ij} - \frac{1}{6} \{J_i, J_j\} + \frac{i}{3} \varepsilon_{ijk} J_k, \tag{3.87}$$

$$G^{(i)} \sigma_j - G^{(j)} \sigma_i = -i \varepsilon_{ijk} G^{(k)}, \tag{3.88}$$



$$i \sum_{i,j} \varepsilon_{ijk} G^{(i)} \sigma_j = G^{(k)}. \quad (3.89)$$

where  $J_i$  are the generators of spin-3/2, derived in the Appendix A. The above relations of  $G^{(i)}$  matrices are derived in Appendix B.

### 3.3.2 Born Term

We now proceed using the results that are given in details in Appendix C. The Born term is given by

$$iB_{ji}^{\beta\alpha}(d_i \rightarrow d_j) = (-ig_{d_j})(-ig_{d_i}) \int d^4x d^4y \langle 0 | T \{ d_j(\infty) N_\beta(\infty) \left[ d_k^\dagger(y) N_\gamma(y) \mathcal{P}_{\gamma\delta}^k N_\delta(y) \right] \times \left[ N_\epsilon^\dagger(x) \mathcal{P}_{\epsilon\sigma}^{s\dagger} N_\sigma^\dagger(x) d_s(x) \right] d_i^\dagger(-\infty) N_\alpha^\dagger(-\infty) \} | 0 \rangle. \quad (3.90)$$

The contractions are given in Appendix C. The final expression for the Born term can be written as

$$iB_{\beta\alpha}^{ji} = (-ig_{d_j})(-ig_{d_i}) \left( -\frac{1}{2} \mathcal{O}^i \mathcal{O}^j \right)_{\beta\alpha} i\bar{S}_N(k_{d_0} - B_d - k_{n_0} + \varepsilon; \mathbf{p} + \mathbf{k}), \\ = i \frac{g_{d_j} g_{d_i}}{2} \frac{(\mathcal{O}^i \mathcal{O}^j)_{\beta\alpha}}{k_{d_0} - B_d - k_{n_0} + \varepsilon - \frac{(\mathbf{p} + \mathbf{k})^2}{2m_N} + i\epsilon}, \quad (3.91)$$

where we used the kinematics described in Figure 3.8. And the factor  $\mathcal{O}^i \mathcal{O}^j$  stands for combinations of Pauli matrices  $\sigma^i$  (spin) and  $\tau^i$  (isospin).  $B_d$  is the binding energy of the deuteron. The integral equation, then, reads

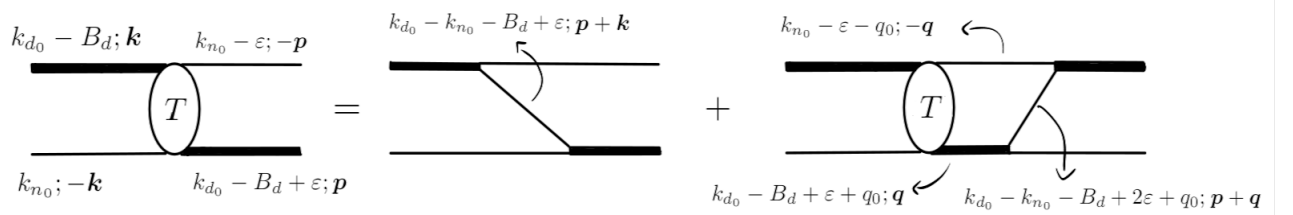


Figure 3.8: The kinematics for the integral equation for the  $nd$  system.

$$\bar{T}_{\beta\alpha}^{ji}(\varepsilon; \mathbf{p}, \mathbf{k}) = B_{\beta\alpha}^{ji}(k_{d_0} - k_{n_0} - B_d + \varepsilon; \mathbf{p} + \mathbf{k}) + H_{\beta\alpha}^{ji}(\varepsilon; \mathbf{p}, \mathbf{k}). \quad (3.92)$$

The homogeneous term  $H_{\beta\alpha}^{ji}(\varepsilon; \mathbf{p}, \mathbf{k})$  is given by

$$\begin{aligned}
H_{\beta\alpha}^{ji}(\varepsilon; \mathbf{p}, \mathbf{k}) &= \sum_{f=s,t} \int \frac{d^4q}{(2\pi)^4} iB_{\beta\gamma}^{j\ell}(k_{d_0} - k_{n_0} - B_d + 2\varepsilon + q_0; \mathbf{p} + \mathbf{q}) i\bar{\mathcal{D}}_f(k_{d_0} - B_d + \varepsilon + q_0; \mathbf{q}) \\
&\quad \times iS_N(k_{n_0} - \varepsilon - q_0; -\mathbf{q}) i\bar{T}_{\gamma\alpha}^{\ell i}(\varepsilon + q_0; \mathbf{q}, \mathbf{k}), \\
&= \sum_{f=s,t} \int \frac{d^4q}{(2\pi)^4} B_{\beta\gamma}^{j\ell}(k_{d_0} - k_{n_0} - B_d + 2\varepsilon + q_0; \mathbf{p} + \mathbf{q}) \bar{\mathcal{D}}_f(k_{d_0} - B_d + \varepsilon + q_0; \mathbf{q}) \\
&\quad \frac{1}{k_{n_0} - \varepsilon - q_0 - \frac{q^2}{2m_N} + i\epsilon} \bar{T}_{\gamma\alpha}^{\ell i}(\varepsilon + q_0; \mathbf{q}, \mathbf{k}), \tag{3.93}
\end{aligned}$$

where the sum is over the singlet and triplet states. Integrating  $q_0$  by contour integration setting  $q_0 = k_{n_0} - \varepsilon - \frac{q^2}{2m_N} + i\epsilon$ , one arrives at

$$\begin{aligned}
H_{\beta\alpha}^{ji}(\varepsilon; \mathbf{p}, \mathbf{k}) &= -i \sum_{f=s,t} \int \frac{d^3q}{(2\pi)^3} B_{\beta\gamma}^{j\ell}(k_{d_0} - B_d + \varepsilon - \mathbf{q}^2/2m_N; \mathbf{p} + \mathbf{q}) \\
&\quad \times \bar{\mathcal{D}}_f(k_{d_0} + k_{n_0} - B_d - \mathbf{q}^2/2m_N; \mathbf{q}) \bar{T}_{\gamma\alpha}^{\ell i}(k_{n_0} - \mathbf{q}^2/2m_N; \mathbf{q}, \mathbf{k}). \tag{3.94}
\end{aligned}$$

Returning to the full equation

$$\begin{aligned}
\bar{T}_{\beta\alpha}^{ji}(\varepsilon; \mathbf{p}, \mathbf{k}) &= B_{\beta\alpha}^{ji}(k_{d_0} - k_{n_0} - B_d + \varepsilon; \mathbf{p} + \mathbf{k}) - \sum_{f=s,t} \int \frac{d^3q}{(2\pi)^3} \\
&\quad \times B_{\beta\gamma}^{j\ell}(k_{d_0} - B_d + \varepsilon - \mathbf{q}^2/2m_N; \mathbf{p} + \mathbf{q}) \bar{\mathcal{D}}_f(k_{d_0} + k_{n_0} - B_d - \mathbf{q}^2/2m_N; \mathbf{q}) \\
&\quad \times \bar{T}_{\gamma\alpha}^{\ell i}(k_{n_0} - \mathbf{q}^2/2m_N; \mathbf{q}, \mathbf{k}), \\
&= \frac{g_{d_j} g_{d_i}}{2} \frac{(\mathcal{O}^i \mathcal{O}^j)_{\beta\alpha}}{k_{d_0} - B_d - k_{n_0} + \varepsilon - \frac{(\mathbf{p}+\mathbf{k})^2}{2m_N} + i\epsilon} \\
&\quad - \sum_{f=s,t} \int \frac{d^3q}{(2\pi)^3} \frac{g_{d_j} g_{d_\ell}}{2} \frac{(\mathcal{O}^\ell \mathcal{O}^j)_{\beta\gamma}}{k_{d_0} - B_d + \varepsilon - \frac{q^2}{2m_N} - \frac{(\mathbf{p}+\mathbf{k})^2}{2m_N} + i\epsilon} \\
&\quad \times \bar{\mathcal{D}}_f(k_{d_0} + k_{n_0} - B_d - \mathbf{q}^2/2m_N; \mathbf{q}) \bar{T}_{\gamma\alpha}^{\ell i}(k_{n_0} - \mathbf{q}^2/2m_N; \mathbf{q}, \mathbf{k}),
\end{aligned}$$

$$\begin{aligned}
&= \frac{g_{d_j} g_{d_i}}{2} \frac{m_N (\mathcal{O}^i \mathcal{O}^j)_{\beta\alpha}}{m_N(k_{d_0} - B_d - k_{n_0} + \varepsilon) - \frac{(\mathbf{p}+\mathbf{k})^2}{2} + i\epsilon} \\
&+ \sum_{f=s,t} \frac{g_{d_j} g_{d_i}}{2} \int \frac{d^3 q}{(2\pi)^3} \left( -\frac{g_{d_\ell}}{g_{d_i}} \right) \frac{m_N (\mathcal{O}^\ell \mathcal{O}^j)_{\beta\gamma}}{m_N(k_{d_0} - B_d + \varepsilon) - \frac{\mathbf{q}^2}{2} - \frac{(\mathbf{p}+\mathbf{k})^2}{2} + i\epsilon} \\
&\quad \times \left( -\frac{4\pi}{m_N g_{d_\ell}^2} \right) \mathcal{D}_f(k_{d_0} + k_{n_0} - B_d - \mathbf{q}^2/2m_N; \mathbf{q}) \bar{T}_{\gamma\alpha}^{\ell i}(k_{n_0} - \mathbf{q}^2/2m_N; \mathbf{q}, \mathbf{k}),
\end{aligned} \tag{3.95}$$

where we used that  $\bar{\mathcal{D}}_f(p_0; \mathbf{p}) = \left( -\frac{4\pi}{m_N g_{d_\ell}^2} \right) \mathcal{D}_f(p_0; \mathbf{p})$ .

$$\begin{aligned}
&= \frac{m_N g_{d_j} g_{d_i}}{2} \left\{ \frac{(\mathcal{O}^i \mathcal{O}^j)_{\beta\alpha}}{m_N(k_{d_0} - B_d - k_{n_0} + \varepsilon) - \frac{(\mathbf{p}+\mathbf{k})^2}{2} + i\epsilon} \right. \\
&+ 2\pi \sum_{f=s,t} \int \frac{d^3 q}{(2\pi)^3} \frac{(\mathcal{O}^\ell \mathcal{O}^j)_{\beta\gamma}}{m_N(k_{d_0} - B_d + \varepsilon) - \frac{\mathbf{q}^2}{2} - \frac{(\mathbf{p}+\mathbf{k})^2}{2} + i\epsilon} \\
&\quad \left. \times \mathcal{D}_f(k_{d_0} + k_{n_0} - B_d - \mathbf{q}^2/2m_N; \mathbf{q}) \left( \frac{2}{m_N g_{d_\ell} g_{d_i}} \right) \bar{T}_{\gamma\alpha}^{\ell i}(k_{n_0} - \mathbf{q}^2/2m_N; \mathbf{q}, \mathbf{k}) \right\}.
\end{aligned} \tag{3.96}$$

Then, defining  $\bar{T}_{\beta\alpha}^{ji}(p_0; \mathbf{p}) \equiv \frac{m_N g_{d_j} g_{d_i}}{2} T_{\beta\alpha}^{ji}(p_0; \mathbf{p})$  and setting  $\varepsilon = k_{n_0} - \mathbf{p}^2/2m_N$  and the initial particles on-shell,  $k_{n_0} = \mathbf{k}^2/2m_N$  and  $k_{d_0} = \mathbf{k}^2/4m_N$ . We calculate the half off-shell amplitude as

$$\begin{aligned}
T_{\beta\alpha}^{ji}(\mathbf{p}, \mathbf{k}) &= \frac{(\mathcal{O}^i \mathcal{O}^j)_{\beta\alpha}}{m_N E - \mathbf{p}^2 - \mathbf{k}^2 - \mathbf{p} \cdot \mathbf{k}} \\
&+ 2\pi \sum_{f=s,t} \int \frac{d^3 q}{(2\pi)^3} \frac{(\mathcal{O}^\ell \mathcal{O}^j)_{\beta\gamma}}{m_N E - \mathbf{p}^2 - \mathbf{q}^2 - \mathbf{p} \cdot \mathbf{q}} \mathcal{D}_f(E - \mathbf{q}^2/2m_N; \mathbf{q}) T_{\gamma\alpha}^{\ell i}(\mathbf{q}, \mathbf{k}),
\end{aligned} \tag{3.97}$$

assuming  $E = k_{d_0} + k_{n_0} - B_d = \frac{3\mathbf{k}^2}{4m_N} - B_d$ .

### 3.3.3 Quartet channel

Only the  ${}^3S_1$  channel contributes, this leads to a single integral equation. Using Eq. (3.102), one can project into quartet channel using the  $G^{(i)}$  matrices. This projection is given by

$$G^{(j)} \sigma^i \sigma^j G^{(i)\dagger} = G^{(j)} (\delta_{ij} + i\epsilon_{ijk} \sigma_k) G^{(i)\dagger} = (G^{(i)} + i\epsilon_{jki} G^{(j)} \sigma_k) G^{(i)\dagger} = 2G^{(i)} G^{(i)\dagger}, \tag{3.98}$$

where we used Eq. (3.89). And remembering that  $J_i^2 |j, m\rangle = j(j+1) |j, m\rangle$  and using (3.87)

$$2G^{(i)}G^{(i)\dagger} = 2 \left[ \frac{3}{4} \sum_{i=1}^3 \delta_{ii} - \frac{1}{6}(J_i^2 + J_i^2) \right] = 2 \left[ \frac{9}{4} - \frac{1}{3} \frac{3}{2} \left( \frac{3}{2} + 1 \right) \right] = 2. \quad (3.99)$$

Using the partial wave expansion and the angular addition theorem in order to integrate over the angle variables leads us to our final expression. As there the procedure is the same as done before, we stress that the only difference is the prefactor  $2\pi$  instead of the  $8\pi$  for the previous case. Knowing this, we can write

$$t_\ell(p, k) = 2b_\ell(p, k) + \frac{2}{\pi} \int_0^\infty dq q^2 b_\ell(p, q) \mathcal{D}_t(E - q^2/2m_N; q) t_\ell(q, k), \quad (3.100)$$

with the same definition for  $b_\ell(p, k)$ .

$$\begin{aligned} b_\ell(p, k) &= \frac{1}{2} \int_{-1}^1 dx P_\ell(x) \frac{1}{p^2 + k^2 - m_N E + kpx}, \\ &= \frac{(-1)^\ell}{pk} Q_\ell \left( \frac{p^2 + k^2 - m_N E}{pk} \right). \end{aligned} \quad (3.101)$$

### 3.3.4 Doublet channel

The doublet channel presents a more complicated scenario as either  $^3S_1$  and  $^1S_0$  channels contribute. The difference is the appearance of a coupled integral equation, specifically, two coupled integral equations. When deriving the equations, we will use Gri bhammer's notation [82] and the Born term can be expressed as a  $2 \times 2$  matrix in cluster-configuration space,

$$\begin{aligned} &\begin{pmatrix} T_{t \rightarrow t}^{ji}(\mathbf{p}, \mathbf{k}) & T_{t \rightarrow s}^{ji}(\mathbf{p}, \mathbf{k}) \\ T_{s \rightarrow t}^{ji}(\mathbf{p}, \mathbf{k}) & T_{s \rightarrow s}^{ji}(\mathbf{p}, \mathbf{k}) \end{pmatrix} = - \frac{1}{\mathbf{p}^2 + \mathbf{k}^2 - m_N E + \mathbf{p} \cdot \mathbf{k}} \begin{pmatrix} \sigma^i \sigma^j & \tau^i \sigma^j \\ \sigma^i \tau^j & \tau^i \tau^j \end{pmatrix} \\ &- \int \frac{d^3 q}{(2\pi)^2} \frac{1}{\mathbf{p}^2 + \mathbf{q}^2 - m_N E + \mathbf{p} \cdot \mathbf{q}} \begin{pmatrix} \sigma^\ell \sigma^j & \tau^\ell \sigma^j \\ \sigma^\ell \tau^j & \tau^\ell \tau^j \end{pmatrix} \\ &\begin{pmatrix} \mathcal{D}_t(E - \mathbf{q}^2/2m_N; \mathbf{q}) & 0 \\ 0 & \mathcal{D}_s(E - \mathbf{q}^2/2m_N; \mathbf{q}) \end{pmatrix} \begin{pmatrix} T_{t \rightarrow t}^{\ell i}(\mathbf{q}, \mathbf{k}) & T_{t \rightarrow s}^{\ell i}(\mathbf{q}, \mathbf{k}) \\ T_{s \rightarrow t}^{\ell i}(\mathbf{q}, \mathbf{k}) & T_{s \rightarrow s}^{\ell i}(\mathbf{q}, \mathbf{k}) \end{pmatrix}. \end{aligned} \quad (3.102)$$

Projecting into initial and final spin-doublet states using Eq. (3.82),

$$\frac{1}{\sqrt{3}} \begin{pmatrix} \sigma^j & 0 \\ 0 & \tau^j \end{pmatrix} \begin{pmatrix} T_{t \rightarrow t}^{ji}(\mathbf{p}, \mathbf{k}) & T_{t \rightarrow s}^{ji}(\mathbf{p}, \mathbf{k}) \\ T_{s \rightarrow t}^{ji}(\mathbf{p}, \mathbf{k}) & T_{s \rightarrow s}^{ji}(\mathbf{p}, \mathbf{k}) \end{pmatrix} \frac{1}{\sqrt{3}} \begin{pmatrix} \sigma^i & 0 \\ 0 & \tau^i \end{pmatrix} = \begin{pmatrix} T_{t \rightarrow t}(\mathbf{p}, \mathbf{k}) & T_{t \rightarrow s}(\mathbf{p}, \mathbf{k}) \\ T_{s \rightarrow t}(\mathbf{p}, \mathbf{k}) & T_{s \rightarrow s}(\mathbf{p}, \mathbf{k}) \end{pmatrix}. \quad (3.103)$$

We use these identities

$$\begin{aligned} \sigma^j \tau^k \sigma^j &= \sigma^j (\delta_{kj} + i\epsilon_{kjl} \sigma^\ell) = \sigma^k + i\epsilon_{kjl} (\delta_{j\ell} + i\epsilon_{j\ell r} \sigma^r) = \sigma^k - \underbrace{(\delta_{\ell\ell} \delta_{kr} - \delta_{\ell r} \delta_{k\ell})}_{=2\delta_{kr}} \sigma^r = -\sigma^k, \\ \sigma^j \tau^k \sigma^j &= 3\tau^k, \quad \tau^j \sigma^k \tau^j = 3\sigma^k, \quad \tau^j \tau^k \tau^j = -\tau^k. \end{aligned} \quad (3.104)$$

Thus, we write

$$\frac{1}{\sqrt{3}} \begin{pmatrix} \sigma^j & 0 \\ 0 & \tau^j \end{pmatrix} \begin{pmatrix} \sigma^i \sigma^j & \tau^i \sigma^j \\ \sigma^i \tau^j & \tau^i \tau^j \end{pmatrix} = \frac{1}{\sqrt{3}} \begin{pmatrix} -\sigma^i & 3\tau^i \\ 3\sigma^i & -\tau^i \end{pmatrix} = \begin{pmatrix} -1 & 3 \\ 3 & -1 \end{pmatrix} \frac{1}{\sqrt{3}} \begin{pmatrix} \sigma^i & 0 \\ 0 & \tau^i \end{pmatrix}. \quad (3.105)$$

Which leads to

$$\begin{aligned} &\begin{pmatrix} T_{t \rightarrow t}(\mathbf{p}, \mathbf{k}) & T_{t \rightarrow s}(\mathbf{p}, \mathbf{k}) \\ T_{s \rightarrow t}(\mathbf{p}, \mathbf{k}) & T_{s \rightarrow s}(\mathbf{p}, \mathbf{k}) \end{pmatrix} = \frac{1}{\mathbf{p}^2 + \mathbf{k}^2 - m_N E + \mathbf{p} \cdot \mathbf{k}} \begin{pmatrix} 1 & -3 \\ -3 & 1 \end{pmatrix} \\ &+ \int \frac{d^3 q}{(2\pi)^2} \frac{1}{\mathbf{p}^2 + \mathbf{q}^2 - m_N E + \mathbf{p} \cdot \mathbf{q}} \begin{pmatrix} 1 & -3 \\ -3 & 1 \end{pmatrix} \\ &\times \begin{pmatrix} \mathcal{D}_t(E - \mathbf{q}^2/2m_N; \mathbf{q}) & 0 \\ 0 & \mathcal{D}_s(E - \mathbf{q}^2/2m_N; \mathbf{q}) \end{pmatrix} \begin{pmatrix} T_{t \rightarrow t}(\mathbf{q}, \mathbf{k}) & T_{t \rightarrow s}(\mathbf{q}, \mathbf{k}) \\ T_{s \rightarrow t}(\mathbf{q}, \mathbf{k}) & T_{s \rightarrow s}(\mathbf{q}, \mathbf{k}) \end{pmatrix}. \end{aligned} \quad (3.106)$$

The projection into partial waves is done using the same procedure as before. We use the partial wave expansion and the angular addition theorem. Thus, we arrive at

$$\begin{aligned} \mathbf{t}_\ell(p, k) &= b_\ell(p, k) \begin{pmatrix} 1 & -3 \\ -3 & 1 \end{pmatrix} + \int_0^\infty \frac{dq q^2}{\pi} b_\ell(p, q) \begin{pmatrix} 1 & -3 \\ -3 & 1 \end{pmatrix} \\ &\times \begin{pmatrix} \tilde{\mathcal{D}}_t(E; q) & 0 \\ 0 & \tilde{\mathcal{D}}_s(E; q) \end{pmatrix} \mathbf{t}_\ell(q, k), \end{aligned} \quad (3.107)$$

with  $b_\ell(p, k)$  as defined earlier,  $\tilde{\mathcal{D}}(E; q) \equiv \mathcal{D}_s(E - \mathbf{q}^2/2m_N; \mathbf{q})$  and the amplitude  $\mathbf{t}_\ell(p, k) = \begin{pmatrix} t_{t \rightarrow t}^\ell(p, k) & t_{t \rightarrow s}^\ell(p, k) \\ t_{s \rightarrow t}^\ell(p, k) & t_{s \rightarrow s}^\ell(p, k) \end{pmatrix}$ .

We need to account the three-body term in the Lagrangian (3.50). The Born term for

the three-body force is written as

$$i\bar{B}_{3B}(d_i \rightarrow d_j) = \pm \left( -i \frac{g_3}{\sqrt{3}} \right)^2 \int d^4x d^4y \quad (3.108)$$

$$\times \langle 0 | T \{ d_j(\infty) N_\beta(\infty) [d_k^\dagger N_\gamma^\dagger \mathcal{O}_{\gamma\delta}^k \phi_\delta]_y [\phi_\epsilon^\dagger \mathcal{O}_{\epsilon\sigma}^{\ell\dagger} N_\sigma d_\ell]_x d_i^\dagger(-\infty) N_\alpha^\dagger(-\infty) \} | 0 \rangle,$$

where the sign depends on the initial and final dimeron states. There is only one possible contraction and is given by

$$\langle 0 | T \{ d_j(\infty) N_\beta(\infty) [d_k^\dagger N_\gamma^\dagger \mathcal{O}_{\gamma\delta}^k \phi_\delta]_y [\phi_\epsilon^\dagger \mathcal{O}_{\epsilon\sigma}^\ell N_\sigma d_\ell]_x d_i^\dagger(-\infty) N_\alpha^\dagger(-\infty) \} | 0 \rangle \quad (3.109)$$

$$= \delta_{jk} i\bar{\mathcal{D}}_{d_j}(\infty - y) \delta_{\beta\gamma} i\bar{S}_N(\infty - x) \delta_{\ell i} i\bar{\mathcal{D}}_{d_i}(x + \infty) \delta_{\sigma\alpha} i\bar{S}_N(y + \infty) \delta_{\delta\epsilon} i\bar{\mathcal{T}}(y - x) \mathcal{O}_{\gamma\delta}^k \mathcal{O}_{\epsilon\sigma}^\ell$$

$$= -i\bar{\mathcal{D}}_{d_j}(\infty - y) i\bar{S}_N(\infty - x) i\bar{\mathcal{D}}_{d_i}(x + \infty) i\bar{S}_N(y + \infty) i\bar{\mathcal{T}}(y - x) \mathcal{O}_{\beta\epsilon}^j \mathcal{O}_{\alpha\sigma}^i, \quad (3.110)$$

with  $i\bar{\mathcal{T}}(z) = i/\Omega$  being the trimer propagator and  $\mathcal{O}_{\alpha\beta}^j = (\sigma_\alpha - \tau^j)_\beta$ . Then, the amputated Born amplitudes are

$$i\mathbf{B}_{3B}^{ji} = i \frac{2}{m_N g_{d_j} g_{d_i}} \bar{\mathbf{B}}_{3B}^{ji} = -i \frac{2g_3^2}{m_N g_{d_j} g_{d_i} \Omega} \frac{1}{3} \begin{pmatrix} \sigma^j \sigma^i & -\sigma^j \tau^i \\ -\tau^j \sigma^i & \tau^j \tau^i \end{pmatrix} = i \frac{\mathcal{H}}{3} \begin{pmatrix} \sigma^j \sigma^i & -\sigma^j \tau^i \\ -\tau^j \sigma^i & \tau^j \tau^i \end{pmatrix}. \quad (3.111)$$

Then, we project into the doublet channel

$$\mathbf{B}_{3B} = \frac{1}{\sqrt{3}} \begin{pmatrix} \sigma^j & 0 \\ 0 & \tau^j \end{pmatrix} \mathbf{B}_{3B}^{ji} \frac{1}{\sqrt{3}} \begin{pmatrix} \sigma^i & 0 \\ 0 & \tau^i \end{pmatrix} = \mathcal{H} \begin{pmatrix} 1 & -1 \\ -1 & 1 \end{pmatrix}. \quad (3.112)$$

(Note that the three body force does not contribute to the quartet channel since  $\sum_i G^{(i)} \sigma^i = 0$ .)

Finally, we can write the doublet channel integral equation

$$\mathbf{t}_\ell(p, k) = b_\ell(p, k) \begin{pmatrix} 1 & -3 \\ -3 & 1 \end{pmatrix} + \delta_{\ell 0} \mathcal{H} \begin{pmatrix} 1 & -1 \\ -1 & 1 \end{pmatrix}$$

$$+ \int_0^\infty \frac{dq q^2}{\pi} \left[ b_\ell(p, q) \begin{pmatrix} 1 & -3 \\ -3 & 1 \end{pmatrix} + \delta_{\ell 0} \mathcal{H} \begin{pmatrix} 1 & -1 \\ -1 & 1 \end{pmatrix} \right] \begin{pmatrix} \tilde{\mathcal{D}}_t(E; q) & 0 \\ 0 & \tilde{\mathcal{D}}_s(E; q) \end{pmatrix} \mathbf{t}_\ell(q, k). \quad (3.113)$$

Note that we need to solve both coupled equations simultaneously, as a matrix equation, in order to properly solve the problem. The doublet channel is the one that exhibits the Efimov physics—the kernel of this channel does not vanish sufficiently fast in the ultraviolet, forcing us to introduce a momentum cutoff  $\Lambda$  as the upper limit of integration

in (3.113). In the absence of a three-body interaction, parametrized by  $\mathcal{H}$ , the solution of the integral equation is quite sensitive to the value of  $\Lambda$  [75, 74, 81]. In the spirit of EFT, proper renormalization of the problem requires an explicit  $\Lambda$ -dependence on  $\mathcal{H}$  in order to absorb the  $\Lambda$ -dependence of the remaining kernel. In position space, the latter is equivalent to the  $-1/R^2$  divergence at the origin in Eq. (3.44) for  $n = 0$ , while the former is equivalent to the boundary condition near  $R = 0$  that fixes the energy of the deepest (ground) bound state. The quartet channel does not exhibit such phenomenon, since in this channel the Pauli exclusion principle precludes the spins to be all aligned at the same position in space.

We reproduced the triton binding energy by solving numerically the homogeneous version of the coupled integral equations in Eq. (3.113). Regardless of being interested mainly in the homogeneous integral equations, we also solved the  $nd$  non-homogeneous equations calculating scattering observables (phase shifts) and comparing with reference [82]. This study of the  $nd$  system, reproducing well-known results in the literature, gives us confidence to move forward and address the  $\Lambda nn$  system, described in the next chapters.

# Chapter 4

## $\Lambda nn$ system

The  $\Lambda nn$  system can be described mathematically in an analogous way as the  $nd$  system, and that is the main reason we described explicitly this system in the previous section. The  $\Lambda nn$  is composed by two different particles: the neutron ( $S = 1/2, I = 1/2$ ) and the  $\Lambda$  ( $S = 1/2, I = 0$ ). Note that the isospin dependence will come just from the neutrons. And, for all possible channels, will be fixed ( $I = 1$ ). The  $\Lambda nn$  is a hypernucleus, due to the  $\Lambda$  particle being a hyperon (a particle containing strange quarks, but no charm, bottom or top quarks [84]). There are three possible channels that contribute to the system:  $^1S_0(nn)$  (singlet),  $^1S_0(\Lambda n)$  (singlet) and  $^3S_1(\Lambda n)$  (triplet).

The Lagrangian that describes the system is given by [85]

$$\mathcal{L} = \mathcal{L}_0 + \mathcal{L}_I + \mathcal{L}_{3B}, \quad (4.1)$$

$$\begin{aligned} \mathcal{L}_0 = & \phi_n^\dagger \left( i\partial_0 + \frac{\nabla^2}{2m_n} \right) \phi_n + \phi_\Lambda^\dagger \left( i\partial_0 + \frac{\nabla^2}{2m_\Lambda} \right) \phi_\Lambda \\ & + \sigma_{s(nn)} s_{nn}^\dagger \left( i\partial_0 + \frac{\nabla^2}{4m_n} + \Delta_{s(nn)} \right) s_{nn} \\ & + \sigma_{s(\Lambda n)} s_{\Lambda n}^\dagger \left( i\partial_0 + \frac{\nabla^2}{2(m_n + m_\Lambda)} + \Delta_{s(\Lambda n)} \right) s_{\Lambda n} \\ & + \sigma_{t(\Lambda n)} t_{\Lambda n}^\dagger \left( i\partial_0 + \frac{\nabla^2}{2(m_n + m_\Lambda)} + \Delta_{t(\Lambda n)} \right) t_{\Lambda n} + \dots, \end{aligned} \quad (4.2)$$

$$\begin{aligned} \mathcal{L}_I = & -y_{s(nn)} \left[ s_{nn}^\dagger (\phi_n^T \mathcal{P}_{s(nn)} \phi_n) + H.c. \right] - y_{s(\Lambda n)} \left[ s_{\Lambda n}^\dagger (\phi_n^T \mathcal{P}_{s(\Lambda n)} \phi_\Lambda) + H.c. \right] \\ & - y_{t(\Lambda n)} \left[ t_{\Lambda n}^{\dagger k} (\phi_n^T \mathcal{P}_{t(\Lambda n)}^k \phi_\Lambda) + H.c. \right] + \dots, \end{aligned} \quad (4.3)$$

$$\mathcal{L}_{3B} = -\frac{1}{6} m_\Lambda y_{t(\Lambda n)}^2 \frac{g(\Lambda)}{\Lambda^2} t_{\Lambda n}^{\dagger i} \phi_n^\dagger \sigma^i \sigma^j \phi_n t_{\Lambda n}^j + \dots, \quad (4.4)$$

where  $\phi_n$  and  $\phi_\Lambda$  being the neutron and  $\Lambda$  fields, respectively;  $s_{nn}$ ,  $s_{\Lambda n}$  and  $t_{\Lambda n}$  are the



dibaryon fields for the  $^1S_0(nn)$ ,  $^1S_0(\Lambda n)$  and  $^3S_1(\Lambda n)$  channels, respectively. The  $\sigma_{s(nn)}$ ,  $\sigma_{s(\Lambda n)}$  and  $\sigma_{t(\Lambda n)}$  are sign factors.  $\Delta_{s(nn)}$ ,  $\Delta_{s(\Lambda n)}$  and  $\Delta_{t(\Lambda n)}$  are the mass differences between the dibaryon and the elementary constituent particle and the couplings  $y_{s(nn)}$ ,  $y_{s(\Lambda n)}$  and  $y_{t(\Lambda n)}$ . The ... stands for higher order operators. The projectors here are different because we do not need to consider isospin projections, then, we write

$$\mathcal{P}_{s(nn)} = -\frac{i}{2}\sigma_2, \quad \mathcal{P}_{s(\Lambda n)} = -\frac{i}{\sqrt{2}}\sigma_2, \quad \mathcal{P}_{t(\Lambda n)}^k = -\frac{i}{\sqrt{2}}\sigma_2\sigma^k. \quad (4.5)$$

The difference between the prefactors of  $\mathcal{P}_{s(nn)}$  and  $\mathcal{P}_{s(\Lambda n)}$  is due to the fact that we have two identical particles in  $^1S_0(nn)$ . Note that, the three-body force Lagrangian only accounts the triplet channel interactions, this is due to the nonexistence of data for the  $\Lambda n$  interaction and we could not estimate the others couplings. Nonetheless, in principle, these terms exist and should be considered.

## 4.1 Integral equation

In order to write the integral equation, one needs to calculate the Feynman rules for Lagrangian (4.1). The propagators are exactly the same as before, except by the fact that we do need to care about the reduced mass for the 2-body system  $\Lambda n$ . Resulting in

- Fermions

$$iS_n(E; \mathbf{q}) = \frac{i}{E - \mathbf{q}^2/2m_n + i\epsilon}, \quad (4.6)$$

$$iS_\Lambda(E; \mathbf{q}) = \frac{i}{E - \mathbf{q}^2/2m_\Lambda + i\epsilon}. \quad (4.7)$$

- Dibaryons (renormalized)

$$iD_{s(nn)}(E, \mathbf{q}) = \frac{4\pi}{y_{s(nn)}^2 m_n} \frac{i}{\frac{1}{a_{nn}} - \sqrt{\frac{1}{4}\mathbf{q}^2 - m_n E - i\epsilon} - i\epsilon}. \quad (4.8)$$

For both  $^1S_0(\Lambda n)$  and  $^3S_1(\Lambda n)$  channels the total energy is given by  $E_T = E - \mathbf{q}^2/2(m_n + m_\Lambda)$ , hence, the renormalized dimer propagators are written as

$$iD_{s(nn)}(E, \mathbf{q}) = \frac{2\pi}{y_{s(\Lambda n)}^2 \mu(\Lambda n)} \frac{i}{\frac{1}{a_{s(\Lambda n)}} - \sqrt{-2\mu(\Lambda n) \left( E - \frac{\mathbf{q}^2}{2(m_n + m_\Lambda)} - i\epsilon \right)} - i\epsilon}, \quad (4.9)$$

$$iD_{s(nn)}(E, \mathbf{q}) = \frac{2\pi}{y_{t(\Lambda n)}^2 \mu(\Lambda n)} \frac{i}{\frac{1}{a_{t(\Lambda n)}} - \sqrt{-2\mu(\Lambda n) \left( E - \frac{\mathbf{q}^2}{2(m_n + m_\Lambda)} - i\epsilon \right)} - i\epsilon}. \quad (4.10)$$

As in [86, 87, 88] the sign factors  $\sigma_{s(nn)}$ ,  $\sigma_{s(\Lambda n)}$  and  $\sigma_{t(\Lambda n)}$  are equal to  $-1$ . Here, we omit the subindex 2 on the scattering lengths, nonetheless all scattering lengths in this chapter stands for the two-body subsystem.

The possible contractions for the Born terms are given in Appendix C. Thus, we proceed defining our operators as  $3 \times 3$  matrices as

$$\bar{\mathbf{T}}^{ji} = \begin{pmatrix} \bar{T}_{t(\Lambda n) \rightarrow t(\Lambda n)}^{ji} & \bar{T}_{s(\Lambda n) \rightarrow t(\Lambda n)}^{ji} & \bar{T}_{s(nn) \rightarrow t(\Lambda n)}^{ji} \\ \bar{T}_{t(\Lambda n) \rightarrow s(\Lambda n)}^{ji} & \bar{T}_{s(\Lambda n) \rightarrow s(\Lambda n)}^{ji} & \bar{T}_{s(nn) \rightarrow s(\Lambda n)}^{ji} \\ \bar{T}_{t(\Lambda n) \rightarrow s(nn)}^{ji} & \bar{T}_{s(\Lambda n) \rightarrow s(nn)}^{ji} & 0 \end{pmatrix}, \quad \bar{\mathbf{D}} = \begin{pmatrix} \bar{\mathcal{D}}_{t(\Lambda n)} & 0 & 0 \\ 0 & \bar{\mathcal{D}}_{s(\Lambda n)} & 0 \\ 0 & 0 & \bar{\mathcal{D}}_{s(nn)} \end{pmatrix},$$

$$\mathbf{S} = \begin{pmatrix} S_\Lambda & 0 & 0 \\ 0 & S_\Lambda & 0 \\ 0 & 0 & S_n \end{pmatrix}, \quad \bar{\mathbf{B}}^{ji} = \begin{pmatrix} y_{t(\Lambda n)}^2 \frac{\sigma^i \sigma^j}{2} S_\Lambda & y_{s(\Lambda n)} y_{t(\Lambda n)} \frac{\sigma^j}{2} S_\Lambda & y_{s(nn)} y_{t(\Lambda n)} \frac{\sigma^i}{\sqrt{2}} S_n \\ y_{t(\Lambda n)} y_{s(\Lambda n)} \frac{\sigma^i}{2} S_\Lambda & y_{s(\Lambda n)}^2 \frac{1}{2} S_\Lambda & y_{s(nn)} y_{s(\Lambda n)} \frac{1}{\sqrt{2}} S_n \\ y_{t(\Lambda n)} y_{t(nn)} \frac{\sigma^j}{\sqrt{2}} S_n & y_{s(\Lambda n)} y_{s(nn)} \frac{1}{\sqrt{2}} S_n & 0 \end{pmatrix}. \quad (4.11)$$

Writing the integral equation with all operators in the unrenormalized form and using the kinematics in Figure 4.1

$$i\bar{\mathbf{T}}^{ji}(\varepsilon; \mathbf{p}, \mathbf{k}) = i\bar{\mathbf{B}}^{ji}(K_{i_0} - k_{i_0} - B_{i_0} + \varepsilon; \mathbf{p} + \mathbf{k}) + \int \frac{d^4 q}{(2\pi)^4} \\ \times i\bar{\mathbf{B}}^{j\ell}(K_{i_0} - k_{i_0} - B_{i_0} + 2\varepsilon + q_0; \mathbf{p} + \mathbf{q}) i\bar{\mathbf{D}}(K_{i_0} - B_{i_0} + \varepsilon + q_0; \mathbf{q}) \\ \times i\mathbf{S}(k_{i_0} - \varepsilon - q_0; -\mathbf{q}) i\bar{\mathbf{T}}^{\ell i}(\varepsilon + q_0; \mathbf{q}, \mathbf{k}), \quad (4.12)$$

with  $K_{i_0} = \frac{k^2}{2(m_j + m_k)}$ ,  $k_{i_0} = \frac{k^2}{2m_i}$  and  $B_{i_0}$  is the binding energy related to the dimer field  $i$ . Note that both  $K_{i_0}$  and  $k_{i_0}$  are matrix dependent elements.

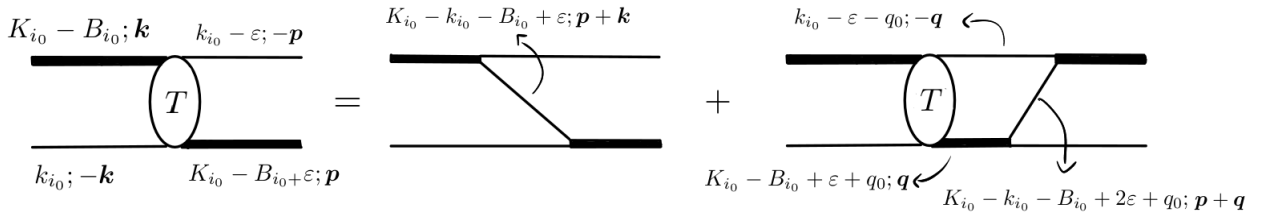


Figure 4.1: The kinematics for the integral equation for the  $\Lambda nn$  system.

We project into doublet channel using the projection operator we derived in Chapter 3

as long as we write the projector as

$$\mathcal{P}_j = \text{diag}(\sigma_j/\sqrt{3}, 1, 1)$$

due to the right projection into singlet and triplet states and neglecting isospin. The projection is given by  $\mathcal{P}_j \mathcal{O}^{ij} \mathcal{P}_i$ , with  $\mathcal{O}^{ij}$  the operators in  $\overline{\mathbf{B}}^{ji}$ . Noting that the projection given by  $\mathcal{P}_j \overline{\mathbf{B}}^{ji} = \overline{\mathbf{B}}^{ji} \mathcal{P}_i$ , the Born term gives

$$\overline{\mathbf{B}} = \begin{pmatrix} -\frac{1}{2}y_{t(\Lambda n)}^2 S_\Lambda & -\frac{\sqrt{3}}{2}y_{s(\Lambda n)}y_{t(\Lambda n)}S_\Lambda & -\sqrt{\frac{3}{2}}y_{s(nm)}y_{t(\Lambda n)}S_n \\ -\frac{\sqrt{3}}{2}y_{t(\Lambda n)}y_{s(\Lambda n)}S_\Lambda & \frac{1}{2}y_{s(\Lambda n)}^2 S_\Lambda & \frac{1}{\sqrt{2}}y_{s(nm)}y_{s(\Lambda n)}S_n \\ -\sqrt{\frac{3}{2}}y_{t(\Lambda n)}y_{t(nm)}S_n & \frac{1}{\sqrt{2}}y_{s(\Lambda n)}y_{s(nm)}S_n & 0 \end{pmatrix}. \quad (4.13)$$

After projecting into doublet channel, the integral equation reads

$$\begin{aligned} \overline{\mathbf{T}}(\varepsilon; \mathbf{p}, \mathbf{k}) &= \overline{\mathbf{B}}(K_{i_0} - k_{i_0} - B_{i_0} + \varepsilon; \mathbf{p} + \mathbf{k}) - i \int \frac{d^4q}{(2\pi)^4} \\ &\times \overline{\mathbf{B}}(K_{i_0} - k_{i_0} - B_{i_0} + 2\varepsilon + q_0; \mathbf{p} + \mathbf{q}) \overline{\mathbf{D}}(K_{i_0} - B_{i_0} + \varepsilon + q_0; \mathbf{q}) \\ &\times \mathbf{S}(k_{i_0} - \varepsilon - q_0; -\mathbf{q}) \overline{\mathbf{T}}(\varepsilon + q_0; \mathbf{q}, \mathbf{k}). \end{aligned} \quad (4.14)$$

Explicitly, the elements of Eq. 4.14 are given by

$$\begin{aligned} \overline{T}_{ba}(\varepsilon; \mathbf{p}, \mathbf{k}) &= \overline{B}_{ba}(K_{a_0} - k_{a_0} - B_{a_0} + \varepsilon; \mathbf{p} + \mathbf{k}) \\ &- i \int \frac{d^4q}{(2\pi)^4} \overline{B}_{bc}(K_{a_0} - k_{a_0} - B_{a_0} + 2\varepsilon + q_0; \mathbf{p} + \mathbf{q}) \\ &\times \overline{D}_c(K_{a_0} - B_{a_0} + \varepsilon + q_0; \mathbf{q}) S_c(k_{a_0} - \varepsilon - q_0; -\mathbf{q}) \overline{T}_{ca}(\varepsilon + q_0; \mathbf{q}, \mathbf{k}), \\ &= y_a y_b \chi_{ba} f_{ba j} S_j(K_{a_0} - k_{a_0} - B_{a_0} + \varepsilon; \mathbf{p} + \mathbf{k}) \\ &- i \sum_{c=1}^3 \int \frac{d^4q}{(2\pi)^4} y_c y_b \chi_{bc} f_{bc i} S_i(K_{a_0} - k_{a_0} - B_{a_0} + 2\varepsilon + q_0; \mathbf{p} + \mathbf{q}) \\ &\times \overline{D}_c(K_{a_0} - B_{a_0} + \varepsilon + q_0; \mathbf{q}) S_c(k_{a_0} - \varepsilon - q_0; -\mathbf{q}) \overline{T}_{ca}(\varepsilon + q_0; \mathbf{q}, \mathbf{k}), \end{aligned} \quad (4.15)$$

with  $f_{ijk} = |\epsilon_{ijk}| + \delta_{ij}(1 - \delta_{jk})\delta_{k3}$ , the Born term  $\overline{B}_{ba} = y_a y_b \chi_{ba} \sum_{c=1}^3 f_{bac} S_c$ , assuming

$S_1 = S_2 = S_n$  and  $S_3 = S_\Lambda$  and  $\chi_{ba}$  is the coefficients matrix written as

$$\chi = \begin{pmatrix} -\frac{1}{2} & -\frac{\sqrt{3}}{2} & -\sqrt{\frac{3}{2}} \\ -\frac{\sqrt{3}}{2} & \frac{1}{2} & \frac{1}{\sqrt{2}} \\ -\sqrt{\frac{3}{2}} & \frac{1}{\sqrt{2}} & 0 \end{pmatrix}, \quad (4.17)$$

$$\begin{aligned} \bar{T}_{ba}(\varepsilon; \mathbf{p}, \mathbf{k}) &= y_a y_b \left\{ \chi_{ba} f_{ba j} S_j(K_{a_0} - k_{a_0} - B_{a_0} + \varepsilon; \mathbf{p} + \mathbf{k}) \right. \\ &\quad - i \sum_{c=1}^3 \left( \frac{y_c}{y_a} \right) \int \frac{d^4 q}{(2\pi)^4} \chi_{bc} f_{bc i} S_i(K_{a_0} - k_{a_0} - B_{a_0} + 2\varepsilon + q_0; \mathbf{p} + \mathbf{q}) \\ &\quad \times \left( \frac{2\pi}{y_c^2 \mu_c} \right) \mathcal{D}_c(K_{a_0} - B_{a_0} + \varepsilon + q_0; \mathbf{q}) S_c(k_{a_0} - \varepsilon - q_0; -\mathbf{q}) \bar{T}_{ca}(\varepsilon + q_0; \mathbf{q}, \mathbf{k}) \left. \right\}, \\ &= y_a y_b \mu_b \left\{ \frac{1}{\mu_b} \chi_{ba} f_{ba j} S_j(K_{a_0} - k_{a_0} - B_{a_0} + \varepsilon; \mathbf{p} + \mathbf{k}) \right. \\ &\quad - i \sum_{c=1}^3 2\pi \int \frac{d^4 q}{(2\pi)^4} \frac{1}{\mu_b} \chi_{bc} f_{bc i} S_i(K_{a_0} - k_{a_0} - B_{a_0} + 2\varepsilon + q_0; \mathbf{p} + \mathbf{q}) \\ &\quad \times \mathcal{D}_c(K_{a_0} - B_{a_0} + \varepsilon + q_0; \mathbf{q}) S_c(k_{a_0} - \varepsilon - q_0; -\mathbf{q}) \frac{1}{y_a y_c \mu_c} \bar{T}_{ca}(\varepsilon + q_0; \mathbf{q}, \mathbf{k}) \left. \right\}. \end{aligned} \quad (4.18)$$

We define the renormalized amplitude as  $T_{ba}(\varepsilon; \mathbf{p}, \mathbf{k}) \equiv \frac{1}{y_a y_b \mu_b} \bar{T}_{ba}(\varepsilon; \mathbf{p}, \mathbf{k})$ , leading to

$$\begin{aligned} T_{ba}(\varepsilon; \mathbf{p}, \mathbf{k}) &= \frac{1}{\mu_b} \chi_{ba} f_{ba j} S_j(K_{a_0} - k_{a_0} - B_{a_0} + \varepsilon; \mathbf{p} + \mathbf{k}) \\ &\quad - i \sum_{c=1}^3 2\pi \int \frac{d^4 q}{(2\pi)^4} \frac{1}{\mu_b} \chi_{bc} f_{bc i} S_i(K_{a_0} - k_{a_0} - B_{a_0} + 2\varepsilon + q_0; \mathbf{p} + \mathbf{q}) \\ &\quad \times \mathcal{D}_c(K_{a_0} - B_{a_0} + \varepsilon + q_0; \mathbf{q}) S_c(k_{a_0} - \varepsilon - q_0; -\mathbf{q}) T_{ca}(\varepsilon + q_0; \mathbf{q}, \mathbf{k}). \end{aligned} \quad (4.19)$$

We can integrate  $q_0$  via residues and write

$$\begin{aligned}
T_{ba}(\varepsilon; \mathbf{p}, \mathbf{k}) &= \frac{1}{\mu_b} \chi_{ba} f_{baj} \frac{1}{K_{a_0} - k_{a_0} - B_{a_0} + \varepsilon - (\mathbf{p} + \mathbf{k})^2/2m_j + i\epsilon} \\
&\quad - \sum_{c=1}^3 2\pi \int \frac{d^3q}{(2\pi)^3} \frac{1}{\mu_b} \chi_{bc} f_{bci} \frac{1}{K_{a_0} - B_{a_0} + \varepsilon - \mathbf{q}^2/2m_c - (\mathbf{p} + \mathbf{q})^2/2m_i + i\epsilon} \\
&\quad \times \mathcal{D}_c(K_{a_0} + k_{a_0} - B_{a_0} - \mathbf{q}^2/2m_c; \mathbf{q}) T_{ca}(k_{a_0} - \mathbf{q}^2/2m_c; \mathbf{q}, \mathbf{k}).
\end{aligned} \tag{4.20}$$

Defining the energy as  $E_i = K_{i_0} + k_{i_0} - B_{i_0} + i\epsilon = k^2/2M_i - B_{i_0} + i\epsilon$ , with  $M_i = \frac{m_i(m_j + m_k)}{m_i + m_j + m_k}$ , the amplitudes read

$$\begin{aligned}
T_{ba}(\varepsilon; \mathbf{p}, \mathbf{k}) &= \frac{1}{\mu_b} \chi_{ba} f_{baj} \frac{1}{E_a - 2k_{a_0} + \varepsilon - (\mathbf{p} + \mathbf{k})^2/2m_j} \\
&\quad - \sum_{c=1}^3 2\pi \int \frac{d^3q}{(2\pi)^3} \frac{1}{\mu_b} \chi_{bc} f_{bci} \frac{1}{E_a - k_{a_0} + \varepsilon - \mathbf{q}^2/2m_c - (\mathbf{p} + \mathbf{q})^2/2m_i} \\
&\quad \times \mathcal{D}_c(E_a - \mathbf{q}^2/2m_c; \mathbf{q}) T_{ca}(k_{a_0} - \mathbf{q}^2/2m_c; \mathbf{q}, \mathbf{k}).
\end{aligned} \tag{4.21}$$

We can obtain the half off-shell amplitudes by setting  $\varepsilon = k_{a_0} - p^2/2m_b = k^2/2m_a - p^2/2m_b$  and then,  $T_{ba}(\mathbf{p}, \mathbf{k}) \equiv T_{ba}(k^2/2m_a - p^2/2m_b; \mathbf{p}, \mathbf{k})$ . With this, we arrive at

$$\begin{aligned}
T_{ba}(\mathbf{p}, \mathbf{k}) &= \frac{1}{\mu_b} \chi_{ba} f_{baj} \frac{1}{E_a - k^2/2m_a - p^2/2m_b - (\mathbf{p} + \mathbf{k})^2/2m_j} \\
&\quad - \sum_{c=1}^3 \int \frac{d^3q}{4\pi^2} \frac{1}{\mu_b} \chi_{bc} f_{bci} \frac{1}{E_a - p^2/2m_b - \mathbf{q}^2/2m_c - (\mathbf{p} + \mathbf{q})^2/2m_i} \\
&\quad \times \mathcal{D}_c(E_a - \mathbf{q}^2/2m_c; \mathbf{q}) T_{ca}(\mathbf{q}, \mathbf{k}), \\
&= \frac{1}{\mu_b} \chi_{ba} f_{baj} \frac{1}{E_a - k^2/2\mu_b - p^2/2\mu_a - \mathbf{p} \cdot \mathbf{k}/m_j} \\
&\quad - \sum_{c=1}^3 \int \frac{d^3q}{4\pi^2} \frac{1}{\mu_b} \chi_{bc} f_{bci} \frac{1}{E_a - p^2/2\mu_c - \mathbf{q}^2/2\mu_b - \mathbf{p} \cdot \mathbf{q}/m_i} \\
&\quad \times \mathcal{D}_c(E_a - \mathbf{q}^2/2m_c; \mathbf{q}) T_{ca}(\mathbf{q}, \mathbf{k}), \\
&= -\frac{\chi_{ba} f_{baj}}{\mu_b} \frac{m_j}{pk \left[ \frac{m_j}{pk} (k^2/2\mu_b + p^2/2\mu_a - E_a) + \cos \theta_{pk} \right]} \\
&\quad + \sum_{c=1}^3 \int \frac{d^3q}{4\pi^2} \frac{\chi_{bc} f_{bci}}{\mu_b} \frac{m_i}{pq \left[ \frac{m_i}{pq} (p^2/2\mu_c - \mathbf{q}^2/2\mu_b - E_a) + \cos \theta_{pq} \right]} \\
&\quad \times \mathcal{D}_c(E_a - \mathbf{q}^2/2m_c; \mathbf{q}) T_{ca}(\mathbf{q}, \mathbf{k}).
\end{aligned} \tag{4.22}$$

Expanding in partial waves, we write

$$\begin{aligned}
T_{ba}(\mathbf{p}, \mathbf{k}) &= \sum_{\ell=0}^{\infty} (2\ell + 1) P_{\ell}(x) t_{ba}^{\ell}(p, k), \\
\Rightarrow t_{ba}^{\ell}(p, k) &= \frac{1}{2} \int_{-1}^1 dx P_{\ell}(x) T_{ba}(\mathbf{p}, \mathbf{k}).
\end{aligned} \tag{4.23}$$

$$\begin{aligned}
\frac{\chi_{ba} f_{baj}}{\mu_b} \frac{m_j}{pk \left[ \frac{m_j}{pk} (k^2/2\mu_b + p^2/2\mu_a - E_a) + \cos \theta_{pk} \right]} &= \sum_{\ell=0}^{\infty} (2\ell + 1) P_{\ell}(x) b_{ba}^{\ell}(p, k), \\
\Rightarrow b_{ba}^{\ell}(p, k) &= \frac{1}{2} \int_{-1}^1 dx P_{\ell}(x) \frac{\chi_{ba} f_{baj}}{\mu_b} \frac{m_j}{pk \left[ \frac{m_j}{pk} (k^2/2\mu_b + p^2/2\mu_a - E_a) + \cos \theta_{pk} \right]}, \\
&= (-1)^{\ell} \frac{\chi_{ba} f_{baj} m_j}{\mu_b pk} Q_{\ell} \left[ \frac{m_j}{pk} (k^2/2\mu_b + p^2/2\mu_a - E_a) \right].
\end{aligned} \tag{4.24}$$

Using angular addition theorem, we write

$$\begin{aligned}
t_{ba}^{\ell}(p, k) &= -b_{ba}^{\ell}(p, k) + \sum_{c=1}^3 \int_0^{\infty} \frac{dq}{\pi} q^2 \mathcal{D}_c(E_a - q^2/2m_c; q) b_{bc}^{\ell}(p, q) t_{ca}^{\ell}(q, k), \\
&= -(-1)^{\ell} \frac{\chi_{ba} f_{baj} m_j}{\mu_b pk} Q_{\ell} \left[ \frac{m_j}{pk} (k^2/2\mu_b + p^2/2\mu_a - E_a) \right] \\
&\quad + \sum_{c=1}^3 \int_0^{\infty} (-1)^{\ell} \frac{\chi_{bc} f_{bci} m_i}{\mu_b pq} Q_{\ell} \left[ \frac{m_i}{pk} (p^2/2\mu_c + q^2/2\mu_b - E_a) \right] \\
&\quad \times \mathcal{D}_c(E_a - q^2/2m_c; q) t_{ca}^{\ell}(q, k).
\end{aligned} \tag{4.25}$$

The  $S$ -wave contribution ( $\ell = 0$ ) is given by

$$\begin{aligned}
t_{ba}^0(p, k) &= -\frac{\chi_{ba} f_{baj} m_j}{\mu_b} \frac{1}{2pk} \ln \left[ \frac{\frac{\mu_b}{\mu_a} p^2 + k^2 - 2\mu_b E_a + \frac{2\mu_b}{m_j} pk}{\frac{\mu_b}{\mu_a} p^2 + k^2 - 2\mu_b E_a - \frac{2\mu_b}{m_j} pk} \right] \\
&\quad + \sum_{c=1}^3 \int_0^{\infty} \frac{\chi_{bc} f_{bci} m_i}{\mu_b} \frac{1}{2pq} \ln \left[ \frac{\frac{\mu_b}{\mu_c} p^2 + k^2 - 2\mu_b E_a + \frac{2\mu_b}{m_i} pk}{\frac{\mu_b}{\mu_c} p^2 + k^2 - 2\mu_b E_a - \frac{2\mu_b}{m_i} pk} \right] \\
&\quad \times \mathcal{D}_c(E_a - q^2/2m_c; q) t_{ca}^0(q, k).
\end{aligned} \tag{4.26}$$

We are interested in resonances, searching for them numerically, requires the calculation of a zero of the determinant of  $(\mathbb{I} - \mathbb{K})$ . Only the homogeneous integral equation matters for this purpose, then, we can solve any column of the matrix of the amplitudes  $\mathbf{T}$ . We will consider the amplitudes  $A(p, k)$  ( $T_{t(\Lambda n) \rightarrow t(\Lambda n)}$ ),  $B(p, k)$  ( $T_{t(\Lambda n) \rightarrow s(\Lambda n)}$ ) and

$C(p, k)$  ( $T_{t(\Lambda n) \rightarrow s(nn)}$ ), leading to eight homogeneous coupled integral equations

$$\begin{aligned}
A(p, k) = & -\frac{1}{2\pi} \frac{m_\Lambda}{\mu(\Lambda n)} \int_0^\Lambda dq q^2 K_1(p, q; E) \frac{1}{\frac{1}{a_{t(\Lambda n)}} - \sqrt{\frac{\mu(\Lambda n)}{M_\Lambda} q^2 - 2\mu(\Lambda n)E}} A(q, k) \\
& -\frac{\sqrt{3}}{2\pi} \frac{m_\Lambda}{\mu(\Lambda n)} \int_0^\Lambda dq q^2 K_1(p, q; E) \frac{1}{\frac{1}{a_{s(\Lambda n)}} - \sqrt{\frac{\mu(\Lambda n)}{M_\Lambda} q^2 - 2\mu(\Lambda n)E}} B(q, k) \\
& -\sqrt{\frac{3}{2}} \frac{1}{\pi} \frac{m_n}{\mu(nn)} \int_0^\Lambda dq q^2 K_2(p, q; E) \frac{1}{\frac{1}{a_{s(nn)}} - \sqrt{\frac{m_n}{2M_n} q^2 - m_n E}} C(q, k),
\end{aligned} \tag{4.27}$$

$$\begin{aligned}
B(p, k) = & -\frac{\sqrt{3}}{2\pi} \frac{m_\Lambda}{\mu(\Lambda n)} \int_0^\Lambda dq q^2 K_1(p, q; E) \frac{1}{\frac{1}{a_{t(\Lambda n)}} - \sqrt{\frac{\mu(\Lambda n)}{M_\Lambda} q^2 - 2\mu(\Lambda n)E}} A(q, k) \\
& +\frac{1}{2\pi} \frac{m_\Lambda}{\mu(\Lambda n)} \int_0^\Lambda dq q^2 K_1(p, q; E) \frac{1}{\frac{1}{a_{s(\Lambda n)}} - \sqrt{\frac{\mu(\Lambda n)}{M_\Lambda} q^2 - 2\mu(\Lambda n)E}} B(q, k) \\
& +\frac{1}{\sqrt{2}\pi} \frac{m_n}{\mu(nn)} \int_0^\Lambda dq q^2 K_2(p, q; E) \frac{1}{\frac{1}{a_{s(nn)}} - \sqrt{\frac{m_n}{2M_n} q^2 - m_n E}} C(q, k),
\end{aligned} \tag{4.28}$$

$$\begin{aligned}
C(p, k) = & -\sqrt{\frac{3}{2}} \frac{1}{\pi} \frac{m_n}{\mu(\Lambda n)} \int_0^\Lambda dq q^2 K_3(p, q; E) \frac{1}{\frac{1}{a_{t(\Lambda n)}} - \sqrt{\frac{\mu(\Lambda n)}{M_\Lambda} q^2 - 2\mu(\Lambda n)E}} A(q, k) \\
& +\frac{1}{\sqrt{2}\pi} \frac{m_n}{\mu(\Lambda n)} \int_0^\Lambda dq q^2 K_3(p, q; E) \frac{1}{\frac{1}{a_{s(\Lambda n)}} - \sqrt{\frac{\mu(\Lambda n)}{M_\Lambda} q^2 - 2\mu(\Lambda n)E}} B(q, k).
\end{aligned} \tag{4.29}$$

with  $M_\Lambda = \frac{m_n(m_n + m_\Lambda)}{2m_n + m_\Lambda}$  and  $M_n = \frac{2m_n m_\Lambda}{2m_n + m_\Lambda}$ . And the kernels  $K_1$ ,  $K_2$  and  $K_3$  are

given by

$$K_1(p, k; E) = \frac{1}{2pk} \ln \left( \frac{p^2 + k^2 - 2\mu_{(\Lambda n)}E + \frac{2\mu_{(\Lambda n)}}{m_\Lambda}pk}{p^2 + k^2 - 2\mu_{(\Lambda n)}E - \frac{2\mu_{(\Lambda n)}}{m_\Lambda}pk} \right), \quad (4.30)$$

$$K_2(p, k; E) = \frac{1}{2pk} \ln \left( \frac{\frac{m_n}{2\mu_{(\Lambda n)}}p^2 + k^2 - m_nE + pk}{\frac{m_n}{2\mu_{(\Lambda n)}}p^2 + k^2 - m_nE - pk} \right), \quad (4.31)$$

$$K_3(p, k; E) = \frac{1}{2pk} \ln \left( \frac{p^2 + \frac{m_n}{2\mu_{(\Lambda n)}}k^2 - m_nE + pk}{p^2 + \frac{m_n}{2\mu_{(\Lambda n)}}k^2 - m_nE - pk} \right). \quad (4.32)$$

We introduced a sharp momentum cutoff  $\Lambda$  assuming  $E, k \sim 1/a_{nn} \sim 1/a_{s,t(\Lambda n)} \lesssim p \ll \Lambda$ . In order to obtain resonances, we run our codes with these coupled equations, the results are presented in Chapter 5. The projection matrix we used in our codes is given by the coefficients and the mass factors and is written as

$$\chi = \begin{pmatrix} -\frac{m_\Lambda}{\mu_{(\Lambda n)}} \frac{1}{2} & -\frac{m_\Lambda}{\mu_{(\Lambda n)}} \frac{\sqrt{3}}{2} & -\frac{m_n}{\mu_{(nn)}} \sqrt{\frac{3}{2}} \\ -\frac{m_\Lambda}{\mu_{(\Lambda n)}} \frac{\sqrt{3}}{2} & \frac{m_\Lambda}{\mu_{(\Lambda n)}} \frac{1}{2} & \frac{m_n}{\mu_{(nn)}} \frac{1}{\sqrt{2}} \\ -\frac{m_n}{\mu_{(\Lambda n)}} \sqrt{\frac{3}{2}} & \frac{m_n}{\mu_{(\Lambda n)}} \frac{1}{\sqrt{2}} & 0 \end{pmatrix}. \quad (4.33)$$



# Chapter 5

## Results

In this chapter, we present our numerical results. It is divided in two main sections: the first one is based on results using the EFT described in Chapter 4, which considers only contact interactions at leading order and the last section presents results using a phenomenological model based on [34], a model that is constructed using separable potentials, specifically rank-one Yamaguchi potentials. The  $nn$  interaction is reasonably well-known [89, 90, 91] but in contrast, the  $\Lambda n$  interaction is poorly known. Efforts have been made to determine a precise value for the  $\Lambda n$  interaction using charge symmetry breaking (CSB) in the data of bound states of a few  $\Lambda$  hypernuclei, specifically the  ${}^4_{\Lambda}\text{H}$  and the  ${}^4_{\Lambda}\text{He}$ , using the binding energy their of ground states to estimate the difference of these mirror hypernuclei [92]. However, recent publications have questioned the data of  ${}^4_{\Lambda}\text{H}$  and  ${}^4_{\Lambda}\text{He}$  [93, 94].

### 5.1 EFT approach

All results in this section are obtained by solving the homogeneous Eqs. (4.27), (4.28), and (4.29). As a first test, we compare our results for a possible  $\Lambda nn$  bound state with the ones from the literature. Although there are several theoretical works that exclude the existence of a  $\Lambda nn$  bound state [26, 27, 28, 29, 30, 31, 32], we wish to ensure that our numbers are at least consistent with previous works. We compare our results with the ones from Ref. [85], which also describes the bound  $\Lambda nn$  system using  $\not\text{EFT}$ . They can be seen in Figures 5.1 and 5.2. Figure 5.1 shows the binding energy of the  $\Lambda nn$  system as a function of the momentum cutoff  $\Lambda$  without contribution from the three-body force. The first bound state appears at  $\Lambda \sim 1.5$  GeV and the second at  $\Lambda \sim 80$  GeV. The results were in perfect agreement with reference [85]. Figure 5.2 presents the plot of the strength of the three-body contact interaction,  $g(\Lambda)$  as a function of the cutoff  $\Lambda$ . This plot is obtained with the binding energy value  $B = 0$ . It shows the universal discrete

scaling factor  $g(\Lambda_{n+1}) = g(\Lambda_1) = 0$  for  $\Lambda_{n+1} = \Lambda_1 e^{n\pi/s_0}$ . Theoretical calculations give  $s_0 \approx 0.803$  and the values obtained from the plot are  $\Lambda_1 \approx 1.52$  GeV and  $\Lambda_2 \approx 76.55$  GeV, which gives  $s_0 = \pi \ln(\Lambda_2/\Lambda_1) \approx 0.801$ . This result suggests a universal behavior of the  $\Lambda nn$  system. As both ours and Ref. [85] results are in good agreement, we adapted our codes in order to search for resonances. In Appendix E, one can understand in details the algorithm we used to search for resonances.

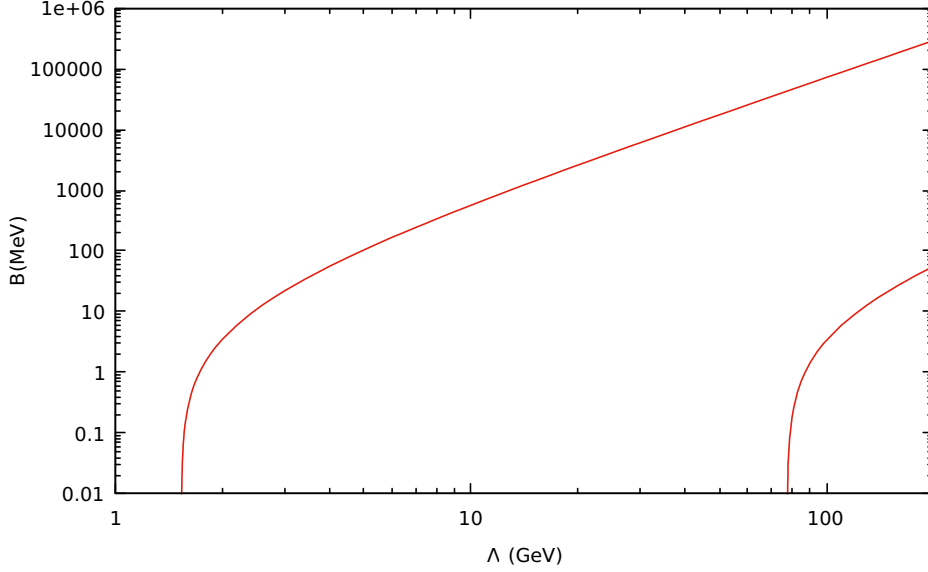


Figure 5.1: Plot of the binding energy as a function of the cutoff  $\Lambda$ . There is no contribution from the three-body force in this plot,  $g(\Lambda) = 0$ .

The values for the scattering parameters used as input for the  $nn$  interaction are  $a_{nn} = -18.9 \pm 0.4$  fm and  $r_{nn} = 2.75 \pm 0.11$  fm [89]. As there are no experimental data for the  $\Lambda n$  interaction and, as pointed out by [34, 95], the difference between the  $\Lambda p$  and the  $\Lambda n$  interaction might be substantially different, we avoid using the scattering parameters from [85]. Instead, we opt to use numbers from the Nijmegen potential model D [37]. The scattering parameters are given in Table 5.1.

	$\Lambda p$	$\Lambda n$
$a_s$	$-1.77 \pm 0.28$ fm	$-2.03 \pm 0.32$ fm
$r_s$	$3.78 \pm 0.35$ fm	$3.66 \pm 0.32$ fm
$a_t$	$-2.06 \pm 0.12$ fm	$-1.84 \pm 0.10$ fm
$r_t$	$3.18 \pm 0.12$ fm	$3.32 \pm 0.11$ fm

Table 5.1: The effective range parameters for both singlet ( $a_s, r_s$ ) and triplet ( $a_t, r_t$ ) channels of  $\Lambda n$  given by the Nijmegen model D [37]. We present the values for the  $\Lambda p$  interaction just for completeness.

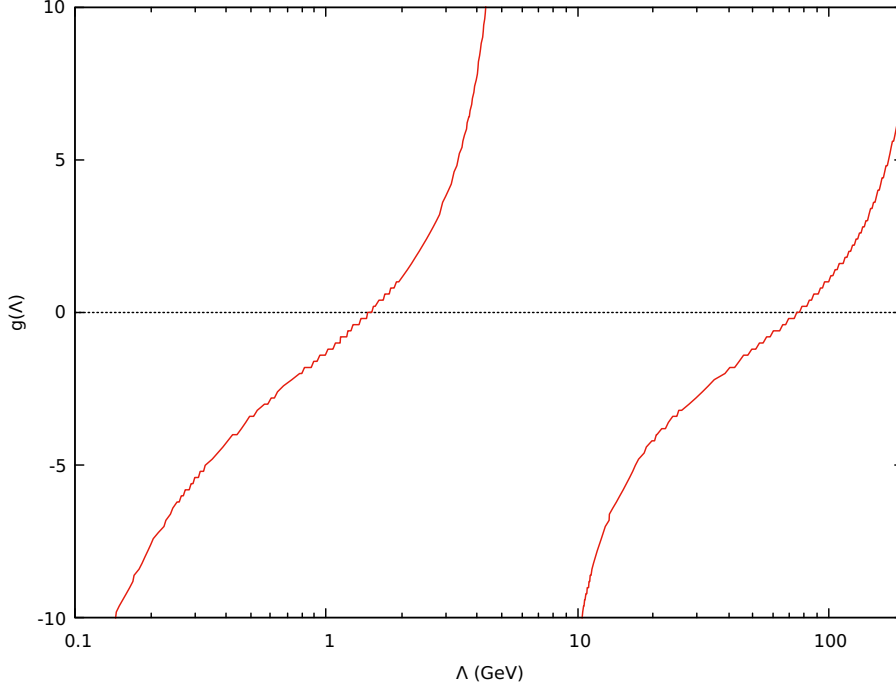


Figure 5.2: The three-body force strength  $g(\Lambda)$  as a functions of the cutoff  $\Lambda$ . The binding energy was set equal to zero,  $B = 0$ .

Although the values from Table 5.1 suggests that the condition  $r_2/a_2 \ll 1$  is not satisfied, we will assume that it holds knowing that there are no experimental numbers for these quantities and that the phenomenological numbers from [37] may not reproduce these unknown physical values. It is important to note that the  $^1S_0(nn)$  channel does satisfy  $r_2/a_2 \ll 1$ . Assuming all channels satisfy a perturbative expansion, we are allowed to work with only the scattering length  $a_2$  (in their respective channels) at LO. In the next section, we will consider a phenomenological model already used by [34], in which both scattering parameters,  $a_2$  and  $r_2$  are effectively taken into account.

For the purpose of searching for the pole trajectory of the  $S$ -matrix, we artificially multiply our scattering amplitude of both singlet and triplet channels of the  $\Lambda n$  interaction by a scaling factor  $s_{EFT}$ . Our strategy is to set a momentum cutoff  $\Lambda$  that would return a zero binding energy state for  $s_{EFT} = 1.0$ . The value for such cutoff is  $\Lambda = 1357.5$  MeV. One then would expect to find resonances for decreasing values of  $s_{EFT} < 1.0$ . The contrary is also true, when one increases the value of the scaling factor  $s_{EFT} > 1.0$ , deeper bound states appear. We also use the strength of the three-body contact interaction  $g(\Lambda)$  as a parameter. We expect that negative values of  $g(\Lambda)$  would lead to a more attractive state, resulting in a deeper bound state, since we fix  $g(\Lambda) = 0$  to the zero binding energy state. On the other hand, positive values of  $g(\Lambda)$  would lead to resonances, as it adds a more repulsive interaction. For all plots in this section, we use the contour rotation described

in E.2 of type  $\int_0^\Lambda$  as we need to integrate over a finite cutoff within EFT.

### 5.1.1 Scattering length $a_2$ as a parameter

Our first result is shown in Figure 5.3. For this plot, we set the effective range  $r_2$  in all channels, as well as the strength of the three-body force  $g(\Lambda)$ , to zero. The lowest value of the scaling factor we consider is  $s_{EFT} = 0.66$ . Points located at the negative real axis are bound states with  $s_{EFT} > 1.0$ , for instance, the point with energy  $E = -0.22 - 0.0i$  MeV is obtained with  $s_{EFT} = 1.05$ . The point with  $s_{EFT} = 1.0$  is located at  $E = -0.0006 - 0.0i$  MeV. In principle, by construction, at  $\Lambda = 1357.5$  MeV the corresponding binding energy would be zero. However, to the decimal precision we are working, a 0.1 MeV smaller cutoff already gives us a resonance. As soon as the scaling factor decreases from 1.0, the first resonance appears, located at  $E = 0.02987 - 0.00282i$  MeV with  $s_{EFT} = 0.99$ . A specific behavior is shown in this plot—for certain values of the resonance energy, they become an accumulation point and jump to poles with almost the same imaginary value, but with different real values of the energy. For instance, the point with energy  $E = 1.3500 - 0.6353i$  MeV has  $s_{EFT} = 0.71$ . When  $s_{EFT}$  is decreased to  $s_{EFT} = 0.70$ , the resonance energy moves to  $E = 1.6838 - 0.6363i$  MeV. For all  $s_{EFT}$  values we could investigate our poles have shown  $\text{Re}[E] > 0$ , and by definition, they are called physical resonances. It is important to highlight that if  $\text{Re}[E] < 0$  the respective pole lies below the break-up threshold, therefore, it is called an unphysical pole. In Appendix F we provide the numerical values of the energy poles in Table F.2.

### 5.1.2 Strength $g(\Lambda)$ as a parameter

Before we proceed, an important information comes in order here. In Eq. (4.4) we consider only a three-body interaction in the  $\Lambda n$  triplet channel and neglect the others in the singlet  $^1S_0(nn)$  and the singlet  $^1S_0(\Lambda n)$  channels. As pointed out in Ref. [85], there are not enough data to pin down all these (in principle) three couplings, and the choice is based on the assumption that the triplet  $\Lambda n$  channel ought to be phenomenologically more important than the others.

Figure 5.4 shows the pole trajectory as a function of the strength of the three-body interaction,  $g(\Lambda)$ . For this plot, we varied  $g(\Lambda)$  from  $-0.3$  to  $1.6$ . The scaling factor is fixed at  $s_{EFT} = 1.0$ . As before, we set the effective range  $r_2$  to zero in all channels. Negative values of  $g(\Lambda)$  produce a bound state, for instance,  $E = -0.135 - 0.0i$  MeV with  $g(\Lambda) = -0.1$ . The point with  $g(\Lambda) = 0$  is located at  $E = -0.0006 - 0.0i$  MeV. For a value of  $g(\Lambda)$  slightly above 0, a resonance appears, for instance, at  $g(\Lambda) = 0.05$  one gets a pole at the energy is  $E = 0.04452 - 0.00657i$  MeV. The same pattern behavior

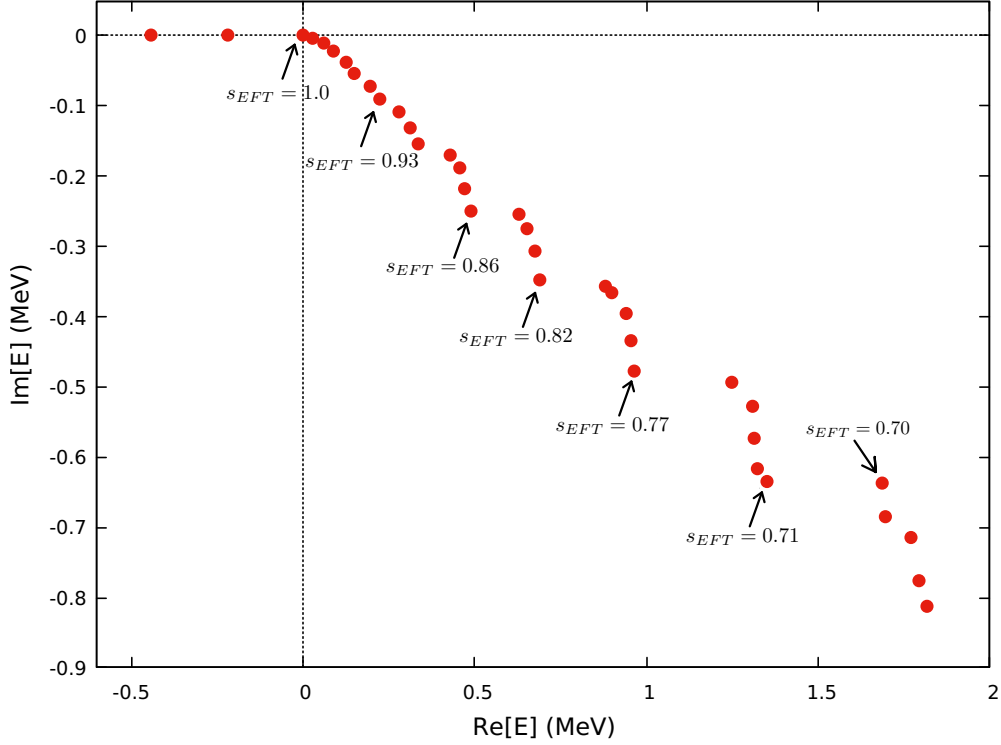


Figure 5.3: Pole trajectory as a function of the scattering length  $a_2$ .

observed in Figure 5.3 is also shown when we vary  $g(\Lambda)$ , in Figure 5.4. In the latter, as in the former, there are accumulation points of poles up to a specific value of  $g$ , and above that, a considerable change in the real part, but not in the imaginary part, takes place. For example, a pole with energy  $E = 0.6622 - 0.3521i$  MeV is obtained with  $g(\Lambda) = 1.0$ , and when  $g$  changes to  $g(\Lambda) = 1.1$ , the pole moves abruptly to  $E = 0.8518 - 0.3581i$  MeV. In Figure 5.4, all resonances are physical, in the sense that  $\text{Re}[E] > 0$ . In Appendix F we provide the numerical values of the energy poles in Table F.3

When combining Figures 5.3 and 5.4 as shown in Figure 5.5, one can see not just a similar behavior, but that both plots are in good agreement for small values of the resonance energy  $\text{Re}[E] \sim 0.4$  MeV. As the energy increases they start to deviate from each other, although, the general behavior is present.

We introduce another scaling factor that multiplies only the effective range  $r_{2(\Lambda n)}$ , both in the triplet and the singlet channels. This factor is fixed to  $s_{r_{2(\Lambda n)}} = 10^{-2}$ . The main reason for introducing this factor is trying to understand how a perturbative value of  $r_{2(\Lambda n)}$  would change the previous results. For this case, we also vary the scattering length  $a_2$ , with the same scaling factor  $s_{EFT}$  used previously. The effective range of the  $nn$  interaction is fixed at  $r_{2(nn)} = 0$ . The values assumed by  $s_{EFT}$  are in the range  $[1.1, 0.79]$ . The results for a perturbative  $r_{2(\Lambda n)}$  in the  $\Lambda n$  interaction, with varying  $a_2$ , are shown in Figure 5.6. One can notice that a value of  $r_{2(\Lambda n)}$  that is different from zero starts to deviate

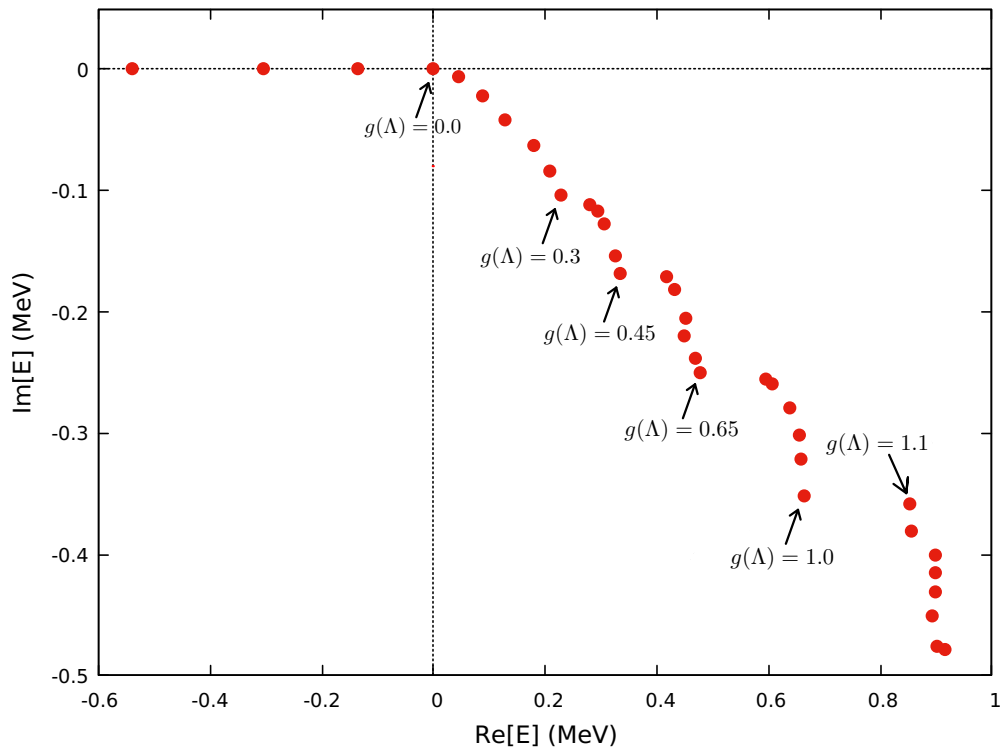


Figure 5.4: Pole trajectory as a function of the three-body strength  $g(\Lambda)$ .

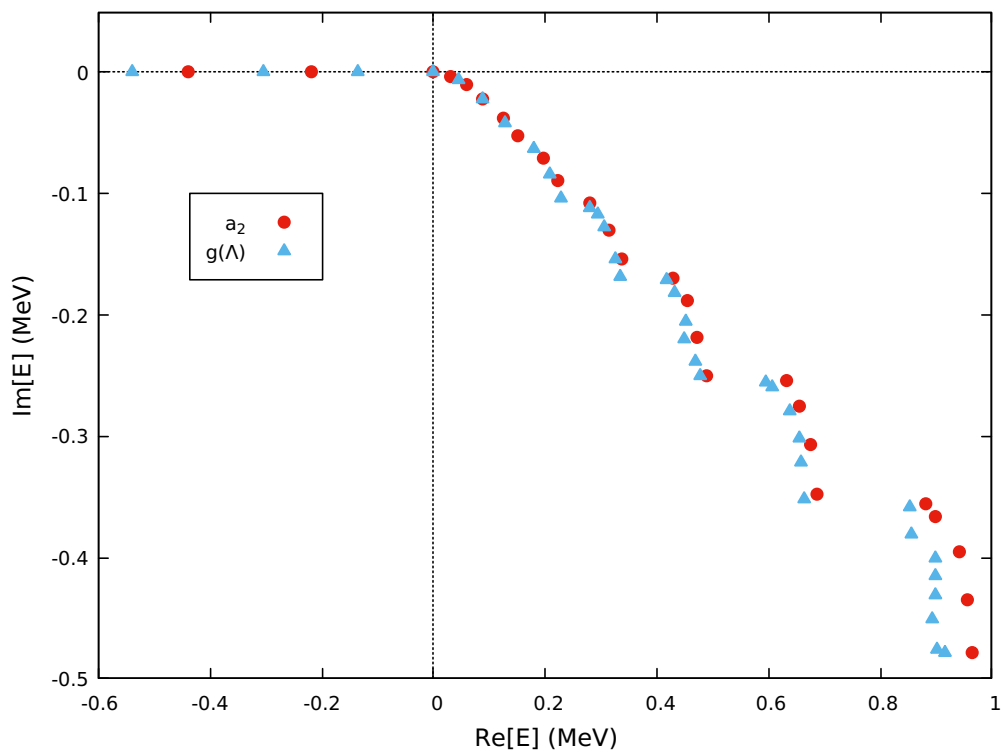


Figure 5.5: Combined plot of Figure 5.3 and 5.4.

for energies with  $\text{Re}[E] > 0.4$  MeV from the case with  $r_{2(\Lambda n)} = 0$ . Nevertheless, such deviations remain relatively small, given the fact that we keep  $s_{r_{2(\Lambda n)}} = 10^{-2}$  well within the perturbative regime.

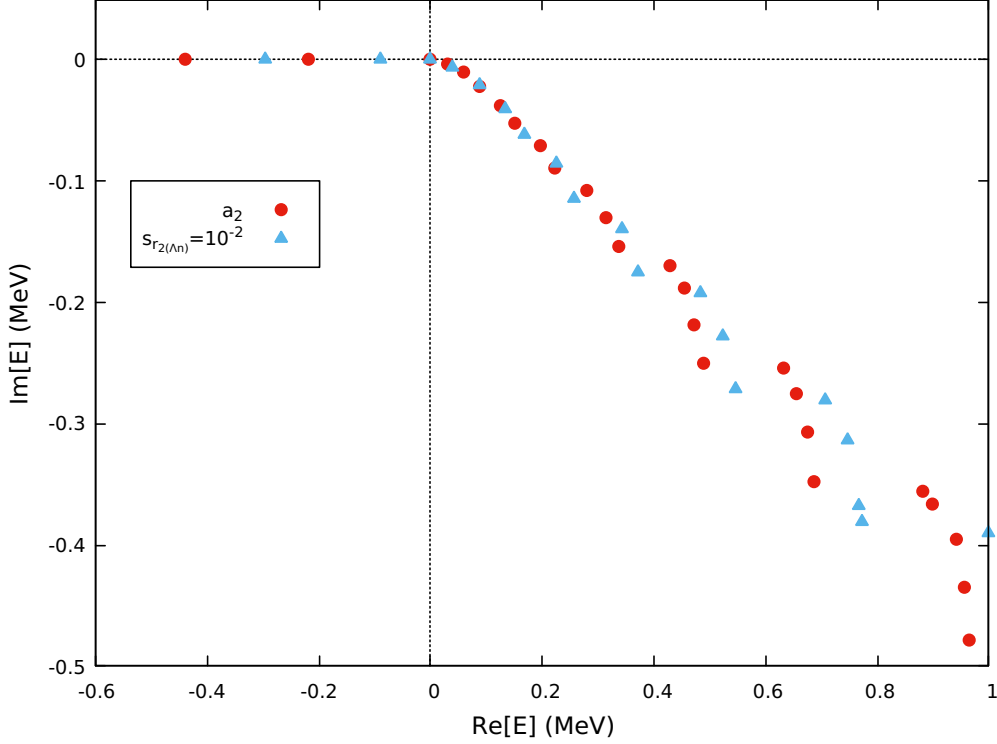


Figure 5.6: Combined plot of  $r_{2(\Lambda n)}$  perturbative and 5.3

## 5.2 Phenomenological approach: Separable potentials

In this section we approach the problem in a different way. If in Section 5.1, we wanted to work in a perturbative scenario with  $r_2/a_2 \ll 1$ , now we are going to properly include the effective range into our calculations, even in the case where the assumption  $r_2/a_2 \ll 1$  fails. This justifies the use of this model, to describe the physics where possibly the EFT assumptions fail. Appendix D presents the theory of the two-body sector of the separable potentials. We need to solve the Faddeev equations for the three-body systems with the abovementioned two-body separable potentials to obtain the pole trajectory.

For convenience, we collect the relevant two-body expressions for the rank-one separable Yamaguchi potential [98]. It is given by

$$V(k', k) = g(k')Cg(k) \quad \text{with} \quad g(k) = \frac{1}{k^2 + \alpha^2}, \quad (5.1)$$

where  $C$  is the strength of the potential and  $\alpha$  is the range of the interaction. Using

Eqs. (D.6) and (D.9) from Appendix D, we match the scattering parameters with the coefficients  $C$  and  $\alpha$ , which gives

$$\frac{1}{a_2} = \frac{\alpha}{2} \left( 1 + \frac{2\alpha^3}{\pi\mu C} \right) \quad \text{and} \quad r_2 = \frac{1}{\alpha} \left( 1 - \frac{4\alpha^3}{\pi\mu C} \right). \quad (5.2)$$

Solving for  $\alpha$  and  $C$  we get

$$\alpha = \frac{1}{2r_2} \left[ 3 + \sqrt{9 - 16 \frac{r_2}{a_2}} \right] \quad \text{and} \quad C = \frac{4\alpha^3}{\pi\mu(1 - \alpha r_2)}. \quad (5.3)$$

The values of the parameters of the separable potential are given in Table 5.2 We write

$\alpha_{s(nn)}$	1.1574 fm <sup>-1</sup>
$\alpha_{s(\Lambda n)}$	1.2503 fm <sup>-1</sup>
$\alpha_{t(\Lambda n)}$	1.3786 fm <sup>-1</sup>
$C_{s(nn)}$	-0.37986 fm <sup>-2</sup>
$C_{s(\Lambda n)}$	-0.2692 fm <sup>-2</sup>
$C_{t(\Lambda n)}$	-0.3608 fm <sup>-2</sup>

Table 5.2: The separable potential parameters determined in terms of the scattering parameters for channels  $^1S_0(nn)$ ,  $^1S_0(\Lambda n)$  and  $^3S_1(\Lambda n)$ .

the homogeneous Faddeev equation as [96]

$$T_i(p; E) = \sum_j \int_0^\infty dq K_{ij}(p, q; E) T_j(q; E), \quad (5.4)$$

where the kernel of the integral equation is given by

$$K_{ij}(p, q; E) = q^2 B_{ij}(p, q; E) S_j(q; E - q^2/2\mu), \quad (5.5)$$

with  $\mu$  the reduced mass of the three-body system and  $S_j(q; E)$  being the quasiparticle propagator written as

$$S_j(E^+) = \left\{ C_j^{-1} - \frac{\pi\mu}{2\mu E^+ + \alpha_j^2} \left( \frac{2\mu E^+ - \alpha_j^2}{2\alpha_j} - i\sqrt{2\mu E^+} \right) \right\}^{-1}. \quad (5.6)$$

The Born term  $B_{ij}(p, q; E)$  reads

$$B_{ij}(q, q'; E) = \int_{-1}^1 dx C_i C_j \frac{g(p)g(p')P_\ell(x)}{E - \frac{q^2}{2m_1} - \frac{q'^2}{2m_2} - \frac{(q+q')^2}{2m_3} + i\epsilon}, \quad (5.7)$$

with  $\mathbf{p} = -\mathbf{q}' - \frac{m_2}{m_2+m_3}\mathbf{q}$  and  $\mathbf{p}' = \mathbf{q} - \frac{m_1}{m_1+m_3}\mathbf{q}'$ . The subindices  $i$  and  $j$  stand for the possible different channels. For each channel, we assume different ranges  $\alpha_{s(nn)}$ ,  $\alpha_{s(\Lambda n)}$ ,



and  $\alpha_{t(\Lambda n)}$ . The above expression contains an integral that can be solved analytically. After integration one gets

$$B_{ij}(p, q; E) = m_3 C_i C_j \frac{(-1)^{\ell+1}}{pq} \left[ \frac{1}{(a-b)(a-c)} Q_\ell \left( \frac{a}{pq} \right) + \frac{1}{(b-a)(b-c)} Q_\ell \left( \frac{b}{pq} \right) + \frac{1}{(c-a)(c-b)} Q_\ell \left( \frac{c}{pq} \right) \right], \quad (5.8)$$

where  $Q_\ell(x)$  is the Legendre polynomials of the second kind, and

$$\begin{aligned} a &= \frac{q^2}{2\xi_{13}} + \frac{q'^2}{2\xi_{23}} - m_3(E + i\epsilon), \\ b &= q'^2 + \xi_{13}q^2 + \alpha_2^2, \\ c &= q^2 + \xi_{23}q'^2 + \alpha_1^2, \end{aligned} \quad (5.9)$$

with  $\xi_{13} = \frac{m_1}{m_1+m_3}$  and  $\xi_{23} = \frac{m_2}{m_2+m_3}$ .

It is important to mention that we use the same spin projection matrix as calculated in Chapter 4 and used in our expressions of Section 5.1. The contour rotation described in E.2 is of the type  $\int_0^\infty$  and we make the change of variable  $q \sim \frac{x}{1-x}$  to map the range of integration from  $[0, \infty[$  to  $[0, 1]$ . That requires multiplying  $x/(1-x)$  by a constant with units of momentum. A convenient choice is the deuteron binding momentum,  $\gamma_d = 45.7169$  MeV, as in the  $\Lambda nn$  system one would not expect a typical momentum much far from this value. The fixed contour deformation angle is  $\theta = 60^\circ$ . In order to trace the trajectory of the pole, we use a scaling factor  $s$  that multiplies the strength of the potential in channels  $^1S_0(\Lambda n)$  and  $^3S_1(\Lambda n)$ , *i.e.*, we only scale the  $\Lambda n$  interaction,

$$C_{s(\Lambda n)} \rightarrow sC_{s(\Lambda n)} \quad C_{t(\Lambda n)} \rightarrow sC_{t(\Lambda n)}. \quad (5.10)$$

Figure 5.7 shows the pole trajectory of the  $\Lambda nn$  system considering our phenomenological model with Yamaguchi form factors. We start by setting the smallest value of  $s$  that holds a bound state. We know that larger values of  $s$  generate tighter bound states, and smaller enough values give rise to resonances. The deeper bound state shown in the figure has the scaling factor of  $s = 1.8$ , with energy  $E = -0.23 - 0.0i$  MeV. The first resonance energy appears at  $E = 0.001627 - 0.000360i$  MeV with scaling parameter  $s = 1.725$ , which is also the closest that we get from the zero energy. The next pole that is important to mention is the last resonance that is physical, whose energy is given by  $E = 0.000119 - 0.15i$  MeV for the scaling factor  $s = 1.625$ . Unphysical resonances, or sometimes called subthreshold resonances,  $\text{Re}[E] < 0$ , are located at the third quadrant of the complex energy plane. The smaller value for the scaling factor that we consider

is  $s = 1.525$ , and that corresponds to an energy of  $E = -0.1915 - 0.3320i$  MeV. In Appendix F we provide the numerical values of the poles in Figure 5.7 in Table F.4.

A value of  $s$  that is larger than 70% of the original parameters may provide unrealistic values for the scattering parameters of the  $\Lambda n$  interaction. A possible way to overcome the mismatch of the  $\Lambda n$  interaction with the possible existence of a  $\Lambda nn$  bound state/resonance is to add a 3-body force  $g(\Lambda)$  in such a way that allows one to lower the value of the scaling parameter  $s$ .

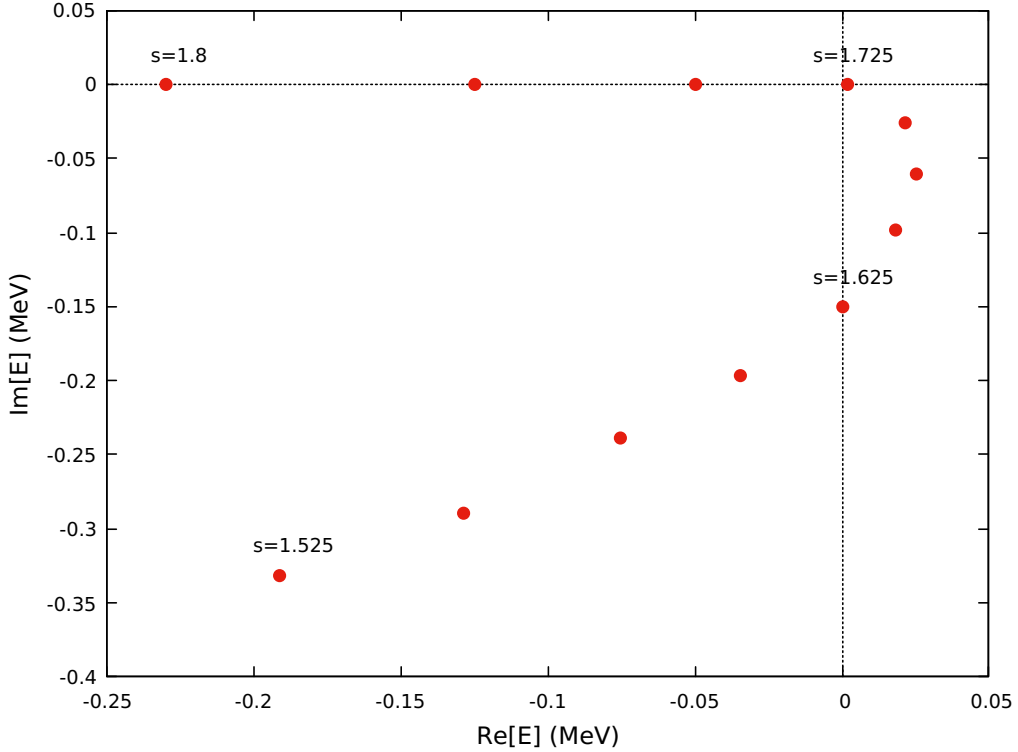


Figure 5.7: Pole trajectory of the  $\Lambda nn$  system using Yamaguchi form factors.

As shown in Chapter 4, the three channels we consider so far involve each pairwise angular momentum and total angular momentum of the three particles equal zero. However, in reference [34], a fourth channel was considered. This fourth channel consists of all three-particle spins aligned ( $S_{tot} = 3/2$ ), with  $\Lambda n$  in the triplet channel aligned with the spin of the remaining neutron), coupled with relative orbital angular momentum  $\mathcal{L} = 2$  (the angular momentum between a neutron and the center-of-mass of the  $\Lambda n$  pair). This channel also contributes to the spin-doublet channel, thought in EFT, due to the higher angular momentum, it shall be considered a higher-order term. In order to simulate such fourth channel, we naively add the same matrix elements of the  ${}^3S_1(\Lambda n)$  channel in the kernel of the integral equation. The results of introducing this naive fourth channel is given in Figure 5.8. One can see that, with this fourth channel, one needs smaller values of the scaling factor  $s$  to achieve a given pole as compared to

Figure 5.7. The last bound state before zero binding energy is achieved with  $s = 1.45$ , whose pole is located at  $E = -0.0125 - 0.0i$  MeV. The deeper bound state is located at  $E = -0.3167 - 0.0i$  MeV with  $s = 1.5$ . The first physical resonance appears with a pole  $E = 0.04496 - 0.02188i$  MeV for a scaling factor  $s = 1.425$ . By decreasing the scaling factor, the last physical resonance we could find is at  $s = 1.3$  with energy pole given by  $E = 0.05434 - 0.41311i$  MeV, since for  $s = 1.275$ , the real part of the corresponding pole energy is already negative,  $E = -0.000105 - 0.51666i$  MeV. The smaller value we plot is with scaling factor  $s = 1.2$ , with pole energy  $E = -0.2965 - 0.8144i$  MeV. As said before, we expect that introducing a fourth channel would be a higher order correction, however, from Figure 5.8 it appears that the addition of the fourth channel gives a sizeable contribution. A attempt to match the EFT expectation and this phenomenological calculation is to add a three-body force in the latter, that could simulate the bulk of changes of the fourth channel within the original three-channel approach, and hopefully making the fourth channel perturbative. More reliable calculations are needed to confirm this speculation.

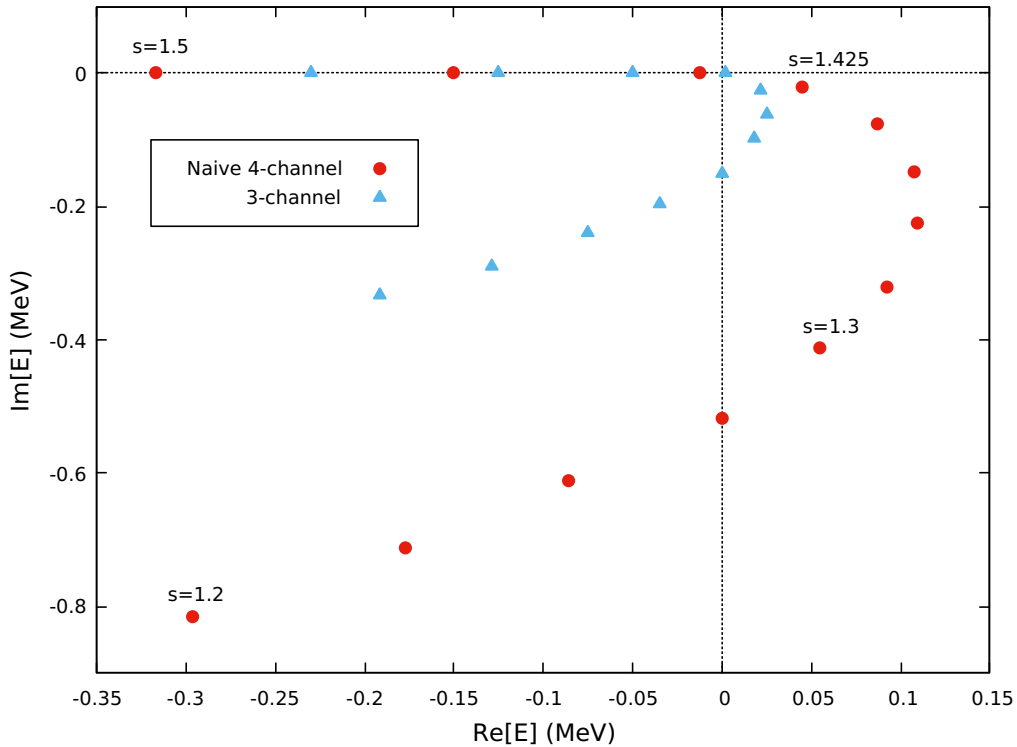


Figure 5.8: Pole trajectory when adding a naive fourth channel and compared with the three-channel plot.

Figure 5.9 compares our results with the naive fourth channel (shown in Figure 5.8) and the trajectory of Afnan and Gibson [34]. For the sake of visualisation, we changed the name of the scaling factor used by Afnan and Gibson to  $s_A$ . In comparing our energy

located at  $E = 0.04496 - 0.02189i$  MeV with  $s = 1.425$  with the closest energy by the authors at  $E = 0.043 - 0.014i$  MeV with  $s_A = 1.325$ , we notice a difference of  $\Delta_s = 0.1$ . When comparing their last bound state located at  $E = -0.158 - 0.0i$  MeV with  $s_A = 1.4$  with our energy at  $E = -0.15 - 0.0i$  MeV with  $s = 1.475$ , we notice that the difference is smaller, around 7.5%. On the other hand, if we compare our unphysical resonance located at  $E = -0.1773 - 0.7116i$  MeV with  $s = 1.225$  with their last (and actually, the potential without any scaling factor, *i.e.*,  $s_A = 1.0$ ) located at  $E = -0.154 - 0.753i$  MeV, the difference is larger and around 22.5%. Therefore, the differences between our naive four-channel and the four-channel approach of Ref. [34] appear to be more sensitive as we decrease our scaling factor.

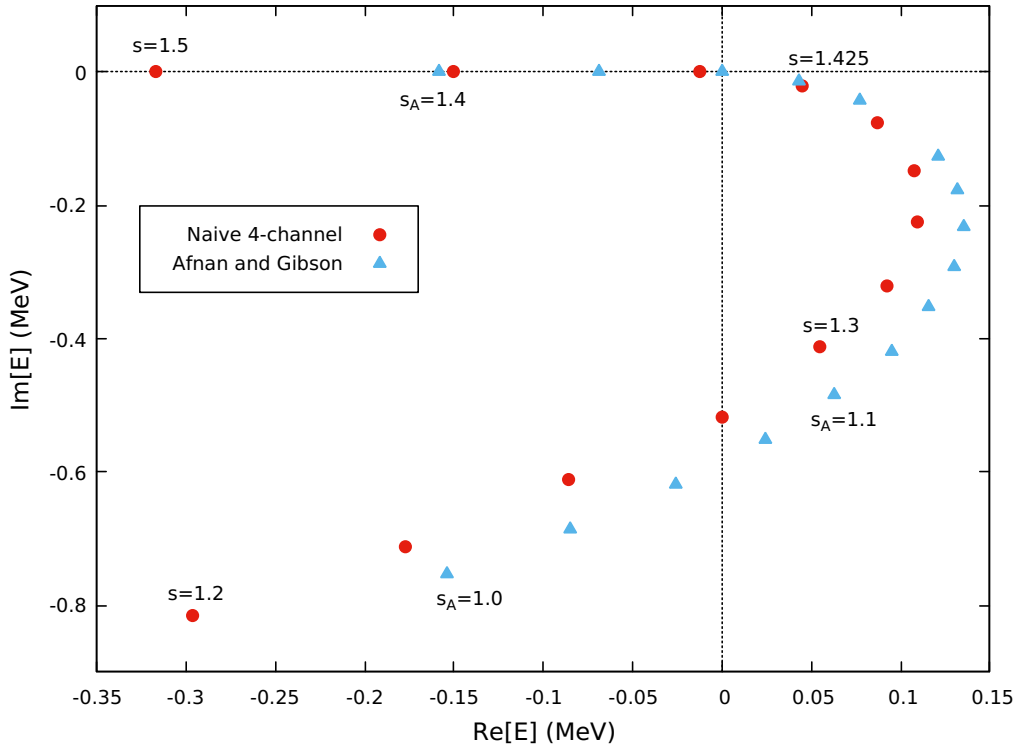


Figure 5.9: Combined plot of Figure 5.8 and reference [34].

# Chapter 6

## Conclusions and perspectives

In this work, we studied the pole trajectory of  $\Lambda nn$  system from bound to resonance states by changing the  $\Lambda n$  interaction. We present trajectories both in the EFT formalism, where and expansion in  $r_2/a_2$  is assumed, and using a phenomenological model that does not have to assume such assumption.

In Chapter 4 we outlined the derivation of the three-body integral equations pertinent to the  $\Lambda nn$  system in effective field theory. The technical details are quite similar to the one presented in more detail for the  $nd$  system in Section 3.3. The set of integral equations are the same used in Ref. [85]. We reproduced the numerical results of this reference for bound states and in this work we make an extension to explore the resonance regime.

Assuming the  $r_2/a_2$  expansion, at LO we multiply the  $\Lambda n$  scattering length (in both  $^3S_1(\Lambda n)$  triplet and  $^1S_0(\Lambda n)$  singlet channels) by a scaling factor  $s_{EFT}$ . By decreasing the scaling factor from 1.1 to 0.66 one could follow the pole trajectory from bound to resonant states. Our LO results show a trajectory that remains in the fourth quadrant of the complex energy plane, therefore, they correspond to physical resonant states. The trajectory, however, shows a strange pattern—it does not seem to be a fully continuous, but a piecewise continuous function as we change the scaling factor. For instance, in Figure 5.3, changing the scaling factor from  $s_{EFT} = 0.71$  to  $s_{EFT} = 0.70$  nearly keeps the imaginary part of the pole to  $\sim -0.635i$  MeV, but changes the real part abruptly from  $\sim 1.35$  MeV to  $\sim 1.68$  MeV.

Still at LO, we keep the  $\Lambda n$  scattering length fixed ( $s_{EFT} = 1.0$ ) and vary the three-body parameter  $g(\Lambda)$  from  $-0.3$  to  $1.6$ . We observe a very similar pattern for the pole trajectory as the previous case, where we varied the scaling factor  $s_{EFT}$ .

We also consider perturbative corrections assuming  $r_2/a_2 \ll 1$ . There is a shortcoming that, phenomenologically,  $r_2/a_2$  is even larger than 1, although the scattering parameters are barely determined experimentally beyond the scattering length. Thus our perturbative expansion multiplies the phenomenological effective range by a factor of

$s_{r_2(\Lambda n)} = 10^{-2}$ . As can be seen in Figure 5.6, as expected, the NLO corrections are relatively small for  $s_{EFT}$  closer to 1.0, but the deviations start to increase as one decreases  $s_{EFT}$ . For an expansion parameter of the order of 1/100, the results with smaller  $s_{EFT}$  do not indicate the expected convergence pattern.

Given the fact that, phenomenologically,  $r_2/a_2$  is slightly greater than 1, we also propose to study the  $\Lambda nn$  system with a separable potential model. We use Yamaguchi form factors, which allows us to relate the parameters of the potential with the scattering parameters (scattering length  $a_2$  and effective range  $r_2$ ). The projections into the three different channels involved remain the same as derived in EFT. Similar as before, we introduce a scaling factor  $s$  that multiplies the  $\Lambda n$  potentials in both  ${}^3S_1(\Lambda n)$  and  ${}^1S_0(\Lambda n)$  channels. The trajectory is given by Figure 5.7. Qualitatively, it shows a similar behavior as the one from Ref [34]. In particular to this case, one goes from a bound state to a resonant state by decreasing  $s$  around 1.725. Further decreasing  $s$  the poles remain in the fourth quadrant of the energy plane up to  $s = 1.625$ , beyond that the real part of the energy pole becomes negative (third quadrant), that is, it becomes an unphysical state. Therefore, in this model, physical resonant states live in the small interval  $1.725 \gtrsim s \gtrsim 1.625$ . Such scaling factors increase considerably the two-body  $\Lambda n$  interaction. However, it is possible that one can decrease the strength of the  $\Lambda n$  interaction by adding a three-body force (*e.g.*, as it happens in the  $nd$  system). In the presence of a  $\Lambda nn$  three-body force it should be possible to keep a shallow bound or resonant state with a smaller scaling factor  $s$ . It would be important to carry out explicit calculations to confirm these statements.

We also study the effect of introducing an extra channel in our three-body calculations. We introduce a naive fourth channel described in Section 5.2, and compare the results with Ref. [34]. With this naive fourth channel, our results get closer to the results of Ref. [34]. Besides, we get physical resonant states for  $1.425 \gtrsim s \gtrsim 1.3$ , that is, smaller values and wider range in  $s$ . To get a more reliable assessment of the effects of a fourth channel, a more rigorous calculation of this channel in our separable potential is needed.

The main conclusions we can get from this study are as follows. In the EFT perspective, with only scattering lengths as LO parameters, we do not need two-body  $\Lambda n$  scaling parameters much different from 1.0 in order to get a bound or resonant  $\Lambda nn$  system. In other words, we do not need to change much the two-body interaction to get a physical  $\Lambda nn$  state. However, we do not know for sure whether the effective range  $r_2$  values are amenable for a perturbative expansion. Phenomenological  $\Lambda n$  potentials indicate that no, with  $r_2/a_2$  of the order of or greater than 1. From our phenomenological separable potential perspective, one cannot get a shallow or resonant  $\Lambda nn$  state without multiplying the  $\Lambda n$  interaction by a considerable factor. In the three-channel approach this multiplication factor is large,  $s$  around 1.6-1.7, while in the four channel approach this factor could be

a bit smaller,  $s$  around 1.3-1.4. Nonetheless this phenomenological conclusion can be substantially altered if one includes a three-body  $\Lambda nn$  interaction. If that is the case, then it is possible to obtain a shallow bound or resonant  $\Lambda nn$  system with the  $\Lambda n$  interaction with a scaling factor  $s$  closer to 1.0. Therefore, a more robust calculation in this direction is needed.

Our aim with this study is, in broader terms, to analyse how much the  $\Lambda n$  interaction ought to be changed in order to produce a bound or resonant  $\Lambda nn$  state. The relevance of this work hinges on the increasing experimental interest in the recent years [25, 33, 36]. An interesting and promising idea is to obtain information about these hard-to-measure interactions by looking at particle correlations in relativistic heavy ions collisions, by means of femtoscopy techniques, as done by the ALICE Collaboration for  $p\Lambda$  and  $\Lambda\Lambda$  interactions [100, 101, 102].

# Appendices



# Appendix A

## Generators of the angular momentum

### 3/2

One can obtain the Cartesian components of the angular momentum operator  $\vec{J}$  for  $j = 3/2$  using the matrix elements of the  $J_{\pm}$  operators, which are given by

$$J_{\pm} |jm\rangle = \sqrt{(j \mp m)(j \pm m + 1)} |j(m \pm 1)\rangle. \quad (\text{A.1})$$

We can also express the lowering and raising operators  $J_{\pm}$  in terms of the Cartesian components  $J_i$  as

$$J_+ = J_1 + iJ_2, \quad J_- = J_1 - iJ_2. \quad (\text{A.2})$$

The inverse relation is

$$J_1 = \frac{1}{2} (J_+ + J_-), \quad J_2 = -\frac{i}{2} (J_+ - J_-). \quad (\text{A.3})$$

For our case, we have  $j = 3/2$ , then the matrix elements read

$$\left\langle 1\frac{1}{2}, \frac{3}{2}m' \left| J_{\pm} \right| 1\frac{1}{2}, \frac{3}{2}m \right\rangle = \sqrt{\left(\frac{3}{2} \mp m\right) \left(\frac{5}{2} \pm m\right)} \delta_{m', m \pm 1}. \quad (\text{A.4})$$

From now on, we omit indices that do not play a significant role and write

$$\langle m' | J_1 | m \rangle = \frac{1}{2} \left[ \sqrt{\left(\frac{3}{2} - m\right) \left(\frac{5}{2} + m\right)} \delta_{m', m+1} + \sqrt{\left(\frac{3}{2} + m\right) \left(\frac{5}{2} - m\right)} \delta_{m', m-1} \right]. \quad (\text{A.5})$$

$$\langle m' | J_2 | m \rangle = -\frac{i}{2} \left[ \sqrt{\left(\frac{3}{2} - m\right) \left(\frac{5}{2} + m\right)} \delta_{m', m+1} - \sqrt{\left(\frac{3}{2} + m\right) \left(\frac{5}{2} - m\right)} \delta_{m', m-1} \right]. \quad (\text{A.6})$$

$$\langle m' | J_3 | m \rangle = m \delta_{m', m}. \quad (\text{A.7})$$

By construction, the third Cartesian component forms a basis for the eigenstates of spin-3/2 and is given by simply

$$J_3 = \frac{1}{2} \begin{pmatrix} 3 & 0 & 0 & 0 \\ 0 & 1 & 0 & 0 \\ 0 & 0 & -1 & 0 \\ 0 & 0 & 0 & -3 \end{pmatrix}. \quad (\text{A.8})$$

Then, we can use (A.5) and (A.6) to calculate the elements of  $J_1$  and  $J_2$ . The non-zero elements are

- $m' = 3/2$ :

$$\langle m' | J_1 | \frac{1}{2} \rangle = \frac{\sqrt{3}}{2}, \quad \langle m' | J_2 | \frac{1}{2} \rangle = -\frac{i\sqrt{3}}{2}. \quad (\text{A.9})$$

- $m' = 1/2$ :

$$\begin{aligned} \langle m' | J_1 | \frac{3}{2} \rangle &= \frac{\sqrt{3}}{2}, & \langle m' | J_1 | -\frac{3}{2} \rangle &= 1, \\ \langle m' | J_2 | \frac{3}{2} \rangle &= \frac{i\sqrt{3}}{2}, & \langle m' | J_2 | -\frac{3}{2} \rangle &= -i. \end{aligned} \quad (\text{A.10})$$

- $m' = -1/2$ :

$$\begin{aligned} \langle m' | J_1 | \frac{1}{2} \rangle &= 1, & \langle m' | J_1 | -\frac{1}{2} \rangle &= \frac{\sqrt{3}}{2}, \\ \langle m' | J_2 | \frac{1}{2} \rangle &= i, & \langle m' | J_2 | -\frac{1}{2} \rangle &= -\frac{i\sqrt{3}}{2}. \end{aligned} \quad (\text{A.11})$$

- $m' = -3/2$ :

$$\langle m' | J_1 | -\frac{1}{2} \rangle = \frac{\sqrt{3}}{2}, \quad \langle m' | J_2 | -\frac{1}{2} \rangle = \frac{i\sqrt{3}}{2}. \quad (\text{A.12})$$

Then, the Cartesian components is written as

$$J_1 = \frac{1}{2} \begin{pmatrix} 0 & \sqrt{3} & 0 & 0 \\ \sqrt{3} & 0 & 2 & 0 \\ 0 & 2 & 0 & \sqrt{3} \\ 0 & 0 & \sqrt{3} & 0 \end{pmatrix}, \quad J_2 = \frac{1}{2} \begin{pmatrix} 0 & -i\sqrt{3} & 0 & 0 \\ i\sqrt{3} & 0 & -2i & 0 \\ 0 & 2i & 0 & -i\sqrt{3} \\ 0 & 0 & i\sqrt{3} & 0 \end{pmatrix} \quad (\text{A.13})$$

$$J_3 = \frac{1}{2} \begin{pmatrix} 3 & 0 & 0 & 0 \\ 0 & 1 & 0 & 0 \\ 0 & 0 & -1 & 0 \\ 0 & 0 & 0 & -3 \end{pmatrix}.$$

Properties of  $J_i$ 's matrices

$$J_1 J_2 = \frac{1}{4} \begin{pmatrix} 3i & 0 & -2i\sqrt{3} & 0 \\ 0 & i & 0 & -2i\sqrt{3} \\ 2i\sqrt{3} & 0 & -i & 0 \\ 0 & 2i\sqrt{3} & 0 & -3i \end{pmatrix}, \quad J_2 J_1 = \frac{1}{4} \begin{pmatrix} -3i & 0 & -2i\sqrt{3} & 0 \\ 0 & -i & 0 & -2i\sqrt{3} \\ 2i\sqrt{3} & 0 & i & 0 \\ 0 & 2i\sqrt{3} & 0 & 3i \end{pmatrix}, \quad (\text{A.14})$$

$$J_2 J_3 = \frac{1}{4} \begin{pmatrix} 0 & -i\sqrt{3} & 0 & 0 \\ 3i\sqrt{3} & 0 & 2i & 0 \\ 0 & 2i & 0 & 3i\sqrt{3} \\ 0 & 0 & -i\sqrt{3} & 0 \end{pmatrix}, \quad J_3 J_2 = \frac{1}{4} \begin{pmatrix} 0 & -3i\sqrt{3} & 0 & 0 \\ i\sqrt{3} & 0 & -2i & 0 \\ 0 & -2i & 0 & i\sqrt{3} \\ 0 & 0 & -3i\sqrt{3} & 0 \end{pmatrix},$$

$$J_3 J_1 = \frac{1}{4} \begin{pmatrix} 0 & 3\sqrt{3} & 0 & 0 \\ \sqrt{3} & 0 & 2 & 0 \\ 0 & -2 & 0 & -\sqrt{3} \\ 0 & 0 & -3\sqrt{3} & 0 \end{pmatrix}, \quad J_1 J_3 = \frac{1}{4} \begin{pmatrix} 0 & \sqrt{3} & 0 & 0 \\ 3\sqrt{3} & 0 & -2 & 0 \\ 0 & 2 & 0 & -3\sqrt{3} \\ 0 & 0 & -\sqrt{3} & 0 \end{pmatrix}.$$

Leading to the algebra of the generators of spin-3/2

$$[J_i, J_j] = i\varepsilon_{ijk} J_k. \quad (\text{A.15})$$

There is also an important relation that will be useful when calculating the  $G^{(i)}$  matrix-

ces, the anti-commutation of  $J_i$ 's

$$\{J_1, J_2\} = \begin{pmatrix} 0 & 0 & -i\sqrt{3} & 0 \\ 0 & 0 & 0 & -i\sqrt{3} \\ i\sqrt{3} & 0 & 0 & 0 \\ 0 & i\sqrt{3} & 0 & 0 \end{pmatrix}, \{J_2, J_3\} = \begin{pmatrix} 0 & -i\sqrt{3} & 0 & 0 \\ i\sqrt{3} & 0 & 0 & 0 \\ 0 & 0 & 0 & i\sqrt{3} \\ 0 & 0 & -i\sqrt{3} & 0 \end{pmatrix}, \quad (\text{A.16})$$

$$\{J_2, J_3\} = \begin{pmatrix} 0 & \sqrt{3} & 0 & 0 \\ \sqrt{3} & 0 & 0 & 0 \\ 0 & 0 & 0 & -\sqrt{3} \\ 0 & 0 & -\sqrt{3} & 0 \end{pmatrix}.$$

And they squared

$$J_1^2 = \frac{1}{4} \begin{pmatrix} 3 & 0 & 2\sqrt{3} & 0 \\ 0 & 7 & 0 & 2\sqrt{3} \\ 2\sqrt{3} & 0 & 7 & 0 \\ 0 & 2\sqrt{3} & 0 & 3 \end{pmatrix}, J_2^2 = \frac{1}{4} \begin{pmatrix} 3 & 0 & -2\sqrt{3} & 0 \\ 0 & 7 & 0 & -2\sqrt{3} \\ -2\sqrt{3} & 0 & 7 & 0 \\ 0 & -2\sqrt{3} & 0 & 3 \end{pmatrix}, \quad (\text{A.17})$$

$$J_3^2 = \frac{1}{4} \begin{pmatrix} 9 & 0 & 0 & 0 \\ 0 & 1 & 0 & 0 \\ 0 & 0 & 1 & 0 \\ 0 & 0 & 0 & 9 \end{pmatrix}.$$

# Appendix B

## $G^{(i)}$ matrices and its properties

As derived in the text, the matrices are given by

$$G^{(1)} = \frac{1}{\sqrt{6}} \begin{pmatrix} -\sqrt{3} & 0 \\ 0 & -1 \\ 1 & 0 \\ 0 & \sqrt{3} \end{pmatrix}, \quad G^{(2)} = \frac{i}{\sqrt{6}} \begin{pmatrix} \sqrt{3} & 0 \\ 0 & 1 \\ 1 & 0 \\ 0 & \sqrt{3} \end{pmatrix}, \quad (\text{B.1})$$

$$G^{(3)} = \frac{2}{\sqrt{6}} \begin{pmatrix} 0 & 0 \\ 1 & 0 \\ 0 & 1 \\ 0 & 0 \end{pmatrix}.$$

The Hermitian conjugate

$$G^{(1)} = \frac{1}{\sqrt{6}} \begin{pmatrix} -\sqrt{3} & 0 & 1 & 0 \\ 0 & -1 & 0 & \sqrt{3} \end{pmatrix}, \quad G^{(2)} = -\frac{i}{\sqrt{6}} \begin{pmatrix} \sqrt{3} & 0 & 1 & 0 \\ 0 & 1 & 0 & \sqrt{3} \end{pmatrix}, \quad (\text{B.2})$$

$$G^{(3)} = \frac{2}{\sqrt{6}} \begin{pmatrix} 0 & 1 & 0 & 0 \\ 0 & 0 & 1 & 0 \end{pmatrix}.$$

Then, we can check explicitly their properties

$$G^{(1)\dagger}G^{(2)} = \frac{i}{6} \begin{pmatrix} -2 & 0 \\ 0 & 2 \end{pmatrix} = -\frac{i}{3}\sigma_3, \quad G^{(2)\dagger}G^{(1)} = -\frac{i}{6} \begin{pmatrix} -2 & 0 \\ 0 & 2 \end{pmatrix} = \frac{i}{3}\sigma_3, \quad (\text{B.3})$$

$$G^{(2)\dagger}G^{(3)} = -\frac{i}{3} \begin{pmatrix} 0 & 1 \\ 1 & 0 \end{pmatrix} = -\frac{i}{3}\sigma_1, \quad G^{(3)\dagger}G^{(2)} = \frac{i}{3} \begin{pmatrix} 0 & 1 \\ 1 & 0 \end{pmatrix} = \frac{i}{3}\sigma_1,$$

$$G^{(3)\dagger}G^{(1)} = \frac{1}{3} \begin{pmatrix} 0 & -1 \\ 1 & 0 \end{pmatrix} = -\frac{i}{3}\sigma_2, \quad G^{(1)\dagger}G^{(3)} = \frac{1}{3} \begin{pmatrix} 0 & 1 \\ -1 & 0 \end{pmatrix} = \frac{i}{3}\sigma_2,$$

$$G^{(1)\dagger}G^{(1)} = G^{(2)\dagger}G^{(2)} = G^{(3)\dagger}G^{(3)} = \frac{2}{3}\sigma_0. \quad (\text{B.4})$$

Which implies

$$\boxed{G^{(i)\dagger}G^{(j)} = \frac{2}{3}\delta_{ij} - \frac{i}{3}\varepsilon_{ijk}\sigma_k.}$$

$$G^{(1)}G^{(2)\dagger} = -\frac{i}{6} \begin{pmatrix} -3 & 0 & -\sqrt{3} & 0 \\ 0 & -1 & 0 & -\sqrt{3} \\ \sqrt{3} & 0 & 1 & 0 \\ 0 & \sqrt{3} & 0 & 3 \end{pmatrix}, \quad G^{(2)}G^{(1)\dagger} = \frac{i}{6} \begin{pmatrix} -3 & 0 & \sqrt{3} & 0 \\ 0 & -1 & 0 & \sqrt{3} \\ -\sqrt{3} & 0 & 1 & 0 \\ 0 & -\sqrt{3} & 0 & 3 \end{pmatrix},$$

$$G^{(2)}G^{(3)\dagger} = \frac{i}{3} \begin{pmatrix} 0 & \sqrt{3} & 0 & 0 \\ 0 & 0 & 1 & 0 \\ 0 & 1 & 0 & 0 \\ 0 & 0 & \sqrt{3} & 0 \end{pmatrix}, \quad G^{(3)}G^{(2)\dagger} = -\frac{i}{3} \begin{pmatrix} 0 & 0 & 0 & 0 \\ \sqrt{3} & 0 & 1 & 0 \\ 0 & 1 & 0 & \sqrt{3} \\ 0 & 0 & 0 & 0 \end{pmatrix}, \quad (\text{B.5})$$

$$G^{(3)}G^{(1)\dagger} = \frac{1}{3} \begin{pmatrix} 0 & 0 & 0 & 0 \\ -\sqrt{3} & 0 & 1 & 0 \\ 0 & -1 & 0 & \sqrt{3} \\ 0 & 0 & 0 & 0 \end{pmatrix}, \quad G^{(1)}G^{(3)\dagger} = \frac{1}{3} \begin{pmatrix} 0 & -\sqrt{3} & 0 & 0 \\ 0 & 0 & -1 & 0 \\ 0 & 1 & 0 & 0 \\ 0 & 0 & \sqrt{3} & 0 \end{pmatrix},$$

$$G^{(1)}G^{(1)\dagger} = \frac{1}{6} \begin{pmatrix} 3 & 0 & -\sqrt{3} & 0 \\ 0 & 1 & -\sqrt{3} & 0 \\ -\sqrt{3} & 0 & 1 & 0 \\ 0 & -\sqrt{3} & 0 & 3 \end{pmatrix}, \quad G^{(2)}G^{(2)\dagger} = \frac{1}{6} \begin{pmatrix} 3 & 0 & \sqrt{3} & 0 \\ 0 & 1 & \sqrt{3} & 0 \\ \sqrt{3} & 0 & 1 & 0 \\ 0 & \sqrt{3} & 0 & 3 \end{pmatrix},$$

$$G^{(3)}G^{(3)\dagger} = \frac{2}{3} \begin{pmatrix} 0 & 0 & 0 & 0 \\ 0 & 1 & 0 & 0 \\ 0 & 0 & 1 & 0 \\ 0 & 0 & 0 & 0 \end{pmatrix}.$$

Leading to

$$G^{(i)}G^{(j)\dagger} = \frac{3}{4}\delta_{ij} - \frac{1}{6}\{J_i, J_j\} + \frac{i}{3}\epsilon_{ijk}J_k.$$

The next property says about multiplying  $G^{(i)}$  and  $\sigma_j$

$$\begin{aligned} G^{(1)}\sigma_2 &= \frac{i}{\sqrt{6}} \begin{pmatrix} 0 & \sqrt{3} \\ -1 & 0 \\ 0 & -1 \\ \sqrt{3} & 0 \end{pmatrix}, G^{(2)}\sigma_3 = \frac{i}{\sqrt{6}} \begin{pmatrix} \sqrt{3} & 0 \\ 0 & -1 \\ 1 & 0 \\ 0 & -\sqrt{3} \end{pmatrix}, G^{(3)}\sigma_1 = \frac{2}{\sqrt{6}} \begin{pmatrix} 0 & 0 \\ 0 & 1 \\ 1 & 0 \\ 0 & 0 \end{pmatrix}, \\ G^{(2)}\sigma_1 &= \frac{i}{\sqrt{6}} \begin{pmatrix} 0 & \sqrt{3} \\ 1 & 0 \\ 0 & 1 \\ \sqrt{3} & 0 \end{pmatrix}, G^{(3)}\sigma_2 = \frac{2i}{\sqrt{6}} \begin{pmatrix} 0 & 0 \\ 0 & -1 \\ 1 & 0 \\ 0 & 0 \end{pmatrix}, G^{(1)}\sigma_3 = \frac{1}{\sqrt{6}} \begin{pmatrix} -\sqrt{3} & 0 \\ 0 & 1 \\ 1 & 0 \\ 0 & -\sqrt{3} \end{pmatrix}, \end{aligned} \tag{B.6}$$

Then, we write

$$G^{(i)}\sigma_j - G^{(j)}\sigma_i = -i\epsilon_{ijk}G^{(k)}.$$

The last property can be evaluated algebraically using the last result we got

$$\begin{aligned} i \sum_{i,j} \epsilon_{ijn} (G^{(i)}\sigma_j - G^{(j)}\sigma_i) &= 2i \sum_{i,j} \epsilon_{ijn} G^{(i)}\sigma_j, \\ &= \sum_{i,j} \epsilon_{ijn} (\epsilon_{ijk} G^{(k)}), \\ &= \sum_j (\delta_{jj}\delta_{nk} - \delta_{jk}\delta_{jn}) G^{(k)} = 2\delta_{nk} G^{(k)}. \end{aligned}$$

$$i \sum_{i,j} \epsilon_{ijk} G^{(i)}\sigma_j = G^{(k)}.$$

where we used the identity  $\sum_i \epsilon_{ijk}\epsilon_{imn} = \delta_{jm}\delta_{kn} - \delta_{jn}\delta_{km}$ .

# Appendix C

## Born terms

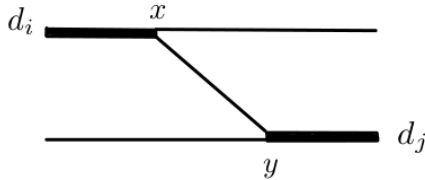
### C.1 $nd$ system

By definition, the particle and the dimer propagators are, respectively

$$iS_N^{\alpha\beta}(y-x) = \langle 0 | T \{ N_\beta(y) N_\alpha^\dagger(x) \} | 0 \rangle = \delta_{\alpha\beta} i\bar{S}_N(y-x), \quad (\text{C.1})$$

$$i\mathcal{D}_d^{ij}(y-x) = \langle 0 | T \{ d_j(y) d_i^\dagger(x) \} | 0 \rangle = \delta_{ij} i\bar{\mathcal{D}}_d(y-x). \quad (\text{C.2})$$

with  $T$  the time-ordered operator.



$$= (-ig_{d_j})(-ig_{d_i}) \int d^4x d^4y \quad (\text{C.3})$$

$$\langle 0 | T \{ d_j(\infty) N_\beta(\infty) [d_k^\dagger(y) N_\gamma(y) \mathcal{P}_{\gamma\delta}^k N_\delta(y)] [N_\epsilon^\dagger(x) \mathcal{P}_{\epsilon\sigma}^{s\dagger} N_\sigma^\dagger(x) d_s(x)] d_i^\dagger(-\infty) N_\alpha^\dagger(-\infty) \} | 0 \rangle.$$

Then, we have four possible Wick contractions

1.

$$\begin{aligned} & \langle 0 | T \{ d_j(\infty) N_\beta(\infty) [d_k^\dagger(y) N_\gamma(y) \mathcal{P}_{\gamma\delta}^k N_\delta(y)] [N_\epsilon^\dagger(x) \mathcal{P}_{\epsilon\sigma}^{s\dagger} N_\sigma^\dagger(x) d_s(x)] d_i^\dagger(-\infty) N_\alpha^\dagger(-\infty) \} | 0 \rangle \\ &= -\delta_{jk} i\bar{\mathcal{D}}_{d_j}(\infty-y) \delta_{\beta\epsilon} i\bar{S}_N(\infty-x) \delta_{si} i\bar{\mathcal{D}}_{d_i}(x+\infty) \delta_{\delta\alpha} i\bar{S}_N(y+\infty) \delta_{\gamma\sigma} i\bar{S}_N(y-x) \mathcal{P}_{\gamma\delta}^k \mathcal{P}_{\epsilon\sigma}^{s\dagger} \\ &= -i\bar{\mathcal{D}}_{d_j}(\infty-y) i\bar{S}_N(\infty-x) i\bar{\mathcal{D}}_{d_i}(x+\infty) i\bar{S}_N(y+\infty) i\bar{S}_N(y-x) \mathcal{P}_{\gamma\alpha}^j \mathcal{P}_{\beta\gamma}^{i\dagger}. \end{aligned} \quad (\text{C.4})$$



2.

$$\begin{aligned}
& \langle 0 | T \{ \overbrace{d_j(\infty) N_\beta(\infty)} \overbrace{[d_k^\dagger(y) N_\gamma(y) \mathcal{P}_{\gamma\delta}^k N_\delta(y)]} \overbrace{[N_\epsilon^\dagger(x) \mathcal{P}_{\epsilon\sigma}^{s\dagger} N_\sigma^\dagger(x) d_s(x)]} \overbrace{d_i^\dagger(-\infty) N_\alpha^\dagger(-\infty)} \} | 0 \rangle \\
&= \delta_{jk} i \overline{\mathcal{D}}_{d_j}(\infty - y) \delta_{\beta\sigma} i \overline{\mathcal{S}}_N(\infty - x) \delta_{si} i \overline{\mathcal{D}}_{d_i}(x + \infty) \delta_{\delta\alpha} i \overline{\mathcal{S}}_N(y + \infty) \delta_{\gamma\epsilon} i \overline{\mathcal{S}}_N(y - x) \mathcal{P}_{\gamma\delta}^k \mathcal{P}_{\epsilon\sigma}^{s\dagger} \\
&= i \overline{\mathcal{D}}_{d_j}(\infty - y) i \overline{\mathcal{S}}_N(\infty - x) i \overline{\mathcal{D}}_{d_i}(x + \infty) i \overline{\mathcal{S}}_N(y + \infty) i \overline{\mathcal{S}}_N(y - x) \mathcal{P}_{\gamma\alpha}^j \mathcal{P}_{\gamma\beta}^{i\dagger}.
\end{aligned} \tag{C.5}$$

3.

$$\begin{aligned}
& \langle 0 | T \{ \overbrace{d_j(\infty) N_\beta(\infty)} \overbrace{[d_k^\dagger(y) N_\gamma(y) \mathcal{P}_{\gamma\delta}^k N_\delta(y)]} \overbrace{[N_\epsilon^\dagger(x) \mathcal{P}_{\epsilon\sigma}^{s\dagger} N_\sigma^\dagger(x) d_s(x)]} \overbrace{d_i^\dagger(-\infty) N_\alpha^\dagger(-\infty)} \} | 0 \rangle \\
&= \delta_{jk} i \overline{\mathcal{D}}_{d_j}(\infty - y) \delta_{\beta\epsilon} i \overline{\mathcal{S}}_N(\infty - x) \delta_{si} i \overline{\mathcal{D}}_{d_i}(x + \infty) \delta_{\gamma\alpha} i \overline{\mathcal{S}}_N(y + \infty) \delta_{\delta\sigma} i \overline{\mathcal{S}}_N(y - x) \mathcal{P}_{\gamma\delta}^k \mathcal{P}_{\epsilon\sigma}^{s\dagger} \\
&= i \overline{\mathcal{D}}_{d_j}(\infty - y) i \overline{\mathcal{S}}_N(\infty - x) i \overline{\mathcal{D}}_{d_i}(x + \infty) i \overline{\mathcal{S}}_N(y + \infty) i \overline{\mathcal{S}}_N(y - x) \mathcal{P}_{\alpha\sigma}^j \mathcal{P}_{\beta\sigma}^{i\dagger}.
\end{aligned} \tag{C.6}$$

4.

$$\begin{aligned}
& \langle 0 | T \{ \overbrace{d_j(\infty) N_\beta(\infty)} \overbrace{[d_k^\dagger(y) N_\gamma(y) \mathcal{P}_{\gamma\delta}^k N_\delta(y)]} \overbrace{[N_\epsilon^\dagger(x) \mathcal{P}_{\epsilon\sigma}^{s\dagger} N_\sigma^\dagger(x) d_s(x)]} \overbrace{d_i^\dagger(-\infty) N_\alpha^\dagger(-\infty)} \} | 0 \rangle \\
&= -\delta_{jk} i \overline{\mathcal{D}}_{d_j}(\infty - y) \delta_{\beta\sigma} i \overline{\mathcal{S}}_N(\infty - x) \delta_{si} i \overline{\mathcal{D}}_{d_i}(x + \infty) \delta_{\gamma\alpha} i \overline{\mathcal{S}}_N(y + \infty) \delta_{\delta\epsilon} i \overline{\mathcal{S}}_N(y - x) \mathcal{P}_{\gamma\delta}^k \mathcal{P}_{\epsilon\sigma}^{s\dagger} \\
&= -i \overline{\mathcal{D}}_{d_j}(\infty - y) i \overline{\mathcal{S}}_N(\infty - x) i \overline{\mathcal{D}}_{d_i}(x + \infty) i \overline{\mathcal{S}}_N(y + \infty) i \overline{\mathcal{S}}_N(y - x) \mathcal{P}_{\alpha\epsilon}^j \mathcal{P}_{\epsilon\beta}^{i\dagger}.
\end{aligned} \tag{C.7}$$

Gathering all the contractions, we can write the amputated (the terms in red) Born amplitudes

$$iB^{\beta\alpha}(d_i \rightarrow d_j) \propto i \overline{\mathcal{S}}_N(y-x) \left[ -(\mathcal{P}^{i\dagger})^T (\mathcal{P}^j)^T + (\mathcal{P}^{i\dagger}) (\mathcal{P}^j)^T + (\mathcal{P}^{i\dagger})^T (\mathcal{P}^j) - (\mathcal{P}^{i\dagger}) (\mathcal{P}^j) \right]_{\beta\alpha}. \tag{C.8}$$

And using the fact that (also holds for  $\tau^i$ )

$$(\sigma_2)^T = -\sigma_2, \quad (\sigma^j)^T = -\sigma_2 \sigma^j \sigma_2 \quad \Rightarrow \quad (\sigma_2 \sigma^j)^T = \sigma_2 \sigma^j, \quad (\sigma^j \sigma_2)^T = \sigma^j \sigma_2. \tag{C.9}$$

- $t_i \rightarrow t_j$ :

$$\begin{aligned}
& \frac{1}{8} [ -(\tau_2 \sigma_2 \sigma^i)^\dagger{}^T (\tau_2 \sigma_2 \sigma^j)^T + (\tau_2 \sigma_2 \sigma^i)^\dagger (\tau_2 \sigma_2 \sigma^j)^T \\
& \quad + (\tau_2 \sigma_2 \sigma^i)^\dagger{}^T (\tau_2 \sigma_2 \sigma^j) - (\tau_2 \sigma_2 \sigma^i)^\dagger (\tau_2 \sigma_2 \sigma^j) ], \\
& = \frac{1}{8} [ -\tau_2^T \tau_2^T (\sigma^i \sigma_2)^T (\sigma_2 \sigma^j)^T + \tau_2 \tau_2^T (\sigma^i \sigma_2) (\sigma_2 \sigma^j)^T \\
& \quad + \tau_2^T \tau_2 (\sigma^i \sigma_2)^T (\sigma_2 \sigma^j) - \tau_2 \tau_2 (\sigma^i \sigma_2) (\sigma_2 \sigma^j) ], \\
& = -\frac{1}{2} \sigma^i \sigma^j. \tag{C.10}
\end{aligned}$$

- $t_i \rightarrow s_j$ :

$$\begin{aligned}
& \frac{1}{8} [ -(\tau_2 \sigma_2 \sigma^i)^\dagger{}^T (\sigma_2 \tau_2 \tau^j)^T + (\tau_2 \sigma_2 \sigma^i)^\dagger (\sigma_2 \tau_2 \tau^j)^T \\
& \quad + (\tau_2 \sigma_2 \sigma^i)^\dagger{}^T (\sigma_2 \tau_2 \tau^j) - (\tau_2 \sigma_2 \sigma^i)^\dagger (\sigma_2 \tau_2 \tau^j) ], \\
& = \frac{1}{8} [ -(\sigma^i \sigma_2)^T \sigma^T \tau_2^T (\tau_2 \tau^j)^T + (\sigma^i \sigma_2) \sigma_2^T \tau_2 (\tau_2 \tau^j)^T \\
& \quad + (\sigma^i \sigma_2)^T \sigma_2 \tau_2^T (\tau_2 \tau^j) - (\sigma^i \sigma_2) \sigma_2 \tau_2 (\tau_2 \tau^j) ], \\
& = -\frac{1}{2} \sigma^i \tau^j. \tag{C.11}
\end{aligned}$$

- $s_i \rightarrow t_j$ :

$$\begin{aligned}
& \frac{1}{8} [ -(\sigma_2 \tau_2 \tau^i)^\dagger{}^T (\tau_2 \sigma_2 \sigma^j)^T + (\sigma_2 \tau_2 \tau^i)^\dagger (\tau_2 \sigma_2 \sigma^j)^T \\
& \quad + (\sigma_2 \tau_2 \tau^i)^\dagger{}^T (\tau_2 \sigma_2 \sigma^j) - (\sigma_2 \tau_2 \tau^i)^\dagger (\tau_2 \sigma_2 \sigma^j) ], \\
& = \frac{1}{8} [ -(\tau^i \tau_2)^T \tau_2^T \sigma_2^T (\sigma_2 \sigma^j)^T + (\tau^i \tau_2) \tau_2^T \sigma_2 (\sigma_2 \sigma^j)^T \\
& \quad + (\tau^i \tau_2)^T \tau_2 \sigma_2^T (\sigma_2 \sigma^j) - (\tau^i \tau_2) \tau_2 \sigma_2 (\sigma_2 \sigma^j) ], \\
& = -\frac{1}{2} \tau^i \sigma^j. \tag{C.12}
\end{aligned}$$

- $s_i \rightarrow s_j$ :

$$\begin{aligned}
& \frac{1}{8} [ -(\sigma_2 \tau_2 \tau^i)^\dagger{}^T (\sigma_2 \tau_2 \tau^j)^T + (\sigma_2 \tau_2 \tau^i)^\dagger (\sigma_2 \tau_2 \tau^j)^T \\
& \quad + (\sigma_2 \tau_2 \tau^i)^\dagger{}^T (\sigma_2 \tau_2 \tau^j) - (\sigma_2 \tau_2 \tau^i)^\dagger (\sigma_2 \tau_2 \tau^j) ], \\
& = \frac{1}{8} [ -(\sigma^i \sigma_2)^T \sigma^T \tau_2^T (\tau_2 \tau^j)^T + (\sigma^i \sigma_2) \sigma_2^T \tau_2 (\tau_2 \tau^j)^T \\
& \quad + (\sigma^i \sigma_2)^T \sigma_2 \tau_2^T (\tau_2 \tau^j) - (\sigma^i \sigma_2) \sigma_2 \tau_2 (\tau_2 \tau^j) ], \\
& = -\frac{1}{2} \tau^i \tau^j. \tag{C.13}
\end{aligned}$$

Then, we can synthesize as

$$\boxed{iB_{\beta\alpha}^{ji} \propto -\frac{1}{2} \mathcal{O}^i \mathcal{O}^j}. \tag{C.14}$$

The final expression for the Born amplitudes are given by

$$\begin{aligned}
iB_{\beta\alpha}^{ji} &= (-ig_{d_j})(-ig_{d_i}) \left( -\frac{1}{2} \mathcal{O}^i \mathcal{O}^j \right)_{\beta\alpha} i\bar{S}_N(k_{d_0} - B_d - k_{n_0} + \varepsilon; \mathbf{p} + \mathbf{k}), \\
&= i \frac{g_{d_j} g_{d_i}}{2} (\mathcal{O}^i \mathcal{O}^j)_{\beta\alpha} \frac{1}{k_{d_0} - B_d - k_{n_0} + \varepsilon - \frac{(\mathbf{p} + \mathbf{k})^2}{2m_N} + i\epsilon}. \tag{C.15}
\end{aligned}$$

## C.2 $\Lambda nn$ system

By definition, the particles and the dimer propagators are, respectively

$$iS_n^{\alpha\beta}(y-x) = \langle 0 | T \{ \phi_\beta^n(y) \phi_\alpha^{n\dagger}(x) \} | 0 \rangle = \delta_{\alpha\beta} i\bar{S}_n(y-x), \tag{C.16}$$

$$iS_\Lambda^{\alpha\beta}(y-x) = \langle 0 | T \{ \phi_\beta^\Lambda(y) \phi_\alpha^{\Lambda\dagger}(x) \} | 0 \rangle = \delta_{\alpha\beta} i\bar{S}_\Lambda(y-x), \tag{C.17}$$

$$i\mathcal{D}_d^{ij}(y-x) = \langle 0 | T \{ d_j(y) d_i^\dagger(x) \} | 0 \rangle = \delta_{ij} i\bar{\mathcal{D}}_d(y-x). \tag{C.18}$$

The Feynman diagram follows the same convention as before, the first diagram should be the  ${}^1S_0(nn) \rightarrow {}^1S_0(nn)$ , which is not possible, then its contribution is zero, the other contractions can be written as

1.  ${}^1S_0(nn) \rightarrow {}^1S_0(\Lambda n)$  and  ${}^1S_0(nn) \rightarrow {}^3S_1(\Lambda n)$

$$\begin{aligned}
& \langle 0 | T \{ \overbrace{s_j^{\Lambda n}(\infty) \phi_\beta^n(\infty)}^{\overbrace{[s_k^{\Lambda n \dagger} \phi_\gamma^n \mathcal{P}_{\gamma\delta}^{(\Lambda n)k} \phi_\delta^\Lambda]_y}^{\overbrace{[\phi_\epsilon^{n \dagger} \mathcal{P}_{\epsilon\sigma}^{(nn)s \dagger} \phi_\sigma^{n \dagger} s_s^{nn}]_x} s_i^{nn \dagger}(-\infty)} \phi_\alpha^{\Lambda \dagger}(-\infty)} \} | 0 \rangle \\
&= -\delta_{jk} i \overline{\mathcal{D}}^{\Lambda n}(\infty - y) \delta_{\beta\epsilon} i \overline{\mathcal{S}}_n(\infty - x) \delta_{si} i \overline{\mathcal{D}}^{nn}(x + \infty) \delta_{\delta\alpha} i \overline{\mathcal{S}}_\Lambda(y + \infty) \delta_{\gamma\sigma} i \overline{\mathcal{S}}_n(y - x) \\
&\quad \times \mathcal{P}_{\gamma\delta}^{(\Lambda n)k} \mathcal{P}_{\epsilon\sigma}^{(nn)s \dagger} \\
&= -i \overline{\mathcal{D}}^{\Lambda n}(\infty - y) i \overline{\mathcal{S}}_n(\infty - x) i \overline{\mathcal{D}}^{nn}(x + \infty) i \overline{\mathcal{S}}_\Lambda(y + \infty) i \overline{\mathcal{S}}_n(y - x) \mathcal{P}_{\gamma\alpha}^{(\Lambda n)j} \mathcal{P}_{\beta\gamma}^{(nn)i \dagger}. \\
&\hspace{15em} \text{(C.19)}
\end{aligned}$$

$$\begin{aligned}
& \langle 0 | T \{ \overbrace{s_j^{\Lambda n}(\infty) \phi_\beta^n(\infty)}^{\overbrace{[s_k^{\Lambda n \dagger} \phi_\gamma^n \mathcal{P}_{\gamma\delta}^{(\Lambda n)k} \phi_\delta^\Lambda]_y}^{\overbrace{[\phi_\epsilon^{n \dagger} \mathcal{P}_{\epsilon\sigma}^{(nn)s \dagger} \phi_\sigma^{n \dagger} s_s^{nn}]_x} s_i^{nn \dagger}(-\infty)} \phi_\alpha^{\Lambda \dagger}(-\infty)} \} | 0 \rangle \\
&= \delta_{jk} i \overline{\mathcal{D}}^{\Lambda n}(\infty - y) \delta_{\beta\sigma} i \overline{\mathcal{S}}_n(\infty - x) \delta_{si} i \overline{\mathcal{D}}^{nn}(x + \infty) \delta_{\delta\alpha} i \overline{\mathcal{S}}_\Lambda(y + \infty) \delta_{\gamma\epsilon} i \overline{\mathcal{S}}_n(y - x) \\
&\quad \times \mathcal{P}_{\gamma\delta}^{(\Lambda n)k} \mathcal{P}_{\epsilon\sigma}^{(nn)s \dagger} \\
&= i \overline{\mathcal{D}}^{\Lambda n}(\infty - y) i \overline{\mathcal{S}}_n(\infty - x) i \overline{\mathcal{D}}^{nn}(x + \infty) i \overline{\mathcal{S}}_\Lambda(y + \infty) i \overline{\mathcal{S}}_n(y - x) \mathcal{P}_{\sigma\alpha}^{(\Lambda n)j} \mathcal{P}_{\beta\sigma}^{(nn)i \dagger}. \\
&\hspace{15em} \text{(C.20)}
\end{aligned}$$

These Born terms are proportional to

$$iB^{\beta\alpha}(s_i^{nn} \rightarrow s_j^{s(\Lambda n)}) \propto i \overline{\mathcal{S}}_n(y - x) [(P^{i\dagger})^T P^j - P^{i\dagger} P^j]_{\beta\alpha}. \quad \text{(C.21)}$$

2.  ${}^1S_0(\Lambda n) \rightarrow {}^3S_1(\Lambda n)$ ,  ${}^1S_0(\Lambda n) \rightarrow {}^1S_0(\Lambda n)$  and  ${}^3S_1(\Lambda n) \rightarrow {}^3S_1(\Lambda n)$

$$\begin{aligned}
& \langle 0 | T \{ \overbrace{s_j^{\Lambda n}(\infty) \phi_\beta^n(\infty)}^{\overbrace{[s_k^{\Lambda n \dagger} \phi_\gamma^n \mathcal{P}_{\gamma\delta}^{(\Lambda n)k} \phi_\delta^\Lambda]_y}^{\overbrace{[\phi_\epsilon^{\Lambda \dagger} \mathcal{P}_{\epsilon\sigma}^{(\Lambda n)s \dagger} \phi_\sigma^{n \dagger} s_s^{\Lambda n}]_x} s_i^{\Lambda n \dagger}(-\infty)} \phi_\alpha^{n \dagger}(-\infty)} \} | 0 \rangle \\
&= -\delta_{jk} i \overline{\mathcal{D}}^{\Lambda n}(\infty - y) \delta_{\beta\sigma} i \overline{\mathcal{S}}_n(\infty - x) \delta_{si} i \overline{\mathcal{D}}^{\Lambda n}(x + \infty) \delta_{\gamma\alpha} i \overline{\mathcal{S}}_n(y + \infty) \delta_{\delta\epsilon} i \overline{\mathcal{S}}_\Lambda(y - x) \\
&\quad \times \mathcal{P}_{\gamma\delta}^{(\Lambda n)k} \mathcal{P}_{\epsilon\sigma}^{(\Lambda n)s \dagger} \\
&= -i \overline{\mathcal{D}}^{\Lambda n}(\infty - y) i \overline{\mathcal{S}}_n(\infty - x) i \overline{\mathcal{D}}^{nn}(x + \infty) i \overline{\mathcal{S}}_n(y + \infty) i \overline{\mathcal{S}}_\Lambda(y - x) \mathcal{P}_{\alpha\epsilon}^{(\Lambda n)j} \mathcal{P}_{\beta\sigma}^{(\Lambda n)i \dagger}. \\
&\hspace{15em} \text{(C.22)}
\end{aligned}$$

These Born terms are proportional to

$$iB^{\beta\alpha}(s_i^{\Lambda n} \rightarrow s_j^{s(\Lambda n)}) \propto -i\bar{S}_\Lambda(y-x) [(P^{i\dagger})^T(P^j)^T]_{\beta\alpha}. \quad (\text{C.23})$$

The final Born term written in matrix form is given by

$$\bar{\mathbf{B}}^{ji} = \begin{pmatrix} y_{t(\Lambda n)}^2 \frac{\sigma^i \sigma^j}{2} S_\Lambda & -y_{s(\Lambda n)} y_{t(\Lambda n)} \frac{\sigma^j}{2} S_\Lambda & -y_{s(nn)} y_{t(\Lambda n)} \frac{\sigma^i}{\sqrt{2}} S_n \\ -y_{t(\Lambda n)} y_{s(\Lambda n)} \frac{\sigma^i}{2} S_\Lambda & y_{s(\Lambda n)}^2 \frac{1}{2} S_\Lambda & y_{s(nn)} y_{s(\Lambda n)} \frac{1}{\sqrt{2}} S_n \\ -y_{t(\Lambda n)} y_{t(nn)} \frac{\sigma^j}{\sqrt{2}} S_n & y_{s(\Lambda n)} y_{s(nn)} \frac{1}{\sqrt{2}} S_n & 0 \end{pmatrix} \quad (\text{C.24})$$

# Appendix D

## Separable Potentials

When considering the two-body sector this model has an exact solution for the scattering amplitude. In order to build the simplest system, he considered spinless particles interacting via a separable potential  $V(\mathbf{p}', \mathbf{p})$ . The form of the potential do not play an important role here, in terms of form factors  $g(\mathbf{p})$  its given by [97]

$$V(\mathbf{p}', \mathbf{p}) = \lambda g(\mathbf{p}')g(\mathbf{p}). \quad (\text{D.1})$$

Plugging into the Lippmann-Schwinger equation

$$\begin{aligned} T(\mathbf{p}', \mathbf{p}) &= \lambda g(\mathbf{p}')g(\mathbf{p}) + \int \frac{dq^3}{(2\pi)^3} \frac{\lambda g(\mathbf{p}')g(\mathbf{q})}{E - \mathbf{q}^2/2\mu + i\epsilon} T(\mathbf{q}, \mathbf{p}), \\ &= \lambda g(\mathbf{p}') \left[ g(\mathbf{p}) + \int \frac{dq^3}{(2\pi)^3} \frac{g(\mathbf{q})}{E - \mathbf{q}^2/2\mu + i\epsilon} T(\mathbf{q}, \mathbf{p}) \right], \\ &= \lambda g(\mathbf{p}') [g(\mathbf{p}) + G(E; \mathbf{p})]. \end{aligned} \quad (\text{D.2})$$

Once knowing an expression for the scattering amplitude  $T(\mathbf{p}', \mathbf{p})$ , one can iterate the expression to write

$$\begin{aligned} T(\mathbf{p}', \mathbf{p}) &= \lambda g(\mathbf{p}') \left[ g(\mathbf{p}) + \int \frac{dq^3}{(2\pi)^3} \frac{g(\mathbf{q})}{E - \mathbf{q}^2/2\mu + i\epsilon} \lambda g(\mathbf{q}) [g(\mathbf{p}) + G(E; \mathbf{p})] \right], \\ &= \lambda g(\mathbf{p}') \left[ g(\mathbf{p}) + \lambda [g(\mathbf{p}) + G(E; \mathbf{p})] \int \frac{dq^3}{(2\pi)^3} \frac{g^2(\mathbf{q})}{E - \mathbf{q}^2/2\mu + i\epsilon} \right]. \end{aligned} \quad (\text{D.3})$$

Which leads to another relation

$$G(E; \mathbf{p}) = \lambda [g(\mathbf{p}) + G(E; \mathbf{p})] I(E), \quad (\text{D.4})$$

with  $I(E) = \int \frac{dq^3}{(2\pi)^3} \frac{g^2(\mathbf{q})}{E - \mathbf{q}^2/2\mu + i\epsilon}$  an integral that depends only on the energy  $E$  and

might be solved analytically.

Eq. (D.4) gives an expression for  $G(E; \mathbf{p})$

$$G(E; \mathbf{p}) = \frac{\lambda g(\mathbf{p})I(E)}{1 - \lambda I(E)}, \quad (\text{D.5})$$

that leads to the final expression for the scattering amplitude

$$\begin{aligned} T(\mathbf{p}', \mathbf{p}) &= \lambda g(\mathbf{p}') \left[ g(\mathbf{p}) + \frac{\lambda g(\mathbf{p})I(E)}{1 - \lambda I(E)} \right], \\ &= \lambda g(\mathbf{p}')g(\mathbf{p}) \left[ \frac{1}{1 - \lambda I(E)} \right]. \end{aligned} \quad (\text{D.6})$$

Which can be expressed in different forms

$$\begin{aligned} T(\mathbf{p}', \mathbf{p}) &= \frac{V(\mathbf{p}', \mathbf{p})}{1 - \lambda I(E)}, \\ &= \frac{g(\mathbf{p}')g(\mathbf{p})}{\lambda^{-1} - I(E)} = \tau(E)g(\mathbf{p}')g(\mathbf{p}). \end{aligned} \quad (\text{D.7})$$

For instance, if the choice for the form factors were

$$g(\mathbf{p}) = \frac{1}{\mathbf{p}^2 + \beta^2}, \quad (\text{D.8})$$

known as Yamaguchi form factors [98]. The integral  $I(E)$  becomes

$$\begin{aligned} I(E) &= - \int \frac{dq^3}{(2\pi)^3} \frac{2\mu}{(\mathbf{q}^2 - \sigma)(\mathbf{q}^2 + \beta_1^2)(\mathbf{q}^2 + \beta_2^2)}, \\ &= - \frac{\mu}{\pi^2} \frac{1}{2(\beta_1 + \beta_2)(\beta_1 - i\sqrt{\sigma})(\beta_2 - i\sqrt{\sigma})}, \quad \text{or} \\ &= \frac{\mu}{\pi} \frac{1}{4\beta(\beta - i\sqrt{\sigma})^2}, \quad \text{if } \beta_1 = \beta_2 \end{aligned} \quad (\text{D.9})$$

with  $\sigma = 2\mu E + i\epsilon$

# Appendix E

## Numerical Methods

In this appendix, we aim to explain the numerical procedures that were used in our routines. The main problem was to solve integral equations, that in most cases could be written as an eigenvalue problem.

For instance, lets consider the integral equation given by

$$t_\ell(p', p) = v_\ell(p', p) + \int_0^\infty \frac{dq q^2}{2\pi^2} \frac{v_\ell(p', q)t_\ell(q, p)}{E - q^2/2m + i\epsilon}, \quad (\text{E.1})$$

The first step when one tries to understand how could this be solved numerically is to discretize all the momentum space. Then, we can write all possible values for  $p = p_1, p_2, \dots, p_n$ , and set  $p' = p$ . With these definitions, a function  $t_\ell(p', p)$  is essentially a  $n \times n$  matrix. Leading to a matrix equation

$$\mathbb{T} = \mathbb{V} + \mathbb{K}\mathbb{T}, \quad (\text{E.2})$$

where the kernel is defined as  $\mathbb{K} = \int_0^\infty \frac{dq q^2}{2\pi^2} \frac{\mathbb{V}}{E - q^2/2m + i\epsilon}$ .

But in most cases, we do not have the driving term  $\mathbb{V}$  which simplifies to a homogeneous equation

$$\begin{aligned} \mathbb{T} &= \mathbb{K}\mathbb{T}, \\ (\mathbb{I} - \mathbb{K})\mathbb{T} &= 0. \end{aligned} \quad (\text{E.3})$$

This condition is satisfied when the determinant of  $(\mathbb{I} - \mathbb{K})$  is equal to zero. Then, our problem is simplified to calculating the zeroes of a determinant [99].



## E.1 Numerical Integration

Among all possible methods that one can implement to numerically solve an integral, we chose to use Gaussian quadratures since it converge really fast. Choosing specifically the Gauss-Legendre quadrature (where the weight function  $W(x) = 1$ ), the integral is approximated by

$$\int_a^b f(x)dx \approx \sum_{j=1}^N f(x_j)w_j \quad (\text{E.4})$$

with  $x_j$  being the abscissas and  $w_j$  are the weights. The abscissas for this specific method are the roots of the  $n$ th Legendre polynomial. The weights can be calculated using  $w_j = \frac{2}{(1 - x_j^2)[P'_n(x_j)]^2}$ .

The idea behind Gaussian quadratures is to choose not only the weighting coefficients, but also the location of the abscissas. This gives to us twice the number of degrees of freedom, which, in general if the integrand is smooth, for a given order  $n$  will give twice the precision of other methods that numerically solve integrals [99].

## E.2 Contour Rotation

### Integrals of type $\int_0^\infty$

In order to access the second Riemann sheet (or the unphysical sheet), we need to deform our integration contour. This can be done by setting

$$q \rightarrow qe^{-i\theta} \quad q' \rightarrow q'e^{-i\theta}, \quad (\text{E.5})$$

and  $\theta > 0$  is a fixed angle.

The exposed section of the second sheet is defined by the real angle and the ray  $|\arg(E)| = 2\theta$ . The limitation of how large can  $\theta$  assume is imposed by the singularities of the kernel  $\mathbb{K}$ . For our work, the only limitation is that  $\theta < \frac{\pi}{2}$ . It is very important to ensure that there are not any singularities from deforming the original contour to the rotated one, in order to properly use the Cauchy's Theorem. Also important is the fact that we can neglect the angular part of the closed contour, as we are evaluating the integrand at  $\infty$ .

The improper integrals were evaluated numerically using a changing of variables

$$x \rightarrow \frac{x}{1-x}, \quad (\text{E.6})$$

which changes the range of integration from  $[0, \infty[$  to  $[0, 1]$ .

### Integrals of type $\int_0^\Lambda$

When working with EFTs, we need to perform the integration over a finite interval setting a momentum cutoff  $\Lambda$  to be the upper limit of integration. In this case we cannot neglect the angular part of the integral and to avoid a calculation of another integral, we perform a different contour rotation that depends on the momentum cutoff  $\Lambda$

$$\bar{q}(\Lambda) = q + 4i\gamma_t \left( \sqrt{1 + \left( \sqrt{\frac{q}{\Lambda}} - \frac{1}{2} \right)^2} - \sqrt{\frac{5}{4}} \right) \quad (\text{E.7})$$

where  $\gamma_t$  is the binding momentum of the deuteron.

This contour was firstly used in [74].

## E.3 Bound States

Once the determinant of  $(\mathbb{I} - \mathbb{K})$  is calculated, determining bound states is simple. Note also that, as they are located at the real axis, we do not need to worry about contour rotating any code that calculates only bound states. Just remembering that, for bound states  $B = -E$ , and only real values are allowed. When searching for them, one just needs to pay attention on the changing of the determinant sign. This change means that there were a zero, and that zero is the point we are looking for. As one finds the zero, we change the range of integration to a smaller one, centered on the zero we found. And we can confirm the value with precision.

One might be aware that the imaginary part of the determinant might be numerically zero in order to properly reproduce a bound state. In Figure E.1 are depicted a typical bound state plot, each value of  $B$  that the determinant are equally zero is a bound state. Depending on the system and on the range of integration, it is possible to find more than one bound state.

## E.4 Resonances

The search for resonances are a bit more complicated, since we need to deal with both real and imaginary parts of the energy. One might naively implement a Cartesian parameterization, but, numerically, the cost is bigger, because it involves a 2D search on a  $n \times n$  grid. A clever way to deal with this is using polar parameterization and write the

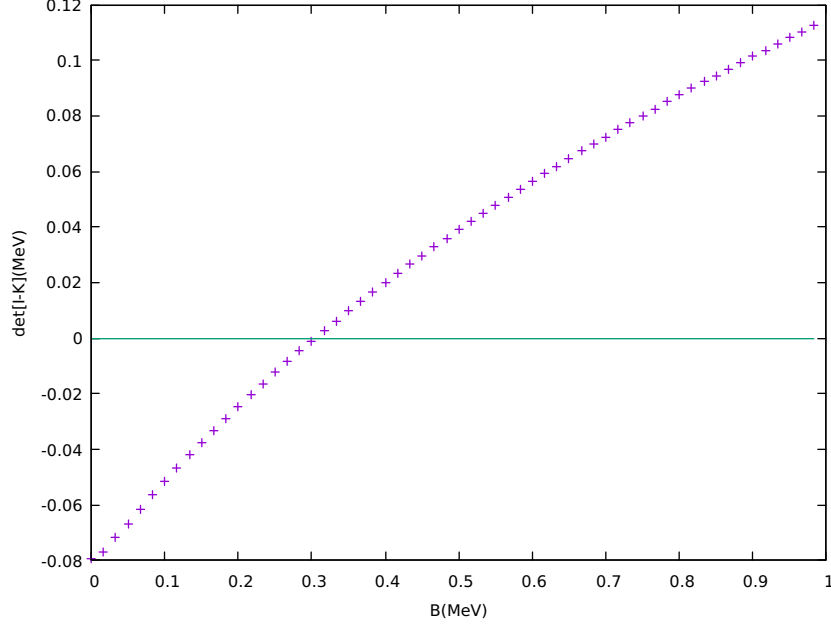


Figure E.1: Plot of the  $\det[(\mathbb{I} - \mathbb{K})]$  vs the binding energy  $B$

resonance energy  $E = E_R - i\frac{\Gamma}{2}$  as  $\tilde{E} = \rho e^{-i\phi}$ . The correspondence is simply the polar transformations

$$\begin{aligned} E_R &= \rho \cos \phi \\ \frac{\Gamma}{2} &= \rho \sin \phi \end{aligned} \quad (\text{E.8})$$

It is important to mention that  $\phi$  is different from  $\theta$ , the contour rotation angle, that is fixed. The angle  $\phi$  sweeps the plane as a loop variable, and for better computational results, we set the  $\phi$  loop as the outer loop.

As we are dealing with a complex number, the best way to search for the zero of the determinant is by searching for a zero of the absolute value of the determinant. Figure E.2 shows the minimum of a typical resonance plot. As the minimum is located, we change the range of integration to a smaller one, centered on the minimum we found. And we can confirm the value with precision.

## E.5 Coupled Channel

A single channel integral equation can be solved very easily, in most cases. There is only one amplitude to be calculated. For instance, the quartet channel in the  $nd$  system is a single channel integral equation. Less trivial is the case when one tries to solve coupled equations, but it turns out to be a simple generalisation.

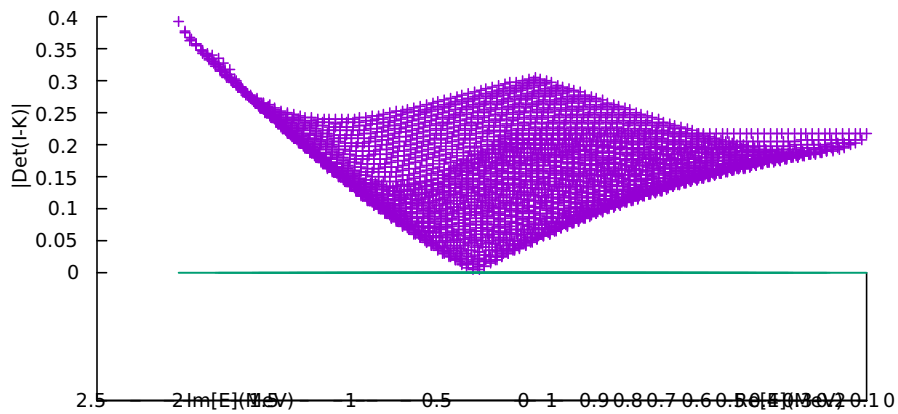
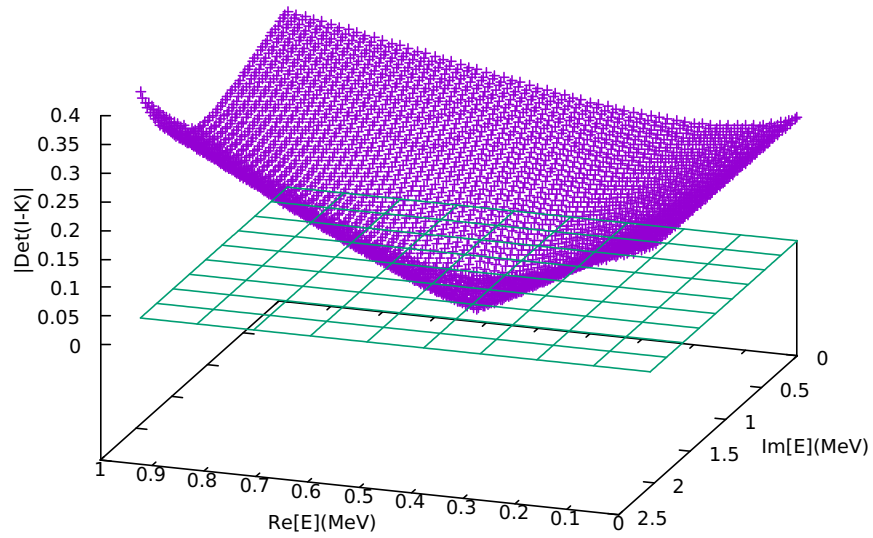


Figure E.2: Different angles of a given resonance plot. The minimum touches numerically the zero, the precision is greater as we restrict the interval of integration.

Consider the  $nd$  system in the doublet channel. There are two integral equations and the amplitudes are coupled. This means that one can completely describe its amplitudes

by solving four different integral equations.

Using matrix notation, we can write the single channel integral equation as

$$\mathbf{t} = \begin{pmatrix} K_{11} & \dots & K_{1n} \\ \vdots & \ddots & \vdots \\ K_{n1} & \dots & K_{nn} \end{pmatrix} \mathbf{t} \quad (\text{E.9})$$

The generalisations for an  $M$ -channel integral equation is straightforward

$$\mathbf{t} = \begin{pmatrix} K_{11} & \dots & K_{1n} & \dots & K_{12n} & \dots & K_{1Mn} \\ \vdots & \ddots & & & & & \vdots \\ K_{n1} & & \ddots & & & & \vdots \\ \vdots & & & \ddots & & & \vdots \\ K_{2n1} & & & & \ddots & & \vdots \\ \vdots & & & & & \ddots & \vdots \\ K_{Mn1} & \dots & \dots & \dots & \dots & \dots & K_{MnMn} \end{pmatrix} \mathbf{t} \quad (\text{E.10})$$

# Appendix F

## Tabulated Values

This Appendix contains the tabulated values of some important results given in Chapter 5.

$s_{EFT}$	$E$ (MeV)
1.1	$-0.295 - 0.0i$
1.05	$-0.09 - 0.0i$
1.0	$-0.0006 - 0.0i$
0.986	$0.0396107 - 0.00556692i$
0.972	$0.0874765 - 0.0211628i$
0.958	$0.134165 - 0.0399964i$
0.944	$0.169145 - 0.0615636i$
0.93	$0.224358 - 0.0852257i$
0.916	$0.255793 - 0.113886i$
0.902	$0.342937 - 0.138904i$
0.888	$0.370979 - 0.17457i$
0.874	$0.483484 - 0.191425i$
0.86	$0.522327 - 0.228199i$
0.846	$0.546384 - 0.271227i$
0.832	$0.70663 - 0.279775i$
0.818	$0.746709 - 0.313888i$
0.804	$0.766558 - 0.367273i$
0.8	$0.771311 - 0.380368i$
0.79	$0.998773 - 0.389405i$

Table F.1: Values for  $s_{r_2(\Lambda_n)} = 10^{-2}$

$s_{EFT}$	$E$ (MeV)
1.1	$-0.44 - 0.0i$
1.05	$-0.22 - 0.0i$
1.0	$-0.0006 - 0.0i$
0.99	$0.0298669 - 0.00282325i$
0.98	$0.0591066 - 0.0103157i$
0.97	$0.0873645 - 0.0216205i$
0.96	$0.124484 - 0.0374655i$
0.95	$0.1511 - 0.0526187i$
0.94	$0.197684 - 0.070859i$
0.93	$0.222681 - 0.0895171i$
0.92	$0.280168 - 0.107266i$
0.91	$0.314119 - 0.130112i$
0.9	$0.336417 - 0.154024i$
0.89	$0.427549 - 0.16971i$
0.88	$0.454549 - 0.18828i$
0.87	$0.472044 - 0.218115i$
0.86	$0.490054 - 0.249695i$
0.85	$0.630929 - 0.253632i$
0.84	$0.654523 - 0.275136i$
0.83	$0.673639 - 0.306285i$
0.82	$0.687291 - 0.347176i$
0.81	$0.880825 - 0.355876i$
0.8	$0.898094 - 0.366506i$
0.79	$0.9403 - 0.395266i$
0.78	$0.955839 - 0.434594i$
0.77	$0.963786 - 0.478427i$
0.75	$1.24683 - 0.493655i$
0.74	$1.30733 - 0.528195i$
0.73	$1.31223 - 0.5733i$
0.72	$1.32375 - 0.615868i$
0.71	$1.35 - 0.635263i$
0.7	$1.6838 - 0.636255i$
0.687	$1.69675 - 0.68553i$
0.68	$1.77092 - 0.715499i$
0.67	$1.79146 - 0.775233i$
0.66	$1.81654 - 0.812578i$

Table F.2: Values plotted in Figure 5.3

$g(\Lambda)$	$E$ (MeV)
-0.3	-0.54 - 0.0 <i>i</i>
-0.2	-0.305 - 0.0 <i>i</i>
-0.1	-0.135 - 0.0 <i>i</i>
0.0	-0.0006 - 0.0 <i>i</i>
0.05	0.0445173 - 0.00657374 <i>i</i>
0.1	0.0872885 - 0.0219254 <i>i</i>
0.15	0.128501 - 0.041381 <i>i</i>
0.2	0.179432 - 0.0624847 <i>i</i>
0.25	0.208543 - 0.0844685 <i>i</i>
0.3	0.227309 - 0.10407 <i>i</i>
0.32	0.27874 - 0.110924 <i>i</i>
0.33	0.292677 - 0.11647 <i>i</i>
0.35	0.304326 - 0.127615 <i>i</i>
0.4	0.325738 - 0.153281 <i>i</i>
0.45	0.335308 - 0.16791 <i>i</i>
0.47	0.416046 - 0.171482 <i>i</i>
0.5	0.431432 - 0.181357 <i>i</i>
0.55	0.450431 - 0.205273 <i>i</i>
0.6	0.449397 - 0.219186 <i>i</i>
0.62	0.467986 - 0.237937 <i>i</i>
0.65	0.478331 - 0.250597 <i>i</i>
0.7	0.5956 - 0.255274 <i>i</i>
0.75	0.607082 - 0.258942 <i>i</i>
0.8	0.637788 - 0.278643 <i>i</i>
0.85	0.654126 - 0.300864 <i>i</i>
0.9	0.657917 - 0.320888 <i>i</i>
1.0	0.662211 - 0.352104 <i>i</i>
1.1	0.851802 - 0.358064 <i>i</i>
1.2	0.855079 - 0.380705 <i>i</i>
1.3	0.898929 - 0.400229 <i>i</i>
1.35	0.8987 - 0.415258 <i>i</i>
1.4	0.898225 - 0.430357 <i>i</i>
1.5	0.892586 - 0.450878 <i>i</i>
1.55	0.902273 - 0.475714 <i>i</i>
1.6	0.915744 - 0.47874 <i>i</i>

Table F.3: Values plotted in Figure 5.4.



$s$	$E$ (MeV)
1.8	$-0.23 - 0.0i$
1.775	$-0.125 - 0.0i$
1.75	$-0.05 - 0.0i$
1.725	$0.00162755 - 0.000360534i$
1.7	$0.0215372 - 0.0255286i$
1.675	$0.025263 - 0.0609736i$
1.65	$0.0182763 - 0.0983157i$
1.625	$0.000119449 - 0.15i$
1.6	$-0.0346648 - 0.196973i$
1.575	$-0.0751219 - 0.238446i$
1.55	$-0.128907 - 0.289278i$
1.525	$-0.191519 - 0.332023i$

Table F.4: Values plotted in Figure 5.7.

$s$	$E$ (MeV)
1.5	$-0.316667 - 0.0i$
1.475	$-0.15 - 0.0i$
1.45	$-0.0125 - 0.0i$
1.425	$0.0449569 - 0.0218832i$
1.4	$0.0873177 - 0.0773594i$
1.375	$0.107758 - 0.148323i$
1.35	$0.109595 - 0.224697i$
1.325	$0.0918899 - 0.320418i$
1.3	$0.0543433 - 0.413108i$
1.275	$-0.000105231 - 0.516665i$
1.25	$-0.0858093 - 0.610666i$
1.225	$-0.17731 - 0.711582i$
1.2	$-0.296531 - 0.814363i$

Table F.5: Values plotted in Figure 5.8.

# Bibliography

- [1] R.P. Feynman, Phys. Rev. **76**, 769 (1949).
- [2] C.N. Yang and R.L. Mills, Phys. Rev. **96**, 191 (1954).
- [3] L. O’Raifeartaigh. The Dawning Of Gauge Theory. Princeton University Press, 1997.
- [4] A. Jaffe and E. Witten, ”Quantum Yang-Mills Theory”. <https://www.claymath.org/wp-content/uploads/2022/06/yangmills.pdf>.
- [5] D.J. Gross and F. Wilczek, Phys. Rev. Lett. **30**, 1343–1346 (1973).
- [6] H.D. Politzer, Phys. Rev. Lett. **30**, 1346–1349 (1973).
- [7] M. Gell-Mann, Phys. Lett. **8**, 214 (1964).
- [8] T. Potter, ”QCD Particle and Nuclear Physics”. [https://www.hep.phy.cam.ac.uk/~chpotter/particleandnuclearphysics/Lecture\\_07\\_QCD.pdf](https://www.hep.phy.cam.ac.uk/~chpotter/particleandnuclearphysics/Lecture_07_QCD.pdf).
- [9] S. Samuel and K.J.M Moriarty, CERN-TH. 4271 (1985). <https://cds.cern.ch/record/163700/files/CM-P00062390.pdf>
- [10] J.J Dudek, R.G. Edwards, K. Orginos and D.G. Richards, J. Phys.: Conf. Ser. **299**, 012007 (2011).
- [11] USQCD Collaboration., W. Detmold, R.G. Edwards, *et al.*, Eur. Phys. J. A **55**, 193 (2019).
- [12] BMW Collaboration, Science **322**, 1224-1227 (2008).
- [13] BMW Collaboration, Phys. Lett. B **705**, 477-481 (2011).
- [14] P.F. Bedaque, A. Boehnlein, M. Cromaz, M. Diefenthaler and L. Elouadrhiri, Eur. Phys. J. A **57** 3, 100 (2021).
- [15] P.F. Bedaque, R. Khadka, G. Rupak and M. Yusef, arXiv:2209.09962v1, <https://arxiv.org/abs/2209.09962>, (2022).
- [16] P.F. Bedaque, H. Kumar and A. Sheng, arXiv:2309.02352v1, <https://arxiv.org/abs/2309.02352>, (2023).

- [17] R.B. Wiringa, V.G.J. Stoks and R. Schiavilla. *Phys. Rev. C* **51**, 38 (1995).
- [18] S. Veerasamy and W. N. Polyzou. *Phys. Rev. C* **84**, 034003 (2011).
- [19] C. Ordonez, L. Ray and U. van Kolck, *Phys. Rev. C* **53**, 2086 (1996).
- [20] R. Machleidt and D.R. Entem, *Phys. Rept.* **503**, 1 (2011).
- [21] E. Epelbaum, H.-W. Hammer and U.-G. Meissner, *Rev. Mod. Phys.* **81**, 1773 (2009).
- [22] R. Higa and M.R. Robilotta, *Phys. Rev. C* **68**, 024004 (2003).
- [23] R. Higa, M.R. Robilotta and C.A. da Rocha, *Phys. Rev. C* **69**, 034009 (2004).
- [24] R. Higa, M.P. Valderrama and E.R. Arriola, *Phys. Rev. C* **77**, 034003 (2008).
- [25] C. Rappold, *et al.*, *Phys. Rev. C* **88**, 041001 (2013).
- [26] R.H. Dalitz and B.W. Downs, *Phys. Rev.* **110**, 958 (1958).
- [27] R.H. Dalitz and B.W. Downs, *Phys. Rev.* **111**, 967 (1958).
- [28] R.H. Dalitz and B.W. Downs, *Phys. Rev.* **114**, 593 (1959).
- [29] H. Garcilazo, *J. Phys. G* **13**, L63 (1987).
- [30] H. Garcilazo and A. Valezarce, *Phys. Rev. C* **89**, 057001 (2014).
- [31] E. Hiyama, S. Ohnishi and B.F. Gibson, T.A. Rijken, *Phys. Rev. C* **89**, 061302(R) (2014).
- [32] A. Gal and H. Garcilazo, *Phys. Lett. B* **736**, 93 (2014).
- [33] K. Itabashi, T. Akiyama, Y. Fujii, *et al.*, *Few-Body Syst* **63**, 16 (2022).
- [34] I.R. Afnan and B.F. Gibson, *Few-Body Syst.* **60**, 51 (2019).
- [35] B.F. Gibson and I.R. Afnan, Proceedings for the 24th edition of European Few Body Conference, (2019).
- [36] B. Pandey, *et al.*, (Hall A Collaboration), *Phys. Rev. C* **105**, L051001 (2022).
- [37] M.M. Nagels, T.A. Rijken and J.J. de Swart, *Phys. Rev. D* **15**, 2547 (1977).
- [38] David Tong. "Quantum Mechanics". *David Tong: Lectures on Quantum Mechanics*. 2021. <http://www.damtp.cam.ac.uk/user/tong/quantum.html>;
- [39] E. Braaten and H.-W. Hammer, *Phys. Rept.* **428**, 259 (2006).
- [40] F.M. Marqués and J. Carbonell, *Eur. Phys. J. A* **57**, 105 (2021).
- [41] R. Littlejohn. "The Lippmann-Schwinger Equation". "Quantum Mechanics". 2016. <https://bohr.physics.berkeley.edu/classes/221/s16/221.html>.

- [42] J.J. Sakurai. Modern Quantum Mechanics (Revised Edition). 1 : Addison Wesley, 1993.
- [43] George Arfken. Mathematical Methods for Physicists. Third San Diego: Academic Press, Inc., 1985.
- [44] C. Itzykson and J.-B. Zuber. Quantum Field Theory. Dover Publications, 2006.
- [45] K.G. Wilson, Rev. Mod. Phys. **47**, 773 (1975).
- [46] M. Schwartz. Quantum Field Theory and the Standard Model: Cambridge Press, 2014.
- [47] M.E. Peskin and D.V Schroeder. An Introduction to Quantum Field Theory: Addison Wesley, 1995.
- [48] P.F. Bedaque and U. van Kolck, Ann. Rev. Nucl. Part. Sci. **52**, 339 (2002).
- [49] S. Weinberg, Phys. Lett. B **251**, 288 (1990).
- [50] S. Weinberg, Nucl. Phys. B **363**, 3 (1991).
- [51] C. Ordóñez and U. van Kolck, Phys. Lett. B **291**, 459 (1992).
- [52] U. van Kolck, Soft Physics: Applications of Effective Chiral Lagrangians to Nuclear Physics and Quark Models, Ph.D. thesis (Texas U.) (1993).
- [53] S. Weinberg, Physica A **96**, 327 (1979).
- [54] J. Gasser and H. Leutwyler, Annals Phys. **158** (1), 142 (1984).
- [55] J. Gasser and H. Leutwyler, Nucl. Phys. B **250** (1-4), 465 (1985).
- [56] P.F. Bedaque and U. van Kolck, Phys. Lett. B **428**, 221 (1998).
- [57] U. van Kolck, Chiral dynamics: Theory and experiment. Proceedings, Workshop, Mainz, Germany, Lect. Notes Phys **513**, 62 (1997).
- [58] D.B. Kaplan, M. J. Savage, and M. B. Wise, Phys. Lett. B **424**, 390 (1998); Nucl. Phys. B **534**, 329 (1998).
- [59] E. Epalbaum, H.-W. Hammer, and U.-G. Meissner, Rev. Mod. Phys. **81**, 1773 (2009).
- [60] A. Nogga, R.G.E. Timmermans, and U. van Kolck, Phys. Rev. C **72**, 054006 (2005).
- [61] H.-W. Hammer, S. König, and U. van Kolck, Rev. Mod. Phys. **92** 2, 025004 (2020).
- [62] S. König, H.W. Griesshammer, H.-W. Hammer, and U. van Kolck, Phys. Rev. Lett. **118** 20, 202501 (2017).
- [63] S. Fleming, T. Mehen, and I.W. Stewart, Nucl. Phys. A **677**, 313 (2000).
- [64] J.-W. Chen, G. Rupak, M. J. Savage, Nucl. Phys. A **653**, 386 (1999).

- [65] Gautam Rupak, Nucl. Phys. A **678**, 405 (2000).
- [66] R. Higa, H.-W. Hammer, and U. van Kolck, Nucl. Phys. A **809**, 171 (2008).
- [67] R. Higa, Mod. Phys. Lett. A **24**, 915 (2009).
- [68] H. -W. Hammer, C. Ji, and D. R. Phillips, J. Phys. G **44** 10, 103002 (2017).
- [69] E. Braaten, M. Lu, Phys. Rev. D **76**, 094028 (2007).
- [70] S. Fleming, M. Kusunoki, T. Mehen, and U. van Kolck, Phys. Rev. D **76**, 034006 (2007).
- [71] H. A. Bethe, Phys. Rev. **76**, 38 (1949).
- [72] D. B. Kaplan, Nucl. Phys. B **494**, 471 (1997).
- [73] U. van Kolck, Proceedings of the Workshop on Chiral Dynamics 1997, Theory and Experiment, Springer–Verlag, 1998.
- [74] P.F. Bedaque H.-W. Hammer and U. van Kolck, Nuc. Phys. A, **646**, 444 (1999).
- [75] P.F. Bedaque, H.-W. Hammer and U. van Kolck, Phys. Rev. Lett. **82**, 463 (1999).
- [76] V. Efimov, Yad. Fiz. **12**, 1080–1091 (1970), [Sov. J. Nucl. Phys. **12**, 589-595 (1971)].
- [77] V. Efimov, Physics Letters B **33**, 563 – 564, 1970.
- [78] P. Naidon and S. Endo, Rep. Prog. Phys. **80**, 056001 (2017).
- [79] T. Frederico, A. Delfino, Lauro Tomio, and M.T. Yamashita, Progress in Particle and Nuclear Physics, **67**, 4, 939-994 (2012).
- [80] V. Efimov, Sov. J. Nucl. Phys. **29**, 546 (1979), [Yad. Fiz. **29**, 1058 (1979)].
- [81] P.F. Bedaque, H.-W. Hammer and U. van Kolck, Nucl.Phys. A **676**, 357-370 (2000).
- [82] H.W. Grißhammer, Nucl. Phys. A **744**, 192 (2004).
- [83] ”*Clebsch-Gordan Coefficients*”. Available in <https://pdg.lbl.gov/2013/reviews/rpp2013-rev-clebsch-gordan-coefs.pdf>.
- [84] W. Greiner, ”Structure of vacuum and elementary matter: from superheavies via hypermatter to antimatter.”. An Advanced Course in Modern Nuclear Physics. Lecture Notes in Physics, **581**, 316 (2001).
- [85] S.-I. Ando, U. Raha and Y. Oh, Phys. Rev. C **92**, 024325 (2015).
- [86] S.R. Beane and M. J. Savage, Nucl. Phys. A **694**, 511 (2001).
- [87] S.-I. Ando and C. H. Hyun, Phys. Rev. C **72**, 014008 (2005).
- [88] S.-I. Ando and K. Kubodera, Phys. Lett. B **633**, 253 (2006).

- [89] C. Chen, *et al.*, Phys. Rev. C **77**, 054002 (2008).
- [90] R. Machleidt and I. Slaus, J. Phys. G: Nucl. Part. Phys. **27** R69 (2001).
- [91] A. Gårdestig, J. Phys. G: Nucl. Part. Phys. **36** 053001 (2009).
- [92] B.F. Gibson and I. R. Afnan, AIP Conference Proceedings **2130**, 020005 (2019).
- [93] J. Esser, *et al.*, Phys. Rev. Lett. **114**, 232501 (2015).
- [94] T.O Yamamoto, *et al.*, Phys. Rev. Lett. **115**, 222501 (2015).
- [95] G.A. Miller, A.K. Opper and E.J. Stephenson, Annu. Rev. Nucl. Part. Sci. **56**, 253 (2006).
- [96] I.R. Afnan and B.F. Gibson, Phys. Rev. C **47**, 1000 (1993).
- [97] R.D. Amado, Phys. Rev. **132**, 485 (1963).
- [98] Y. Yamaguchi, Phys. Rev. **95**, 1628 (1954).
- [99] W. Press, S. Teukolsky, W. Vetterling and B. Flannery. Numerical Recipes, 3rd Edition: The Art of Scientific Computing. Cambridge University Press, 3 edition, (2007)
- [100] ALICE Collaboration, Phys. Lett. B **833** 137272 (2022).
- [101] ALICE Collaboration, Phys. Rev. C **99**, 024001 (2019).
- [102] ALICE Collaboration, Phys. Lett. B **797**, 134822 (2019).